ROLE OF FIBRONECTIN IN TUMOR DEVELOPMENT AND JOINT LUBRICATION

A Dissertation

Presented to the Faculty of the Graduate School

of Cornell University

in Partial Fulfillment of the Requirements for the Degree of

Doctor of Philosophy

by

Roberto Carlos Andresen Eguiluz

January 2015

ROLE OF FIBRONECTIN IN TUMOR DEVELOPMENT AND JOINT LUBRICATION

Roberto Carlos Andresen Eguiluz, Ph.D.

Cornell University 2015

Surfaces in biology are present everywhere, and how biomacromolecules and cells interact with them to form interfaces is crucial in cell biology, biotechnology and medicine. For example, biosensors are based on the specific recognition of sugars such as glucose in the glucose-sensors used by diabetic patients. Another example is found in cancer, where breast cancer cells secrete factors that interact with peripheral stromal cells (the interface) and alter their behavior. Another interesting example can be found in diarthrodial joints, such as the knee or the hip joint, where two opposing surfaces need efficient and durable interfacing as they slide against each other over the lifespan of a healthy person.

In the first part of this thesis, I present a direct quantitative correlation between the mechanics of the fibronectin extracellular matrix at the cellular scale and the conformation of fibronectin constituting the matrix at the molecular scale. Additionally, I analyze the effects of mechanics and conformation on cell behavior (adhesion and secretion) in a model system that represents the interface with the tumor.

Next, I present a phenomenological study of the molecular interactions between fibronectin (present in the superficial zone of cartilage) and synovial fluid components. I do this by examining their synergistic performance under confinement and shear to provide efficient lubrication. These results are compared with the tribological performance of a mimetic lubricin developed by my

coworkers.

Combined, these results have important implications for our understanding of (i) tumor development and vascularization (ii) cell-matrix interactions (by providing new insights into the structure-mechanics relationship of protein networks), and (iii) the molecular mechanisms of boundary lubrication and wear protection of articular surfaces. The findings presented in this work may be applied to future treatments of diseases such as breast cancer and osteoarthritis.

BIOGRAPHICAL SKETCH

Roberto together with his brother Juan Carlos was born and raised in Mexico City by his mother Luz María and grandmother Omi. After completing his basic education at the Swiss College of Mexico, Roberto lived and traveled in France, Germany, and Switzerland, and upon return he attended the National Autonomous University of Mexico (UNAM) were he received a B.S. degree in Mechanical Engineering. During this period, he spent one year at the Eidgenössische Technische Hochschule (ETH) Zurich as part of an exchange program, where he developed an uniaxial strain device to probe protein fibers. Following graduation, Roberto joined the Ibero-American University as a lecturer in the Department of Mechanical and Electrical Engineering. Shortly after, he started as a lecturer in the College of Engineering at the Autonomous University of Mexico while pursuing a masters degree in Materials Science and Engineering. It was there that he discovered the world of tribology while working with Prof. Rafael Schouwenaars.

In January 2010, Roberto moved to Ithaca, NY with Sol and Matias, his wife and son, to pursue a Ph.D. under the supervision of Prof. Delphine Gourdon. His doctoral research focuses on how mechanics, conformation, and interaction of structural and lubricating proteins impact fundamental biological functions. In addition to his dissertation research, he has participated in a range of projects from tumorigenesis to novel and tunable bio-adhesives. After completing his doctoral studies, Roberto will continue pursuing research in mechanobiology and mechanotransduction as a post-doctoral fellow with Prof. Deborah Leckband at the University of Illinois at Urbana-Chapaign.

To Sol,

my Penelope.

ACKNOWLEDGEMENTS

The work presented here is the result of the combined emotional and intellectual environment in which I have been immersed, thanks to family, friends, and colleagues.

First, I want to acknowledge my supervisor Prof. Delphine Gourdon for giving me the opportunity to be her first Ph.D. student, trusting me with the challenging task of mounting the SFA lab, for her guidance in all projects, and for being available to answer so many questions during my thesis. I also thank my co-supervisors and collaborators, Prof. Claudia Fischbach, Prof. Lawrence Bonassar, Prof. Dave Putnam, and Prof. Michael Smith for opening their laboratory spaces, for their fruitful discussions and feedback. They always critically studied the results and pointed out how to improve them. I also want to thank Prof. Xavier Banquy and Dr. Kai Kristiansen for walking me through the SFA world.

To all of those who read this document over and over again in order to make it better, thank you! These people are Juan Carlos, Anna, Sierra, Cory, Noah, Fei, Karin, Sol, and Christine.

The experimental work couldn't have been done without the great assistance provided by the teams of CCMR, NBTC, and CNF. Specially, I want to thank Phil Carubia, who became a good friend. Also, the collegial and respectful working environment at the MSE Department, has been very important. I want to thank Michele Conrad, Karen Jordan, Carol Armstrong, Vicki Conner, Dolores Dewbury, David Rutherford, and Heidi Hart-Gorman who keep it running and help to maintain a friendly environment.

I am very fortunate to have met and shared not only office space but great moments with Markus, Rebecca, Karin, Fei, and Sierra, who during this time

have become much more than colleagues - good friends. This holds for BoRi too, who became an unofficial Gourdon member. They have always been ready to help in any situation, whether work related or personal. The team and friends include Kelly, Cory and Noah, who became my right and left hand in the lab and made it possible to pull all this together. We still have a trip to "The Church" pending. I also want to thank the members of the Bonassar and Putnam Groups at BME, especially to Kirk J. Samaroo, Mingchee Tan, Edward Bonnevie, and Heidi Reesink, with whom I worked and who kindly shared their expertise and materials with me. Thanks for the patience in answering in detail my questions and for the time you took for useful discussions.

There is life in Ithaca outside Cornell! I will start by thanking Victor and Cosette for receiving us with open arms in Ithaca. You made our arrival such an easy thing. Also, to Emily and the Asenath-Smith (Smith-Asenath) family, who became close friends, allies, and partners in crime. Next, I thank Panos Dallas, who started as a colleague, and became a very good and close friend, helping me with long conversations and support. During these almost five years I was part of a unique community which made Ithaca home. I am referring to Pato and the Winckler Urrutia, Amir and the Sadovnik Page, Adam Bisogni, Silvano and the De La Llata Sabido, Santiago "Gorreón" and the Peralta Hernandez, Duncan and the Duke Cardenas, David and the Rhodes Josephson, all West-viewers, and "Lord" Nimish Pujara, friends and confidants. Thanks for all the good moments, support, conversations, barbecues, tears, disagreements, and hangovers. Who knows where the next one will be.

The next lines are for my long-distance friends and colleagues, that remained close despite the many miles or km in between: Piter, Richard, Karel, Glen, Andretti, Brody, Mau-Tse, Marry, Lucciana, Tiririt, Rodrigo, Kaki, Nora, Kimon,

and Mike. The same for my UNAM friends: Hugo, Agustín, David, Everth, and the always supportive Rafael Schouwenaars.

To counter balance work life, my family environment was and is a key factor. I want to start by thanking my wife Sol for always supporting me in any circumstance, for knowing when and how to give me a needed push, love, and for putting her professional career on hold. Without the love and joy she has brought to my life it would have been (almost) impossible to go through these years. Thanks to my son Matias and my daughter Romina for filling me with such amazing feelings, and for guiding me through the world to so many unexpected and unexplored places. Thanks to my mother Luz Maria for teaching me through her example that discipline and hard work are essential tools for life, and for her love, dedication and unconditional support. My brother follows. I have reached a new personal relationship with him, beyond brother and best friend, extended to intellectual collaborator. Thanks for your always supportive words and actions, and thanks also to my extended growing family, Anna and Mo. Thanks to my cousins Conchita, Maricarmen, Melanie, Jaqueline, José Miguel and Manuel, my uncles Miguel, Claus, and aunts Dicky, Doris and Conchis who always have cheered for me and motivated me. Finally, thanks to my in-laws, Selva, David, Sofia, and David.

With *all* of you I constantly redefined the word *family*.

I also acknowledge the founding and support provided by CONACyT, which helped for four years of our stay.

Ah, and to Cuchufli.

TABLE OF CONTENTS

Biographical Sketch . . . iii
Dedication . . . iv
Acknowledgements . . . v
Table of Contents . . . viii
List of Tables . . . xi
List of Figures . . . xii

Acronyms **xix**

1 Scope of the Thesis **2**
1.1 Research objectives . . . 2
1.1.1 Specific objective 1 . . . 3
1.1.2 Specific objective 2 . . . 4
1.1.3 Specific objective 3 . . . 5
1.2 General Conclusion . . . 6

2 General background **8**
2.1 Extracellular matrix . . . 9
2.2 Fibronectin . . . 10
2.3 Breast tissue and breast cancer . . . 12
2.4 Articular cartilage and osteoarthritis . . . 15
2.4.1 Synovial fluid . . . 18
2.5 Polymer brushes . . . 20
2.6 A unique experimental technique: the surface forces apparatus . 22
2.7 Fibronectin molecular conformation via Förster resonance energy transfer . . . 23

3 Stiffening and unfolding of fibronectin increase proangiogenic factor secretion by breast cancer-associated stromal cells **25**
3.1 Abstract . . . 25
3.2 Significance . . . 26
3.3 Introduction . . . 27
3.4 Results . . . 29
3.4.1 Tumor-conditioned cells promote matrix stiffening through altered Fn assembly . . . 29
3.4.2 Tumor-Associated Matrices Comprise Highly Stretched and Unfolded Fn Fibers . . . 33
3.4.3 Tumor-Associated Fn Matrices are Thicker, Denser, and Comprise Thicker Fibers . . . 35
3.4.4 Tumor-associated Fn matrices modify cell adhesion and proangiogenic factor secretion by activating an integrin switch . . . 36

3.5 Discussion . . . 39
3.6 Materials and methods . . . 43
3.7 Acknowledgements . . . 44
3.8 Supplemental information . . . 44
3.8.1 SI Materials and methods . . . 44
3.8.2 SI Figures . . . 51

4 Fibronectin tethers synovial fluid components in the superficial zone of cartilage 56
4.1 Abstract . . . 56
4.2 Significance . . . 57
4.3 Introduction . . . 57
4.4 Materials and Methods . . . 61
4.4.1 Fibronectin conformation studies . . . 61
4.4.2 Surface Forces Apparatus . . . 62
4.5 Results . . . 64
4.5.1 Fibronectin conformation . . . 64
4.5.2 Normal interaction forces between fibronectin tethered molecules . . . 65
4.5.3 Effective brush-like behavior . . . 67
4.5.4 Lubrication and wear protection of mica surfaces by fibronectin tethered molecules . . . 71
4.5.5 Surface damage via FECO spectroscopy . . . 74
4.5.6 Particulate formation and evolution . . . 77
4.6 Discussion . . . 79
4.6.1 Fn conformation and binding of SF components . . . 79
4.6.2 Friction forces, coefficients of friction, and wear protection 82
4.7 Conclusions . . . 85
4.8 Acknowledgements . . . 86

5 Low friction of lubricin-mimicking bottle-brush polymers interacting with fibronectin 87
5.1 Abstract . . . 87
5.2 Significance . . . 88
5.3 Introduction . . . 89
5.4 Materials and methods . . . 91
5.4.1 mimLub synthesis . . . 91
5.4.2 Preparation of mimLub and fibronectin solutions . . . 93
5.4.3 Atomic force microscopy . . . 94
5.4.4 Surface Forces Apparatus . . . 95
5.5 Results . . . 96
5.5.1 Molecular characterization of mimLUB . . . 96
5.5.2 Role of fibronectin in normal interaction forces of mica surfaces across mimLUB . . . 98

5.5.3 Role of fibronectin in lubrication and wear protection of mica surfaces by mimLUB . . . 100
5.5.4 Role of fibronectin on mimLUB confinement and overall film viscosity . . . 103
5.6 Discussion . . . 105
5.7 Conclusion . . . 108
5.8 Acknowledgements . . . 109

6 Conclusions **110**
6.1 Summary . . . 110
6.2 Future directions . . . 113
6.2.1 Cell type generalization and 3-D studies . . . 114
6.2.2 Conformation-dependent binding of lubricin to fibronectin 114
6.2.3 Bi- and multi-synovial fluid component shear experiments on fibronectin films . . . 116
6.2.4 Tweaking mimetic polymer brushes and exposing them to real biological systems . . . 117

A Apendix: Collaborative projects **118**
A.1 Past collaborations . . . 118
A.1.1 Implanted adipose progenitor cells as physicochemical regulators of breast cancer . . . 118
A.1.2 Controlling Adhesion and Elasticity of Mytilus edulis Foot Protein-1 Films via DOPA-DOPA Crosslinking . . . 119
A.2 Current collaborations . . . 121
A.2.1 Obesity-dependent changes of interstitial ECM mechanics and their role in breast tumorigenesis . . . 121

B Apendix: Matlab codes for elastic moduli extraction **123**

C Apendix: Fn strain-induced unfolding appears to promote LUB and pAA-*g*-PEG binding **131**
C.1 Materials and methods . . . 131
C.1.1 Microfabrication of master mold . . . 131
C.1.2 PDMS patterning and preparation . . . 132
C.2 Preliminary strain-binding results . . . 133
C.2.1 LUB binds to Fn in a strain dependent manner . . . 133
C.2.2 pAA-*g*-PEG binds to Fn in a strain dependent manner . . . 134

Bibliography **136**

LIST OF TABLES

4.1 Components found in SF reported to play a role in joint lubrication and used in this study. 61

4.2 Brush lengths (L) and average grafting distances (s) for long range (LR) and short range (SR) interactions obtained from Equation 4.1. 70

4.3 Pressures reported at onset of wear. In brackets max applied pressures without sign of wear. 73

LIST OF FIGURES

2.1 Modular structure of a Fn monomer. (A) Fn type I modules (rectangles), type II modules (violet ovals), and type III modules (ovals). The alternative spliced domains in yellow. Assembly and binding domains indicated along the Fn monomer. (B) Modules type I and II showing the pair of disulfide bonds in purple. (C) Module type III with its stacked β-strands. Fig. from [Mao and Schwarzbauer, 2005] 10

2.2 Schematic illustration of articular cartilage showing the collagen orientation in different zones. Inset 1 shows the superficial zone of cartilage. Inset 2 depicts the lamina splendens. Fig. adapted from [Dedinaite, 2012] 16

2.3 LUB consists of a long heavily glycosylated, mucinous domain separating two SMB domains at the N-terminus and a haemopexin region at the C-terminus. The mucinous domain consists of a polypeptide backbone with the main amino acids being threonine, glutamic acid, proline and lysine. Carbohydrates constitute about 40% (w/w) of LUB with the main residues being galactosamine, galactose, and N-acetylneuraminic acid. Thus, LUB molecules carry a considerable number of anionic side chains and the mucinous part of the molecule has a bottle-brush structure. LUB is associated with phospholipid components that comprise about 10% by weight. Taken from [Dedinaite, 2012]. 19

2.4 HA is a linear high molecular weight polysaccharide, consisting of repeating disaccharide units of D-glucuronic acid and N-acetyl D-glucosamine. At physiological pH, HA carries a high negative charge. 21

3.1 Caption in next page. 30

3.1 Tumor-associated Fn matrices are stiffer and more viscous. (A) Schematics of the Surface Forces Apparatus (SFA) mica surfaces and the setup used for mechanical characterization of the matrices at 37°C. (B) Interference fringes measured with the SFA when shining white light through the confining surfaces at large (uncompressed matrix) and small (compressed matrix) separations. (C) Immunostaining of tumor-conditioned stromal cells embedded in their ECM after 24 hours of culture onto SFA mica surfaces (green, Fn; red, F-actin; and blue, nuclei). (D) Same as (C) after decellularization (cell extraction) showing the Fn matrix left behind. Scale bars = 50 μm. (E) To determine Fn matrix stiffness, compressive force-distance profiles were acquired in quasi-static conditions in control (○) and tumor-associated (●) conditions and fitted using a Hertzian model. (F) Mean tumor-associated matrix elastic moduli (n = 18) were ≈60% higher than those of control matrices (n = 20). (G) The viscoelastic behavior of both control (○) and tumor-associated (●) Fn matrices was next quantified through creep experiments by monitoring matrix relaxation after rapid (instantaneous) force application. All relaxation data were well fitted using a double exponential decay to extract fast (τ_1) and slow (τ_2) characteristic times. (H) There was an overall slower response (hence higher viscosity) of tumor-conditioned matrices (n = 3) compared to that of control matrices (n = 2). Mean ± SD. 31

3.2 Tumor-associated Fn matrices are more unfolded. (A, B) FRET-Fn maps showed lower FRET intensity ratios, IA/ID, in tumor matrices (blue Fn fibers) than in their control counterpart (green/yellow Fn fibers). Scale bars = 50 μm. (C) Corresponding FRET intensity ratios histograms confirmed that tumor-associated Fn matrices comprised mainly stretched/unfolded Fn fibers (low FRET, narrow distribution) while control matrices contained a broader population of Fn conformations (higher FRET, larger distribution). (D) Mean FRET intensity ratios, IA/ID, of tumor-associated Fn matrices (n = 171) were lower than that of control matrices (n = 245), indicating that tumor conditions increased unfolding by ≈10% with respect to control. Mean ± SD. 34

3.3 Tumor-associated Fn matrices are thicker, denser, and comprised of thicker fibers.(A) Tumor-associated Fn matrices (n=21) measured by the SFA were thicker than control matrices (n = 17). (B) Z-projections of immunostained control and tumor-associated Fn matrices. Scale bars = 50 μm. Insets: 300% zooms used to determine the pore size and fiber diameter shown in panels (C) and (D), respectively. (C) Pores measured within tumor associated Fn matrices (n = 72) were significantly smaller than those measured within control matrices (n = 72) ($p < 0.0001$). (D) Tumor-associated Fn fibers (n = 120) possessed larger diameters than those of control Fn fibers (n = 120) ($p < 0.05$). Mean ± SD. 36

3.4 Cells adhere to tumor-associated Fn preferentially through α_v integrins with associated increased VEGF secretion. (A) After 4 hours, fewer adherent cells were detected within unfolded and stiff tumor matrices (1088 ± 522 cells) than within control ones (1851 ± 1504 cells) (n = 3/group). Mean ± SD. (B) After 4 hours, new cells secreted higher levels of VEGF when seeded onto tumor-associated Fn (1.9 ± 0.6 pg/1000 cells) than those seeded onto control Fn (1.3 ± 0.42 pg/1000 cells). (C) Cells treated with β_1-integrin blockers secreted significantly higher amounts of VEGF (2.8 ± 0.93 pg/1000 cells; $p < 0.01$) than untreated cells on control matrices, while cells treated with v-integrin blockers secreted slightly lower levels of VEGF (1.5 ± 0.47 pg/1000 cells) than untreated cells on tumor matrices (1.92 ± 0.6 pg/1000 cells) (n = 6/group). Mean ± SD. 38

3.5 ECM composition and linearization of force-distance profiles. (A) Cell-derived ECMs were immunostained simultaneously for both fibronectin and collagen, showing that early tumor-associated ECMs were comprised exclusively of Fn. Scale bars = 50 μm. (B) Linearization of the representative compressive force-distance profiles for control ECMs (experimental ∘, fit – – –) and for tumor ECMs (experimental •, fit– – ––) shown in Fig. 3.11E. Tumor-associated ECMs show a larger linear regime as compared to the control ECMs. 52

3.6 Chemical crosslinking increases stiffness. Tumor-associated ECM elastic moduli were measured to be 0.1428 ± 0.06070kPa (n = 20), representing an increase in elastic modulus of 60% compared to the control ECM elastic modulus, measured to be 0.09031 ± 0.05266 kPa (n = 30) ($p < 0.05$). 52

3.7 Chemical crosslinking relaxes conformation. (A) Control Fn ECMs were comprised of more close-to-compact Fn fibers (high FRET, red/yellow pixels). (B) Tumor-associated Fn ECMs were comprised of more unfolded Fn fibers (low FRET, blue pixels). (C) Representative histograms of FRET ratios displayed. (D) Mean FRET intensity ratios of tumor-associated Fn ECMs (n = 14) were significantly lower than that of control Fn ECMs (n = 18) ($p < 0.0001$). Scale bars = 50 μm. 53

3.8 Enhanced VEGF secretion. After preconditioned cells deposited Fn matrices for 24 hours, media and decellularized Fn matrix lysates were collected to measure soluble and Fn-bound VEGF, respectively. VEGF values were normalized to cell population, and represented as relative ratios to soluble VEGF detected from control Fn matrix samples. Tumor-associated soluble VEGF secretions were higher than that of control soluble VEGF secretions (n = 2). Tumor-associated Fn-bound VEGF was not different from that of control Fn-bound VEGF (n = 2). 54

3.9 Focal adhesion protein recruitment on tumor-associated Fn ECMs associated with development of focal contacts. After 4 hours, untreated cells on control ECMs developed fibrillar adhesions as shown by talin immunostaining (insets: double arrows). Cells treated with β_1-integrin blockers on control ECMs show adhesion clusters comprised talin not associated with cells (insets: ECM cluster). Untreated cells on tumor ECMs appeared to have developed focal contacts comprised both talin and pFAK (insets: large arrowheads). Cells treated with α_v-integrin blockers were able to develop fibrillar adhesions (insets: double arrows). Cells treated with both integrin blockers on control ECMs were also able to develop fibrillar adhesions (insets: double arrows), however treated cells on tumor ECMs left behind adhesion clusters in the surroundings (insets: ECM cluster). Scale bar = 50 μm. . . 55

4.1 (A) Schematics of articular cartilage showing collagen type II fiber orientation as a function of depth. Inset 1: detail of the superficial zone of articular cartilage illustrating the cellular and acellular regions. Inset 2: representation of some relevant biomolecules present in the lamina splendens. (B) FRET intensity ratio frequency histogram of Fn conformations as measured by FRET-Fn adsorbed to curved mica substrates. 64

4.2 (A) Representative curves of the normal force $F_\perp$ normalized by the surface radius of curvature R as a function of the absolute separation distance D between mica surfaces coated with adsorbed Fn (white squares), with adsorbed Fn and LUB (cyan circles), with adsorbed Fn and ESF (orange triangles), with adsorbed Fn and HA (black squares), and with adsorbed Fn and BSA (green diamonds). (B) Bar charts displaying the average values of the unperturbed film thickness D_0 and (C) the average values for the compressed film thickness (hardwalls) HW of Fn films before (white) and after incubation of LUB (cyan), ESF (orange), HA (black), and BSA (green). Values are reported as mean + standard deviation. In all cases, p ¡ 0.05 is indicated by a single star, p ¡ 0.01 by two stars and p ¡ 0.001 by three stars. 65
4.3 Semi-log plots of representative curves of the normal force $F_\perp$ normalized by the surface radius of curvature R as a function of the film thickness D (A) LUB (cyan circles), (B) ESF (orange triangles), (C) HA (black squares), and (D) BSA (green diamonds) adsorbed to Fn. White squares in each panel represent Fn only. Red lines indicate fits to Eq. 4.1 (AdG) or Eq. **??** (exponential decay). 68
4.4 Friction force $F_\parallel$ as a function of normal force $F_\perp$ between (A) mica surfaces with adsorbed Fn and LUB, (B) with adsorbed Fn and ESF, (C) with adsorbed Fn and HA, and (D) with adsorbed Fn and BSA all sheared in PBS. The surfaces were sheared at sliding velocities of $V = 0.3\mu m/s$ (black circles), $V = 3\mu m/s$ (red triangles), and $V = 30\mu m/s$ (blue squares). Open symbols for HA and BSA indicate measurements after the surfaces became damaged with wear. 71
4.5 Examples of surfaces visualized by MIB of mica substrates (A, E, I) with adsorbed Fn and LUB, (B, F, J) with adsorbed Fn and ESF, (C, G, K) with adsorbed Fn and HA, and (D, H, L) with adsorbed Fn and BSA when shearing started (t_0) and when shearing ended (t_f) at sliding velocities (A, B, C, D) $V = 0.3\mu m/s$, (E, F, G, H) $V = 3\mu m/s$, and (I, J, K, L) $V = 30\mu m/s$. Molecule aggregates without damage is indicated by single sided orange arrows. Damage is indicated by double sided yellow arrows. 75
4.6 Debris size measured as a function of normal force $F_\perp$ at sliding velocities of (A) $V = 0.3\mu m/s$, (B) $V = 3\mu m/s$, and (C) $V = 30\mu m/s$ for mica surfaces with adsorbed Fn and HA (black squares) and with adsorbed Fn and BSA (green diamonds). (D) Schematic representation of Fn+HA and Fn+BSA debris confined between surfaces. 78
4.7 Proposed dimer configurations of (A) LUB at low concentrations and (B) LUB at high concentrations (from synovial fluid). 79

5.1 (A) Molecular structure of the pAA-PEG bottle-brush polymer mimLUB, with x~185 y~650, m~45, and MW ≈ 1400 kDa, (B) Tapping mode AFM height micrograph in air of the polymer chains adsorbed on a freshly cleaved mica surface from a solution at 300 μg/ml, scale bar = 50 nm, (C) number-average contour length l_N and number-average molecular diameter d_N, and (D) schematic representation of the mimLUB with l_N, d_N and hydrodynamic diameter D_H. 97
5.2 Normal force $F_\perp$ normalized by the surface radius of curvature R between mimLub molecules adsorbed on mica surfaces (A) and between two physisorbed Fn layers (B) on mica surfaces with mimLUB as a function of the mica-mica separation distance (film thickness), D. Forces on approach are shown by solid circles and on separation by open circles. Bar charts displaying the average value for film thickness at rest D_0 (C) and average value for the HW (D) for mimLUB adsorbed on mica (white), Fn only (black), and Fn+mimLUB (gray). Average + standard deviation reported. Values reported as mean + standard deviation. In all cases, $p < 0.05$ is indicated by a single star and $p < 0.01$ by two stars. 99
5.3 Friction force $F_\parallel$ as a function of normal force $F_\perp$ between mica surfaces with adsorbed mimLub (A) and with physisorbed Fn layers with mimLub (B), both in PBS. The surfaces were sheared at sliding velocities of $V = 0.3\mu m/s$ (black circles), $V = 3\mu m/s$ (red triangles), and $V = 30\mu m/s$ (blue squares). Open symbols indicate measurements after the surfaces became damaged (with wear). . 101
5.4 Friction forces $F_\parallel$ as a function of the normal force $F_\perp$ between mica surfaces with adsorbed mimLub (A) and with physisorbed Fn layers with mimLub (B) in PBS with free mimLub ($C_{mimLub} = 3mg/ml$) in the solution. The surfaces were sheared at sliding velocities of $V = 0.3\mu m/s$ (black circles), $V = 3\mu m/s$ (red triangles), and $V = 30\mu m/s$ (blue squares). Open symbols indicate measurements after the surfaces became damaged (with wear). 102
5.5 Film thickness D measured as a function of normal force $F_\perp$ at sliding velocities of $V = 0.3\mu m/s$ (A-B) and $V = 30\mu m/s$ (C-D). . . 104
5.6 Experimental effective viscosity of the confined solutions between the surfaces. Results showing that the viscosity of the confined film is inversely proportional to sliding speed, without Fn (A) and with Fn (B) adsorbed to mica surfaces. 105

C.1 (A) Plot of 633 labeled LUB strain-dependent binding to Fn fibers using the relative intensity ratio (IR value) of Alexa-633 to Alexa-488 as a function of strain. (B) Image of 633 labeled Lub additive binding at 14% strain. Scale bar = 50μm. 134

C.2 (A) Plot of a 4 mg/ml solution of 105 kDa-5 kDa pAA-PEG polymer binding in a strain-dependent manner to Fn fibers. Measurements were done using the relative intensity ratio (IR value) of Alexa-594 to Alexa-488 as a function of strain. (B) Image of 594-labeled B-Lub polymer additive binding at 14% macroscopic strain. Scale bar = 50μm. 135

ACRONYMS

AdG Alexander-de Gennes

ASC Adipose stromal cells

BC Breast cancer

BSA Bovine serum albumin

CAF Cancer-associated fibroblasts

ECM Extracellular matrix

ESF Equine synovial fluid

FECO Fringes of equal chromatic order

Fn Fibronectin

FRET Förster Resonance Energy Transfer

GAG Glycosaminoglycans

GdnHCl Guanidine hydrochloride

HA Hyaluronan/hyaluronic acid

HEP Heparin

IL Interleukin

LS Lamina splendens

LUB Lubricin

MBI Multiple beam interferometry

MW Molecular weight

OA Osteoarthritis

PB Polymer brush

PBS phosphate buffered saline

PEX Homepexin

pFAK Phosphorylated focal adhesion kinase

PL Phospholipids

RGD Arginylglycylaspartic acid

SA Serum albumin

SF Synovial fluid

SFA Surface Forces Apparatus

SMB Somatomedin

TGF Transforming growth factor

VEGF Vascular endothelial growth factor

CHAPTER 1

SCOPE OF THE THESIS

In biology, there have been considerable efforts during the course of the last several decades to study fundamental problems outside the context of biochemistry. The understanding of pathological processes that were traditionally considered disruptions of purely biochemical signaling events, such as the binding of a molecule to a specific cell receptor, is changing. Currently, there is a paradigm shift from pure biochemical approaches to that cell and tissue function, and disease development can also be understood by the role of mechanical force. In trying to further understand cell and tissue function and disease development, researchers have bridged cell biology and biochemistry with various disciplines of science and engineering, including mechanics (*e.g.* solid mechanics and tribology) and materials science.

The main goal of this thesis is to address the role of fibronectin (Fn), a prominent protein present in many living organisms, in tumor development and joint lubrication, and further motivate its study by combining knowledge, collaboration and techniques beyond the aforementioned disciplines.

1.1 Research objectives

The overall research objectives of this thesis are to elucidate the relationship between Fn conformation and the mechanical properties of the extracellular matrix imposed by Fn's conformation and matrix topology, and to investigate the tribological roles of Fn in the context of tumor development and joint lubrication, respectively. The thesis has three sections, each containing a specific

objective.

1.1.1 Specific objective 1

The extracellular matrix (ECM) of living tissues is a dynamic environment that is constantly being remodeled by its resident cells. Dysregulated remodeling results in biomechanical and biochemical changes. In breast cancer, these processes are regulated by stromal cells, which are simultaneously controlled by intracrine, paracrine, or endocrine signaling. More specifically, paracrine signaling allows the tumorous environment to recruit neighboring cells to the growing malignant domain by altering cellular remodeling processes. The resulting ECM presents conformational and compositional changes. However, how stiffness directly correlates with conformational changes and further affects biological regulation (such as cell adhesion and pro-angiogenic secretion) has not been addressed.

In specific objective 1, we aim to test the hypothesis that Fn-ECM stiffness and conformation assembled by pre-adipocytes exposed to tumor soluble factors is dysregulated, altering cellular adhesion and secretion.

Decellularized ECMs composed of Fn and assembled by pre-adipocytes previously exposed to tumor soluble factors were indented quasi-statically with the surface forces apparatus (SFA) to determine matrix stiffness and matrix thickness. Control experiments where cells were not exposed to tumor soluble factors were performed and results compared. In parallel, exogenous FRET-labeled Fn was added during the cellular matrix assembly process to map Fn conformations within ECM fibers. Combined, both experiments allowed correlation of

matrix stiffness, matrix thicknesses and Fn conformation. A third experiment, where decellularized matrices were reseeded with unexposed pre-adipocytes, allowed determinations of alterations in cell adhesion and cell secretion (of vascular endothelial growth factors) in matrices assembled by exposed and unexposed pre-adipocytes. This aim focused on correlating Fn-ECM stiffness, topology, and biological function with Fn conformation across several length scales, from the cellular (via SFA) to the molecular (via FRET) scale.

1.1.2 Specific objective 2

Articular cartilage surfaces slide against each other very efficiently during the lifespan of a healthy person without inflicting damage. Such remarkable tribological properties have been attributed to the complex architecture of the cartilage ECM. In cartilage, internal pressurization provided by high water content trapped by glycosoaminoglycans and glycoproteins in the porous media dissipates energy, in combination with synergistic interactions of surface active proteins. Cartilage boundary lubrication research has focused on various surface active proteins, individually and synergystically, including collagen type II, hyaluronan (or hyaluronic acid)(HA), lubricin (LUB), phospholipids (PL), and serum albumin (SA), which are also present in the natural lubricant of joints, the synovial fluid (SF). Fn is another protein present in high amounts only in the superficial zone of cartilage. However, how Fn contributes to boundary joint lubrication is not known.

In specific objective 2, we aim to test the hypothesis that Fn interacts synergistically with SF components in order to provide low friction and wear protec-

tion of sliding surfaces.

Atomically smooth mica surfaces were saturated with physisrobed Fn, followed by incubation with one of three SF components known to play a role in joint lubrication, either LUB, HA, or SA. After incubation, samples were rinsed and tested in phosphate buffered saline (PBS). One set of experiments consisted of incubating Fn with equine SF (as extracted) for comparison. Normal force measurements using the SFA were performed for each condition to determine film behavior upon confinement. Additional experiments where incubated surfaces were sheared relative to each other, allowed determination of the coefficients of friction as well as the onset of damage at different shearing velocities. Efficient lubrication and wear protection were consistently observed for Fn incubated with LUB and with equine SF. Poor wear protection was consistently observed for Fn incubated with HA and with SA. This aim focused on ascertaining whether or not Fn is capable of tethering synovial fluid molecules, as an attempt to understand Fn's presence in the superficial zone of articular cartilage.

1.1.3 Specific objective 3

Articular cartilage surfaces, as stated previously, are capable of sliding very efficiently against each other as long as no cartilage surface damage is present. Cartilage injury can arise from aging or trauma, inducing changes in the cartilage ECM and modifying its tribological performance. One key signature of cartilage damage is a significant decrease in proteoglycan content. Among these proteoglycans is LUB, one of the molecules responsible for boundary lubrication. The decrease in LUB, and the already damaged cartilage surface yield in a poor sur-

face protection and inefficient wound healing process. For several decades, HA has been used to relieve pain in osteoarthritis (OA) patients, with poor results. As an alternative treatment, a mimetic LUB consisting of a polymer brush synthesized by our collaborators is being developed.

In specific objective 3, we aim to test the hypothesis that a mimetic polymer brush differentially alters boundary mode lubrication if it is physisorbed or soluble in the bulk lubricant in the presence or absence of Fn.

A mimetic LUB polymer consisting of a polyacrylic acid backbone and polyethylene glycol side chains was designed, synthesized, and characterized at the molecular scale, to determine molecular contour length, diameter, and weight. Normal and lateral (friction) force measurements of the polymer either physisorbed on mica or free floating in solution revealed that only a few polymer molecules remained trapped in the shearing junction upon pressure, leading to poor lubrication and no wear protection. A second experiment with Fn present revealed that the polymer remained firmly bound to the surfaces upon confinement, providing efficient lubrication and robust wear protection. This aim focused on identifying the ability of a mimetic LUB molecule to lubricate in the absence or presence of Fn.

1.2 General Conclusion

In our research, *in vitro* model systems were used to investigate the roles of Fn in (i) tumor development and in (ii) joint boundary lubrication. We first found that the early Fn matrix assembled by tumor-associated stromal cells was thicker, denser, and more unfolded than in the control case, resulting in signif-

icant ECM stiffening. Additionally, we showed that cells secrete more vascular endothelial growth factor when reseeded onto tumor-associated Fn matrices, most likely promoting vascularization and growth of the breast tumor. We then found that Fn (i) effectively tethers synovial fluid components to surfaces (with mica to model cartilage) providing good wear protection despite high friction coefficients; (ii) tethers LUB providing good wear protection with low friction coefficients; however, (iii) weakly tethers HA and SA and does not provide wear protection. Our results suggest that Fn function in the superficial zone of cartilage most likely promotes LUB binding to the cartilage surface. Finally, we found that the mimetic LUB remained bound to surfaces saturated with Fn, effectively modifying friction coefficients and delaying onset the of wear.

CHAPTER 2

GENERAL BACKGROUND

Breast cancer (BC) [Bissell and Hines, 2011] and osteoarthritis (OA) [Chevalier, 1993] are characterized by progressive changes in the composition of the ECM. The ECM consists of a network of proteins assembled by cells that provides structural support as well as biochemical and biomechanical cues. This network finely regulates cellular behavior such as adhesion, differentiation, and proliferation [Cox and Erler, 2011, Ingber, 2003] and assembly of ECM components [Singh et al., 2010]. When the conformation and ratio of the ECM proteins change [Rhee et al., 2005, Lu et al., 2012, Martino et al., 2011], this leads to alterations of both the biomechanical [Kempson, 1982, Assoian and Klein, 2008] and biochemical [López-Otín and Diamandis, 1998] properties of healthy tissue. A prominent component of the ECM is Fn. Fn is a crucial glycoprotein in several biological processes, including embryogenesis and wound healing. Fn is also involved in tumorigenesis and in diarthoidal joint lubrication. Therefore, understanding the role of Fn in biological processes such as tumor development or joint lubrication is crucial for obtaining further insight into the development and evolution of such diseases.

This chapter presents a general background for understanding the study of Fn and its role in BC development and joint lubrication. The chapter begins by introducing the ECM, followed by Fn. Next, the tissues of interest for the present work are introduced - breast tissue and articular cartilage - with their functions and pathologies. I then shortly describe polymer brushes (PB), which are explored here as a biomimetic alternative to joint treatments such as OA. In the final section, I give a brief and by no means complete introduction to our

main analysis tools: the surface forces apparatus (SFA) and Förster resonance energy transfer (FRET).

2.1 Extracellular matrix

The ECM of living tissues is a complex and highly dynamic fibrillar microenvironment that tightly regulates cellular behavior such as adhesion, differentiation, migration [Cox and Erler, 2011, Ingber, 2003], and self-assembly of ECM components [Singh et al., 2010]. The ECM is comprised of a variety of proteins, glycoproteins, and proteoglycans that provide not only structural support but also biomechanical and biochemical signals to cells [Kempson, 1982, Assoian and Klein, 2008, López-Otín and Diamandis, 1998, Engler et al., 2006]. Depending on tissue, age, and disease, the architecture and composition of the ECM vary. For example, BC [Bissell and Hines, 2011] and OA [Chevalier, 1993] are characterized by progressive changes in the composition of the ECM. These changes in the connective tissue have been connected with proteglycans and collagen content [Rhee et al., 2005, Lu et al., 2012, Martino et al., 2011] and lead to alterations of both biomechanical [Kempson, 1982, Assoian and Klein, 2008] and biochemical [López-Otín and Diamandis, 1998] properties of healthy tissue. One particular protein of the ECM, Fn (see Fig. 2.1), has shown crucial matrix assembly and cellular regulating properties. Additionally, Fn has been found to be dysregulated in BC [Chandler et al., 2011] and OA [Chevalier, 1993, Sofat et al., 2012]. Given that the composition, material properties, and function of the ECM vary drastically from physiological to pathological conditions, a more detailed background on breast tissue and articular cartilage is presented bellow (sections 2.3 and 2.4).

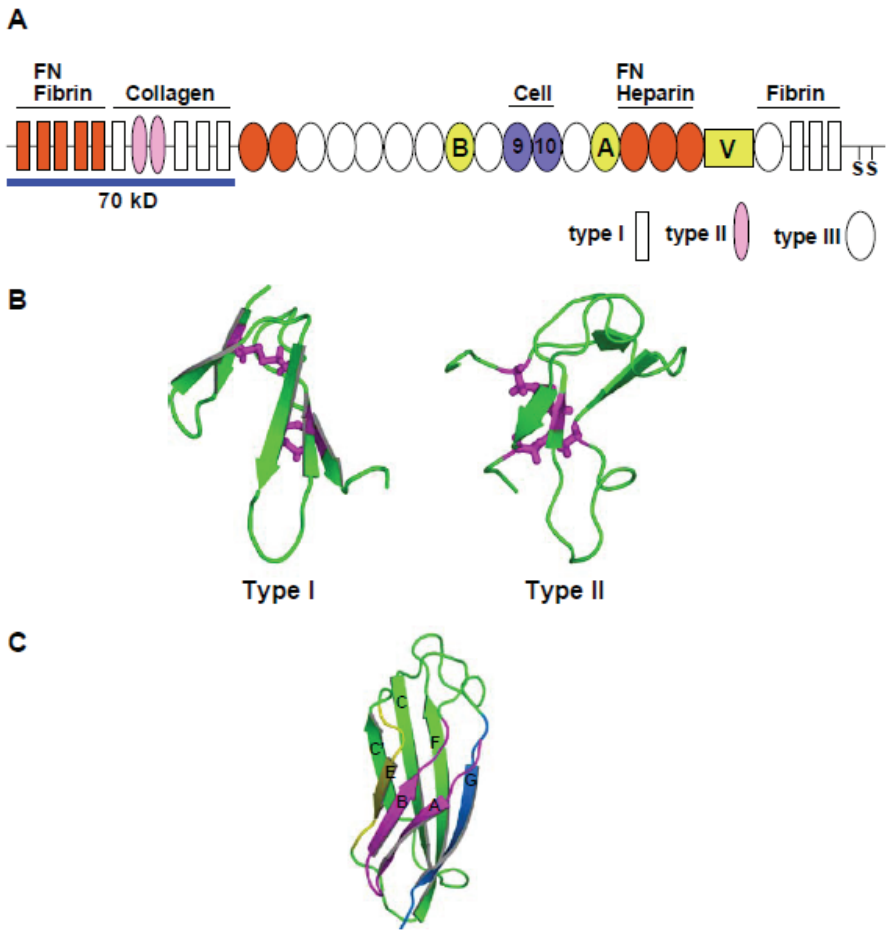

Figure 2.1: Modular structure of a Fn monomer. (A) Fn type I modules (rectangles), type II modules (violet ovals), and type III modules (ovals). The alternative spliced domains in yellow. Assembly and binding domains indicated along the Fn monomer. (B) Modules type I and II showing the pair of disulfide bonds in purple. (C) Module type III with its stacked β-strands. Fig. from [Mao and Schwarzbauer, 2005]

2.2 Fibronectin

Fn is a large dimer with monomers (Fig. 2.1) 230-270 kDa in size composed of three types of repeating modules, denominated type I, II, and III. Type I and II modules contain piled β-sheets stabilized by a pair of disulfide bonds [Potts and Campbell, 1996, Pickford et al., 1997]. Type III modules, however,

lack disulfide bonds and hide cryptic/buried binding sites [Leahy et al., 1996, Dickinson et al., 1994], making them more sensible to structural changes such as β-sheet unraveling due to external tensile forces, including cellular traction forces [Smith et al., 2007, Singh et al., 2010].

Fn can be found in a soluble inactive form (plasma Fn) as well as in an insoluble active form, which consists of elastic polymerized fibrils formed by integrin mediated forces [Geiger, 2001, Mao and Schwarzbauer, 2005]. Neither Fn fibrillogenesis nor the arrangement/conformation of Fn molecules within fibers are fully understood, but important self-association interactions (domain dependent) have been identified. These self-association domains contain binding sites for matrix proteins, such as collagen, fibrin, and itself [Pankov, 2002]. Fn also contains sites for cell receptors, such as integrins. Some of Fn's binding sites are cryptic, or hidden when the molecule is in its equilibrium (folded) form. These cryptic sites may become exposed when Fn conformation changes to a more extended or unfolded state [Vogel, 2006], altering its function in a conformation-dependent manner.

Integrins function as transmembrane cellular receptors to interact with other cells or the ECM. Currently, it is known that integrin signaling and downstream cell behavior can be affected by altering Fn module's spacing and orientation, thereby changing its recognition sites [Grant et al., 1997, Altroff et al., 2003]. This can be achieved by inserting peptide spacers. A similar situation results upon mechanical strain, which, for example, changes the distance and orientation of the RGD loop located on Fn-III_{10} and PHSRN "synergy" site on Fn-III_9 [Grant et al., 1997, Altroff et al., 2003]. Spatial alterations decrease Fn's affinity for specific integrins, such as $\alpha_5\beta_1$ [Mott and Werb, 2004], which

binds to both domains simultaneously. Contrary to $\alpha_5\beta_1$, another integrin, $\alpha_v\beta_3$, binds only to Fn-III$_{10}$, and seems to be insensitive to Fn conformational changes. These changes in integrin affinity have a direct impact in cell life cycle, *i.e.* adhesion, differentiation, proliferation, secretion and/or apoptosis [Wan et al., 2013, Levental et al., 2009, Obara et al., 1988].

2.3 Breast tissue and breast cancer

Breast tissue consists primarily of soft matter containing connective tissue cells (stromal cells) and energy reservoir cells (adipocytes), termed ASCs. ACSs include fibroblasts, endothelial cells, and immune cells such as macrophages. Adipose tissue has been mainly considered an energy reservoir, however, it also plays a role in morphogenesis. This morphogenic characteristic arises from the synthesis of benign or inflammatory morphogens, such as TGF-β, ILIL-6,IL-8 cytokines, among others.

The breast tissue hosts the mammary gland, which is separated by the mammary gland epithelium from the mammary adipose tissue [Cinti, 2012]. The mammary gland epithelium plays a critical role in mammary gland formation, due to its highly organized and stratified cellular layers. A complex organization arises from a delicate balance of ECM derived physico-chemical signals that instruct epithelial and stromal cells on how to assemble the functional mammary gland. During this process, ECM assembly is mediated by TGF-β, promoting epithelial cell growth and branching [Robinson et al., 1991, Sakai et al., 2003]. Additionally, when the mammary gland activity changes (involution), mammary adipose tissue is fully remodeled by both stimulating

epithelial cell apoptosis, but also conserving the stem cell niche for recovery [Robinson et al., 1991]. Both processes, deconstruction and reconstruction of the adipose stroma, are in a delicate homeostasis. Imbalance between them can lead to tumorigenesis.

Currently, BC is one of the leading threats to women's health worldwide [Polyak, 2007]. It is characterized by mutation of mammary epithelial cells due to various factors, including ageing, obesity, and genetic mutations, among others [Polyak, 2007]. The mentioned risk factors play important roles in determining a favorable tumorigenic microenvironment which regulates tumor malignancy [Sørlie et al., 2006]. The tumorigenic microenvironment is highly dynamic during various stages of tumor progression. Each stage is regulated by specific processes, which can be identified by their unique signatures. These signatures are defined as hallmarks of cancer, and consist of growth stimulation, resistance to inhibitory signals, apoptosis resistance, angiogenesis stimulation, unlimited replicability, and local tissue invasion [Bissell and Radisky, 2001]. All processes occur in parallel, influence each other, and require participation of tumor-associated and host stromal cells, giving rise to the possibility of an endless brail.

One well known hallmark of cancer commonly used in diagnosis is tumor stiffness. The fibrotic process that culminates as a rigid lump originates from abnormal growth of cancerous epithelial cells. Abnormal growth creates an oxygen deprived environment that results in hypoxia, stimulating chronic inflammation. Inflammatory morphogens recruit inflammatory cells into the tumor, which in turn secrete paracrine factors that activate surrounding cells, some of which are fibroblasts. These surrounding fibroblasts consequently participate

in fibrotic reactions. Fibrotic reactions densify the tissue by up-regulating ECM protein deposition. However, tumor stiffness is not just a passive outcome of tumorigenesis, but in turn actively promotes tumor progression by stimulating cancer cell growth as well as promoting some of the key processes, such as angiogenesis [Caino et al., 2013, Pollard, 2004, Park et al., 2011].

As previously described, the tumorous microenvironment is very dynamic and actively promotes tumor progression. This is achieved by a continuous change in tissue structure that facilitates and enhances tumor growth. The recruitment of cancer-associated fibroblasts CAFs marks the initiation of desmoplasia, the deposition of fibrotic tissue. Recruited CAFs deposit abundant amounts of fibrillar ECM molecules which include collagen I and Fn [De Wever et al., 2008]. These dysregulations in ECM composition create structural and mechanical alterations [Egeblad et al., 2010, Cox and Erler, 2011, Butcher et al., 2009]. In addition to deposition, CAFs control the partial unfolding of Fn [Chandler et al., 2011]. This, in turn, likely increases the stiffness of Fn fibers in the matrix, although it has not yet been measured [Chandler et al., 2011, Klotzsch et al., 2009]. The partial unfolding accompanied by stiffening consequently alters Fn ability to bind to other ECM molecules, such as glycosaminoglycans (GAGs), collagen and even itself [Tomasek et al., 2002].

Fn is not only extensively upregulated in tumors but it is also present in a more unfolded conformation, which further promotes tumor growth, angiogenesis and invasion [Chandler et al., 2011, Akiyama et al., 1995]. For example, the presence of unfolded Fn influences cell-matrix interactions by disrupting the distance and orientation of the RGD loop and PHSRN "synergy" site [Grant et al., 1997, Altroff et al., 2003], forcing cells to utilize $\alpha_v\beta_3$ and favor-

ing over-secretion of vascular endothelial growth factor (VEGF) [De et al., 2005, Wan et al., 2013]. VEGF is used by the tumor microenvironment for the formation of new blood vessels (angiogenesis). Additionally, unfolded Fn influences collagen assembly orientation and quantity [Kadler et al., 2008], as manifested in desmoplasia and fibrosis. As a result, the microenvironment provided by a dysregulated ECM is perceived differently by the surrounding cells. In order to identify and understand the pathology of diseases such as cancer, it becomes fundamental to study the effects that conformational changes bring to the tumorous microenvironment and compare with healthy conditions.

2.4 Articular cartilage and osteoarthritis

Articular cartilage acts as the natural bearing of diarthroidal joints, covering the ends of articulating bones, and efficiently supporting normal and shear forces over the lifespan of a healthy person [Mow et al., 1993]. Cartilage consists of a complex heterogeneous and heavily stratified ECM built and maintained by specific cells, called chondrocytes. Cartilage consists of an intricate network of mostly collagen and highly hydrated proteoglycans.

Chondrocytes in cartilage comprise about 2% in volume in adults [Hunziker, 2010], which produce and maintain the ECM. The ECM is approximately 90% of the tissue dry weight. The main chemical components of cartilage are water (80%), collagen (50% to 75%), proteoglycans (15% to 30%), and PL, which comprises up to 10% of the dry weight [Loret and Simões, 2004]. Proteoglycans are made up of a large core protein with covalently attached sulfated glycosaminoglycan (GAG) chains. Another fundamental protein of the extra-

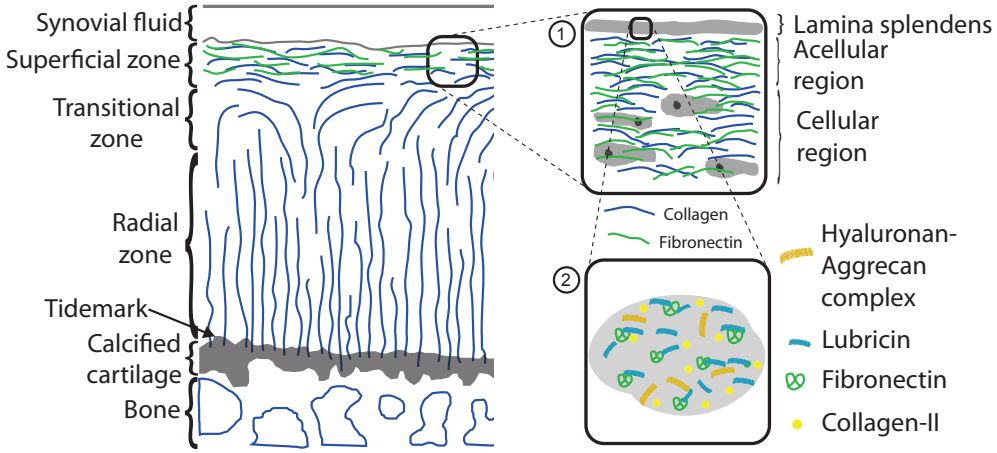

Figure 2.2: Schematic illustration of articular cartilage showing the collagen orientation in different zones. Inset 1 shows the superficial zone of cartilage. Inset 2 depicts the lamina splendens. Fig. adapted from [Dedinaite, 2012]

cellular matrix of cartilagenous tissues is aggrecan. Aggrecan attaches non-covalently but strongly to HA, and the association is strengthened by a link protein. These aggrecan-HA compelxes have been associated with important biological lubrication systems [Horkay et al., 2008]. Collagen fibers, mostly type II, are cross-linked by collagen type IX [Eyre et al., 2004], forming a collagen network that encloses hydrated proteoglycan gels with an internal pressure of 0.2 to 0.3 MPa [Hunziker, 2010].

The superficial zone of cartilage (Fig. 2.2) consists of collagen layers tangential to the sliding direction. It is acellular and is covered by the lamina splendens [M.A. MacConail, 1951], a gel that constitutes the interface with the SF [Jurvelin et al., 1996]. This gel's composition varies from the rest of the cartilage. It lacks collagen fibrils [Jeffery et al., 1991] and Fn and LUB, a boundary lubricating glycoprotein, are present in high amounts [Balazs, 2009]. Interestingly, the lamina splendens is formed in situ under shear by the confined

SF. The lamina splendens is not affected by any mechanical or physicochemical removal process, since it is reformed under the action of shear. However, it is extremely sensitive to any chemical or genetic degradation of the SF [Krishnan et al., 2004, Jay et al., 2007, Coles et al., 2010]. This leads to the question of whether or not the LS plays a major role in degenerative diseases, such as OA.

OA is a degenerative disease associated with increased wear of the cartilage, and it is one of the most frequent and rapidly growing causes of permanent disability across the world, affecting more than 40 million people in the United States alone [Morrell et al., 2005]. In OA, the composition of the ECM changes over the lifespan of a person, depending on age, injury and disease, resulting in cartilage biomechanical and biochemical alterations.

A key signature of cartilage aging is the decrease in molecular weight (MW) of proteoglycans and GAG chains [Martin and Buckwalter, 2002], accompanied by a decrease in chondrocyte biosynthetic activity [Martin et al., 1997]. Partially due to the aforementioned causes, dysregulation in enzymatic and non-enzymatic homeostasis in the crosslinking process of collagen increases cartilage imbalance [Bailey, 2001]. Another cartilage ECM dysregulation mechanism is trauma, which induces disruption of the collagen matrix and significant proteoglycan loss at the site of injury. Generated fissures in the cartilage surface enhance collagen fibrillar formation and increase Fn synthesis and deposition [Chevalier, 1993]. These changes due to age and injury lead to the deterioration of mechanical properties and a predisposition to develop OA.

2.4.1 Synovial fluid

SF is the natural thick and viscous lubricant of joints, and has long been believed to be responsible for remarkable joint lubrication. It is composed of a mixture of specialized components including LUB [Radin et al., 1970], Fn [Balazs, 2009], PL [Hills, 2002, Hills and Crawford, 2003], HA [Balazs, 2009], SA [Fan et al., 2012] and GAGs. SF's main components, *i.e.* LUB and HA, are described next.

Lubricin and boundary lubrication

LUB is a glycoprotein present in SF, and is believed to lubricate and protect the cartilage surfaces in boundary lubrication, preventing cartilage-cartilage contact, and thus, wear [Schaefer et al., 2004]. In boundary lubrication mode, lubrication and wear are governed by the interacting surface properties. It is a condition, condition in which surface separation is usually smaller than the average surface roughness [Bhushan, 2013]. Like any other efficient boundary lubricant, LUB is capable of binding to the cartilage surface. Apart from providing extremely low friction coefficients, LUB also protects the cartilage surfaces from excessive protein adsorption and cell overgrowth, being both a causes of joint failure diseases [Rhee et al., 2005]. LUB is a structureless flexible high MW molecule, of the order of 230 kDa, and it has an extended length of 210 nm. This molecule, represented in Fig. 2.3, is composed of a large heavily glycosylated central domain, carrying negative charges and heavily hydrated in an aqueous environment; it also has two end-domains that are not glycosylated, carrying positive charges [Zappone et al., 2007]. The two end-domains, the somatomedin (SMBSMB), heparin (HEP) and homepexin (PEX)-like domains are

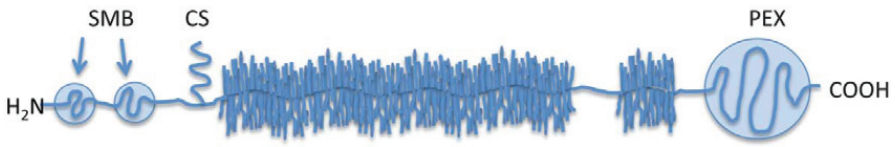

Figure 2.3: LUB consists of a long heavily glycosylated, mucinous domain separating two SMB domains at the N-terminus and a haemopexin region at the C-terminus. The mucinous domain consists of a polypeptide backbone with the main amino acids being threonine, glutamic acid, proline and lysine. Carbohydrates constitute about 40% (w/w) of LUB with the main residues being galactosamine, galactose, and N-acetylneuraminic acid. Thus, LUB molecules carry a considerable number of anionic side chains and the mucinous part of the molecule has a bottle-brush structure. LUB is associated with phospholipid components that comprise about 10% by weight. Taken from [Dedinaite, 2012].

of special interest, since they are known to play specific roles in cell-cell and cell-ECM interactions [Jones et al., 2007, Jay, 2004].

As previously described, boundary lubrication takes place when the lubricating film thickness is less than the asperity height of the interacting surfaces [Bhushan, 2013]. As opposed to boundary lubrication, hydrodynamic lubrication takes place when friction coefficients and wear are governed by the viscosity of a lubricating liquid film that fully separates the interacting surfaces [Bhushan, 2013]. The transition from boundary lubrication to hydrodynamic lubrication is known as mixed lubrication, and the lubricating liquid film thickness is on the order of the surface roughness [Bhushan, 2013].

Hyaluronan

HA, one of the main glycoproteins present in SF and connective tissues, is found in many different concentrations, depending on location, age, and species. A concentration of 3.5 mg/ml is normally found in a regular adult knee [Tadmor et al., 2002a]. HA is a large (circa 20 times bigger than LUB), negatively charged and unbranched glycosaminoglycan (specialized glycoprotein with polysaccharide side-chains), with a high MW, ranging from 6-7 MDa for healthy to 3-5 MDa for rheumatoidal fluid [Dahl et al., 1985], with a polymer length $\approx$2 μm [Mow et al., 1984, Toole, 2004]. It also possesses a hydrophilic region due to the presence of carboxyl groups. A number of specific functions like lubrication, macromolecular filtering, cartilage surfaces protection, water homeostasis, selective binding of proteins (known cell-surface receptors) have been attributed to HA [Laurent et al., 1996]. Over the last few decades, HA has been thought to be responsible for the ultra low friction and wear rates in articular joints, although Radin *et al.* questioned this claim [Radin et al., 1970]. Despite controversy about whether HA acts as an effective boundary lubricant or not, it has been used for the treatment of degenerative joint diseases and total or partial joint replacements [Kirchner and Marshall, 2006], providing temporary pain relief for patients. A schematic of a HA molecule is shown in Fig. 2.4.

2.5 Polymer brushes

Chapter 5 of this thesis deals with PB, used as an attempt to mimic the biological architecture and function of native LUB. PB have potential as a therapeutic approach for joint diseases, *i.e.* OA.

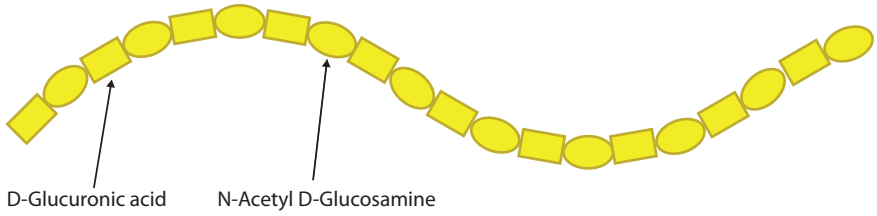

Figure 2.4: HA is a linear high molecular weight polysaccharide, consisting of repeating disaccharide units of D-glucuronic acid and N-acetyl D-glucosamine. At physiological pH, HA carries a high negative charge.

PBs have been proposed to be responsible for efficient lubrication in biological tribosystems subjected to low external pressures [Raviv et al., 2003, Gourdon et al., 2008]. Examples include the eye or the respiratory system, mediating not only low friction, but also permeability and/or bacteria and dust adhesion. PB generally consist of a dense array of polymer chains (neutral or charged) endgrafted to a surface. The vicinity between adjacent polymer chains forces the chains to stretch and extend perpendicularly to the supporting substrate, resulting in a dense robust array covering the surface [Brittain and Minko, 2007]. To control the formation of dense brushes, specific conditions have to be fulfilled, *i.e.* a complex balance between MW, surface density, quality of solvent, and charge distribution, among others. Instead of brushes, the polymer chains may also adopt less desirable conformations, such as pancake or mushroom, leading to weaker stability and non functional properties of the coatings. Among the controlled properties achieved by brushes are wettability, adhesion and lubricity [Klein et al., 1993, Brittain and Minko, 2007]. The ability to easily manipulate these properties makes brushes smart surfaces that have attracted attention for applications in biosensors, tissue engineering, drug delivery and lubricants [Dong et al., 2009]. An increasing number of groups have been clarifying the main parameters governing the tribological be-

havior of PB coated surfaces [Zappone et al., 2008, Liberelle and Giasson, 2008, Chen et al., 2009, Hartung et al., 2008, Kampf et al., 2004]. It is well established that under low loads, almost any pair of polymer coated surfaces will slide with low friction coefficients, μ = 0.01 [Raviv et al., 2003, Liberelle and Giasson, 2008]. An extreme case has been found to be of the order of μ = 0.001 [Raviv et al., 2003] when end-grafted charged polymers were sheared at low pressure (0.5 MPa), across very small distances (0.7 μm).

PB appear to be efficient for modifying surface properties, and thus for controlling tribological behavior of shearing junctions. However, controlling the coverage density of brushes and their attachment to surfaces has been of great concern, especially in resisting high pressures and large distances sheared, such as in hip or knee joints. Highly packed synthetic PB have been used to successfully lubricate artificial joints at low pressures [Hartung et al., 2008].

2.6 A unique experimental technique: the surface forces apparatus

A key technique used throughout this thesis is the SFA. The SFA technique was developed in the 1970's to measure the normal and friction forces on the molecular and atomic scale on a wide variety of systems, such as colloids, amorphous polymers, and metals [Israelachvili, 1973, Israelachvili and McGuiggan, 1990]. Two cylindrical silica lenses of radius R (typically between 1 and 2 cm), wearing a thin sheet of back-silvered and atomically smooth mica, face each other and are used as preliminary surfaces. These surfaces can be modified before being mounted into the SFA. The surfaces separation, D, is obtained by multiple

beam interferometry (MBI), together with surface shape, contact radius, contact area and refractive index in both static and dynamic conditions. Normal and friction forces are measured with a double cantilever spring while shearing is done with a piezoelectric bimorph slider allowing large displacements. Three enormous advantages of the direct visualization of the contact region with MIB using fringes of equal chromatic order (FECO) are: i) the contact area is measured rather than calculated, and ii) any damage to the surfaces can be easily detected, as well as undesirable particles/contaminants, and iii) SFA junction covers the micron (cellular) scale, while the normal (film thickness) is extremely accurate covering the nanometer scale.

2.7 Fibronectin molecular conformation via Förster resonance energy transfer

Another very important technique for the studies presented in this thesis is Förster resonance energy transfer (FRET) technique, which enables the mapping of the molecular conformations. FRET relies upon a phenomenom where an excited donor chromophore transfers energy by a non-radiative, dipole-dipole interacting mechanism to an acceptor chromophore. The efficiency of the energy transfer is inversely proportional to the sixth power of the distance between both chromophores, making it very sensitive to small changes in distance, typically less than 10 nm. The efficiency of energy transfer depends on i) the relative orientation of the donor emission dipole moment and the acceptor absorption dipole moment, ii) the spectral overlap between donor emission and acceptor absorption spectrum, and iii) the distance between the center of both

chromophores. The FRET energy transfer can be described by:

$$E_T = \frac{1}{1 + \left(\frac{r}{R_0}\right)^6} \tag{2.1}$$

where E_T is the efficiency of energy transfer, r is the distance between the center of the two chromophores, and R_0 is the Förster distance between the two, *i.e.* where E_T is 50%.

CHAPTER 3

STIFFENING AND UNFOLDING OF FIBRONECTIN INCREASE PROANGIOGENIC FACTOR SECRETION BY BREAST CANCER-ASSOCIATED STROMAL CELLS

The work presented in this chapter has been submitted: **Roberto C. Andresen Eguiluz**, Karin C. Wang, Fei Wu, BoRi Seo, Claudia Fischbach, and Delphine Gourdon. Author contributions: R.C.A.E., K.C.W., C.F. and D.G. designed research; R.C.A.E., K.C.W., and F.W. performed research; R.C.A.E., K.C.W., F.W. and B.R.S. contributed new reagents/analytic tools; R.C.A.E., K.C.W. and D.G. analyzed data; and R.C.A.E., K.C.W., C.F., and D.G. wrote the paper.

3.1 Abstract

Fibronectin (Fn) forms a fibrillar network that controls not only physiological cell behaviors such as early tissue development and wound healing, but also the progression of diseases including cancer. Indeed, breast cancer-associated stromal cells upregulate the quantity of deposited Fn and modify Fn conformation by increasing fibrillar stretching. However, (i) the interplay between structural and mechanical properties of the tumor-associated Fn network and (ii) its effect on tumor vascularization remain unclear. Here, we used the Surface Forces Apparatus to quantify the stiffness of cell-free Fn matrices deposited by control and tumor associated 3T3-L1 preadipocytes that were obtained by preconditioning with tumor-derived soluble factors. Our results reveal that tumor-associated cells promote matrix stiffening and thickening relative to control cells. The stiffening of these tumor-associated Fn matrices was then shown to correlate with increased molecular unfolding in Fn fibers, as determined by Foerster Res-

onance Energy Transfer. Finally, changes in cell adhesion and proangiogenic capability of newly seeded 3T3-L1s were assessed via cell counting and quantification of vascular endothelial growth factor (VEGF) secretion, respectively. Additionally, α_v and β_1 integrin-blocking antibodies were utilized to examine altered integrin specificity as a potential mechanism of modified cell-matrix signaling. Our findings indicate that tumor associated Fn decreases adhesion while enhancing VEGF secretion by breast cancer associated stromal cells, and that altered integrin specificity is likely responsible for such changes. Collectively, our data suggest that simultaneous stiffening and unfolding of tumor associated Fn alters both the adhesion and the proangiogenic behavior of surrounding stromal cells.

Keywords: fibronectin, surface forces apparatus (SFA), foerster resonance energy transfer (FRET), tumor angiogenesis

3.2 Significance

We have combined a set of physical sciences tools with cancer biology to: (i) characterize structural and mechanical properties of tumor-associated matrices at both the molecular and matrix/cellular scales, and (ii) correlate those properties with stromal cell behavior. Our findings indicate that the early matrix assembled by tumor-associated stromal cells is thicker, denser, and more unfolded than control matrices, resulting in significant stiffening. Additionally, cells secrete more vascular endothelial growth factor when reseeded onto these tumor-associated matrices, likely promoting vascularization and growth of the breast tumor. These results have important implications for our under-

standing of tumor development and vascularization, and enhance our knowledge of cell-matrix mechanobiological interactions that may be exploited for other biomaterials-based applications including advanced tissue engineering approaches.

3.3 Introduction

Varied physicochemical properties of the extracellular matrix (ECM), a dynamic and complex fibrillar network, modulate cellular behavior. In tumors, the ECM is primarily generated by cancer-associated cells (e.g. fibroblasts and adipogenic precursors) and contributes to sustained tumor growth and survival [Spaeth et al., 2009, Mishra et al., 2008, Karnoub et al., 2007, Chandler et al., 2012, Butcher et al., 2009, Paszek et al., 2005, Kumar and Weaver, 2009, Lu et al., 2012]. It exhibits numerous altered materials properties relative to normal ECM including variations in protein composition, structure, and rigidity. In fact, analysis of tumorous ECMs revealed differences in collagen I deposition relative to normal ECMs as suggested by elevated quantities, crosslinking, and stiffness of collagen [Chandler et al., 2012, Levental et al., 2009]. Moreover, fibronectin (Fn) might be responsible for additional ECM structural alterations, as indicated by the presence of highly stretched and unfolded Fn fibers in tumor-associated matrices [Chandler et al., 2011]. It is important to recognize that tumor-associated Fn and collagen alterations are functionally linked since Fn (i) is essential for the deposition of collagen I in ECMs [Midwood et al., 2004, Sottile and Hocking, 2002, Anderson, 2001] and (ii) is also used as an indicator for increased tumor aggressiveness [Zhang et al., 2004]. Nevertheless, a clear correlation between struc-

tural, conformational, and mechanical properties of the tumorous ECM network and the role of Fn in this process has not been established. This correlation has been hindered partly by the intrinsic complex composition of the ECM, and by the lack of analytical tools that permit simultaneous assessment of ECM materials properties from the matrix/cellular scale to the molecular scale. Indeed, both collagen and Fn fibers are present in mature ECM and likely synergize to modulate the bulk properties of the tumor ECM [Sottile and Hocking, 2002, Curran and Keely, 2013]. Additionally, there is a lack of materials science tools to separately assess morphology and mechanics of native (uncrosslinked) ECM at both matrix/cellular and molecular scales under physiologically relevant conditions.

Altered materials properties of the tumor ECM are clinically relevant as they promote tumor malignancy via direct effects on tumor cells [Paszek et al., 2005] and indirectly by enhancing the formation of new blood vessels (angiogenesis) [Fischbach et al., 2009, Calvo et al., 2013]. In fact, altered ECMs can enhance angiogenesis either by increasing the activity of surrounding endothelial cells [Mammoto et al., 2009] or by stimulating the secretion of pro-angiogenic factors (e.g. vascular endothelial growth factor (VEGF)) from cancer-associated fibroblasts [Chandler et al., 2012]. However, the specific ECM properties and associated mechanisms responsible for the pro-angiogenic capability of tumor-associated cells remain unclear.

Here, we integrated a set of physical sciences tools with cancer biology to: (i) characterize the mechanics, conformation, and topology of tumor-associated Fn matrices at both the matrix and molecular scales, and (ii) correlate these materials properties with adhesion and pro-angiogenic factor (VEGF) secretion of

adipose stromal cells. Our results revealed that tumor-conditioned Fn matrices were stiffer and more unfolded than control matrices, and that these dysregulated matrices contributed to enhanced VEGF secretion by stromal cells.

3.4 Results

3.4.1 Tumor-conditioned cells promote matrix stiffening through altered Fn assembly

To evaluate if tumor cell-secreted factors alter ECM deposition by adipose stromal cells, a major cell type in the mammary microenvironment, we first used the Surface Forces Apparatus (SFA) to assess the overall rigidity of matrices deposited by tumor-associated and control 3T3-L1 preadipocytes. (See Fig. 3.1 and SI Fig. 3.8). The SFA allows one to run compressive tests by determining the absolute distance D between two semi-reflecting smooth mica surfaces mounted on silica discs (Fig. 3.1A) using interferometric fringes patterns (Fig. 3.1B) while applying normal forces $F_{\perp}$ via a double cantilever spring [Israelachvili, 1973, Israelachvili and McGuiggan, 1990]. Briefly, tumor-associated and control 3T3-L1 cells were seeded onto the lower SFA mica disk in Fn-containing medium for 24 hours (Fig. 3.1C) and later removed with decellularization buffer, leaving behind a cell-free fibrillar ECM comprising Fn fibers (Fig. 3.1D, SI Fig. 3.5A). Compressive measurements over areas ≈20 - 30 μm in diameter (length scale of a cell) were then performed in the quasistatic regime via the upper SFA (bare) mica disk and force-distance profiles were acquired (Fig. 13.1E). Data were further analyzed to extract elastic moduli using Johnson

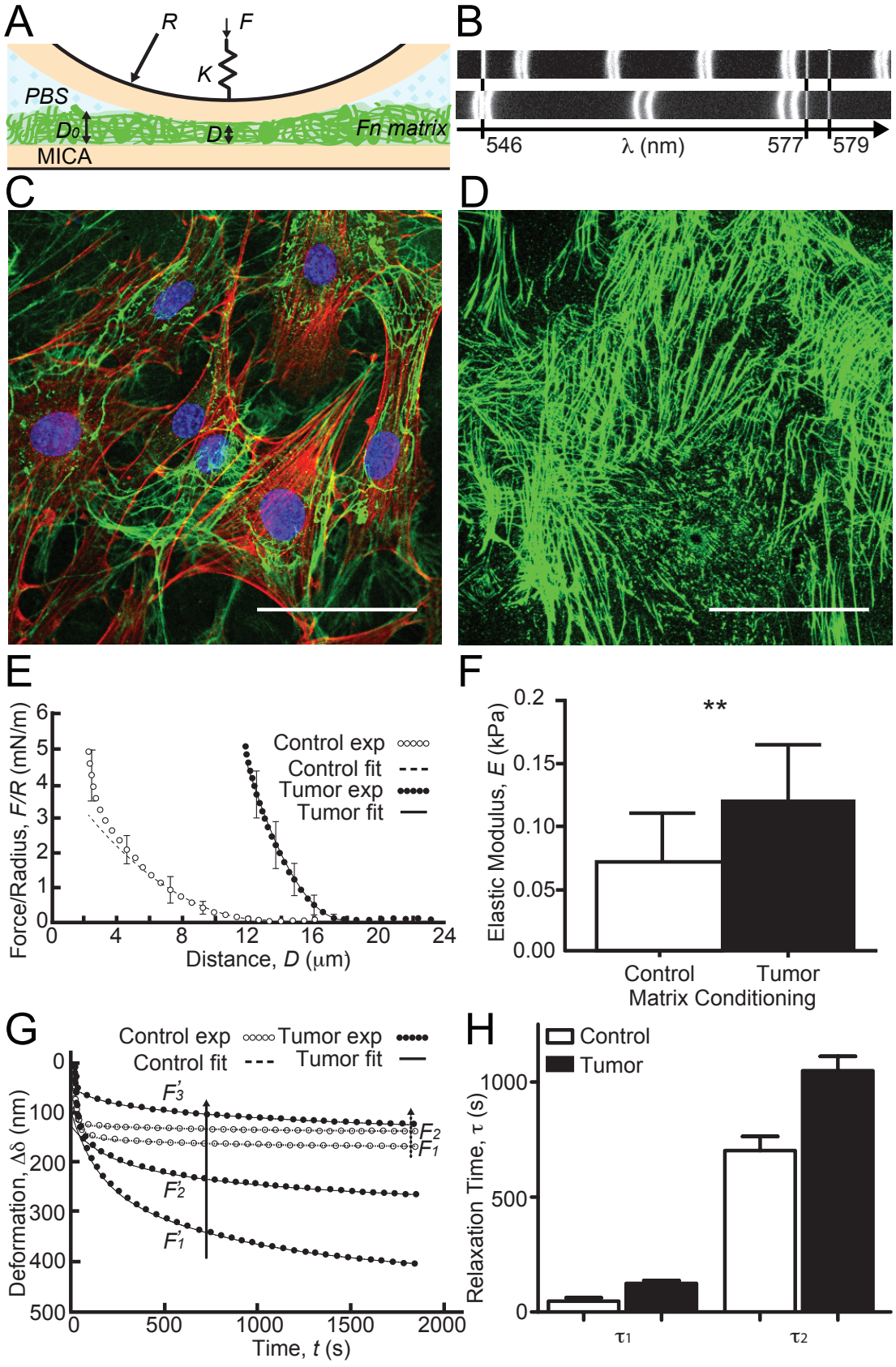

Figure 3.1: Caption in next page.

Figure 3.1: Tumor-associated Fn matrices are stiffer and more viscous. (A) Schematics of the Surface Forces Apparatus (SFA) mica surfaces and the setup used for mechanical characterization of the matrices at 37°C. (B) Interference fringes measured with the SFA when shining white light through the confining surfaces at large (uncompressed matrix) and small (compressed matrix) separations. (C) Immunostaining of tumor-conditioned stromal cells embedded in their ECM after 24 hours of culture onto SFA mica surfaces (green, Fn; red, F-actin; and blue, nuclei). (D) Same as (C) after decellularization (cell extraction) showing the Fn matrix left behind. Scale bars = 50 μm. (E) To determine Fn matrix stiffness, compressive force-distance profiles were acquired in quasi-static conditions in control (○) and tumor-associated (●) conditions and fitted using a Hertzian model. (F) Mean tumorassociated matrix elastic moduli (n = 18) were ≈60% higher than those of control matrices (n = 20). (G) The viscoelastic behavior of both control (○) and tumor-associated (●) Fn matrices was next quantified through creep experiments by monitoring matrix relaxation after rapid (instantaneous) force application. All relaxation data were well fitted using a double exponential decay to extract fast (τ_1) and slow (τ_2) characteristic times. (H) There was an overall slower response (hence higher viscosity) of tumor-conditioned matrices (n = 3) compared to that of control matrices (n = 2). Mean ± SD.

contact mechanics [Johnson, 1985], in which the indentation of the matrix under compression δ is related to the normal force $F_\perp$ by the following equation:

$$\frac{F_\perp}{R} = E\pi\frac{\delta^2}{D_0} \tag{3.1}$$

where R is the radius of curvature of the discs, D_0 is the matrix thickness at rest, and E the resulting Young modulus. Elastic moduli were calculated over a 25% strain range (Fig. 3.1F) and force normalized by radius of curvature ($F_\perp/R$) plotted as a function of thickness parameter δ^2/D_0 was used as control for the fit quality (SI, Fig. 3.5B). We found that the mean elastic moduli of fresh tumor-

associated ECM were significantly higher than those of control matrices (E = 0.12 ± 0.04 vs. 0.07 ± 0.03 kPa, $p < 0.001$).

We have also tested the effect of *in situ* chemical fixation (with neutral buffered formalin) on ECM rigidity and found it increased the stiffness of both tumor-associated and control matrices by 22% and 19%, respectively (E = 0.14 ± 0.06 vs. 0.09 ± 0.05 kPa, $p < 0.002$) (SI, Fig. 3.6), while the overall stiffening of tumor-associated matrices was maintained. These data indicate how essential it is to assess mechanical properties of cell-derived materials in their native state instead of using fixatives, which promotes extra stiffening (here by ≈20%).

Since the ECM is a viscoelastic material, we next analyzed its creep response by applying instantaneous force and recording ECM relaxation $\Delta\delta$ over time (Fig. 3.1G). Our results indicate two relaxation regimes that could be well fitted by a double exponential decay:

$$\Delta\delta(t) = A_1 exp\Big[-\frac{t}{\tau_1}\Big] + A_2 exp\Big[-\frac{t}{\tau_2}\Big] \tag{3.2}$$

where $\Delta\delta(t)$ is the matrix thickness decay, τ_1 and τ_2 are the fast and slow relaxation times, respectively, and A_1 and A_2 are the decay amplitudes used as fitting parameters. Tumor associated matrices revealed longer relaxation times than control matrices in both the fast (τ_1 = 125 ± 30 vs. 47 ± 25 s) and the slow (τ_2 = 1048 ± 152 vs. 701 ± 107 s) regimes, indicative of an overall slower response of tumor-associated Fn matrices to external forces (Fig. 3.1H). Collectively, these data indicate that, besides being stiffer, tumor-conditioned matrices are also more viscous than their control counterparts, which is likely able to dysregulate mechanosignaling to surrounding cells. Although we could not find any previ-

ous report of tumor ECM viscoelasticity, our matrix creep data are in agreement with the enhanced viscosity detected in breast cancer [Sinkus et al., 2005] and prostate cancer [Zhang et al., 2008] tissues.

3.4.2 Tumor-Associated Matrices Comprise Highly Stretched and Unfolded Fn Fibers

We next combined FRET and confocal microscopy to monitor the incorporation of FRET-labeled Fn into newly developed fibrils over 24 hours, as previously described in [Smith et al., 2007] and calibrated in detail in [Chandler et al., 2011] (Fig. 3.2 and Sec. 3.6). Our *in situ* FRET mapping shows that control cells (Fig. 3.2A) deposited high and medium FRET Fn fibers (yellow and green pixels) indicative of the coexistence of close-to-compact and extended Fn conformations. In contrast, tumor associated cells (Fig. 2B) generated mostly stretched and unfolded Fn fibers, as indicated by low FRET fibrillar sections (blue pixels). Overall, tumor-associated matrices displayed both a more homogenous Fn population (narrower FRET histogram in Fig. 3.2C) and more stretched Fn fibers than control matrices (mean FRET intensity ratio = 0.35 ± 0.047 vs. 0.38 ± 0.05, $p < 0.0001$) (Fig. 3.2D). This trend is in agreement with previously published results [Chandler et al., 2011]. Collectively, our data suggest that tumor-conditioned cells deposit Fn fibers with altered conformations that might alter Fn signaling either by exposing new binding sites to cells or by disrupting strain-sensitive binding motives such as the PHSRN synergy site and the RGD loop sequence responsible for $\alpha_5\beta_1$ integrins binding [Ruoslahti, 1988, Pierschbacher and Rouslahti, 1984].

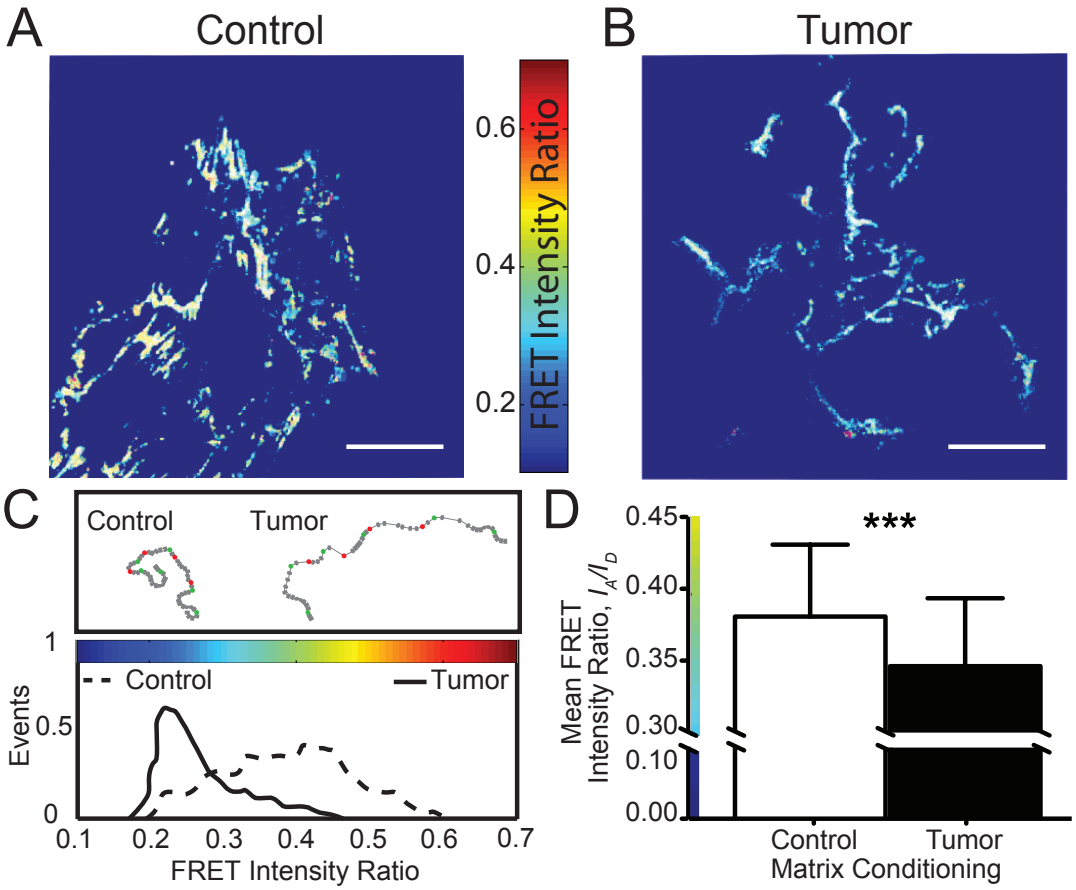

Figure 3.2: Tumor-associated Fn matrices are more unfolded. (A, B) FRET-Fn maps showed lower FRET intensity ratios, IA/ID, in tumor matrices (blue Fn fibers) than in their control counterpart (green/yellow Fn fibers). Scale bars = 50 μm. (C) Corresponding FRET intensity ratios histograms confirmed that tumor-associated Fn matrices comprised mainly stretched/unfolded Fn fibers (low FRET, narrow distribution) while control matrices contained a broader population of Fn conformations (higher FRET, larger distribution). (D) Mean FRET intensity ratios, IA/ID, of tumor-associated Fn matrices (n = 171) were lower than that of control matrices (n = 245), indicating that tumor conditions increased unfolding by ≈10% with respect to control. Mean ± SD.

When testing the effect of Fn matrix chemical fixation on FRET, we found it increased the FRET ratio of control matrices (SI Fig. 3.7A) but had no effect on the FRET of tumor-associated (SI Fig. 3.7B) matrices relative to unfixed conditions, denoting an overall strain relaxation and enhancing the differences between tumor-associated and control matrices (mean FRET intensity ratio = 0.35 ± 0.06 vs. 0.45 ± 0.05) (SI Fig. 3.7C, D).

3.4.3 Tumor-Associated Fn Matrices are Thicker, Denser, and Comprise Thicker Fibers

We next investigated the topology of the Fn matrices. We first used the SFA to assess ECM thickness (Fig. 3.3A) and show that tumor-associated cells generated a 37% thicker matrix than control cells (D_0 = 18.9 ± 1.7 vs. 13.7 ± 0.8 μm, $p <$ 0.03). Next, z-projections of 3D reconstructed confocal image stacks (Fig. 3.3B) were used to quantify pore sizes and fiber diameters using ImageJ (NIH). We found that tumor-associated matrices were also denser, as indicated by smaller pores than in control matrices (73.3 ± 96.5 vs. 131.8 ± 179.8 μm^2) (Fig. 3.3C) and displayed Fn fibers with larger diameters (Tumor = 1.10 ± 0.42 μm) than control matrices (Control = 0.89 ± 0.31 μm) (Fig. 3.3D). Collectively, our data show that the topology of tumor-associated matrices is also altered: indeed, narrower pores and thicker Fn fibers likely contribute to enhanced matrix rigidity as well as altered cell binding and migration.

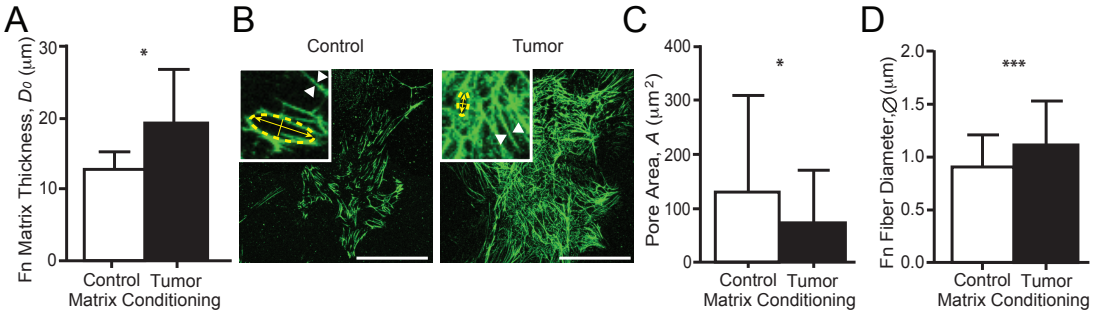

Figure 3.3: Tumor-associated Fn matrices are thicker, denser, and comprised of thicker fibers.(A) Tumor-associated Fn matrices (n=21) measured by the SFA were thicker than control matrices (n = 17). (B) Z-projections of immunostained control and tumor-associated Fn matrices. Scale bars = 50 μm. Insets: 300% zooms used to determine the pore size and fiber diameter shown in panels (C) and (D), respectively. (C) Pores measured within tumor associated Fn matrices (n = 72) were significantly smaller than those measured within control matrices (n = 72) ($p < 0.0001$). (D) Tumor-associated Fn fibers (n = 120) possessed larger diameters than those of control Fn fibers (n = 120) ($p < 0.05$). Mean ± SD.

3.4.4 Tumor-associated Fn matrices modify cell adhesion and proangiogenic factor secretion by activating an integrin switch

To determine the relevance of our results in tumor angiogenesis, we next assessed the adhesion and proangiogenic capability of newly seeded cells (after 4 hours) on the Fn matrices, via cell counting and quantification of vascular endothelial growth factor (VEGF) secretion, respectively. Our data show that ≈40% fewer cells adhered on tumor-associated ECMs (Fig. 3.4A) while VEGF secretion per cell increased by ≈45% (Fig. 3.4B) in tumor conditions. We attributed different levels of VEGF to altered secretion (1.33 ± 0.019 vs. 1 ± 0.075) rather than different matrix sequestration after we analyzed Fn-matrix lysates

indicating negligible amounts of Fn matrix-bound VEGF, and no significant differences between tumor and control matrix conditions (0.086 ± 0.0017 vs. 0.091 ± 0.018) (SI Fig. 3.8). Because Fn conformational changes were previously shown to modulate the binding specificity of integrins [Krammer et al., 1999, Petrie et al., 2006, Friedland et al., 2009, Wan et al., 2013, Seong et al., 2013], we also examined altered integrin specificity as a potential mechanism of tumor-induced modified signaling. We first tested the role of $\alpha_5\beta_1$ integrins in regulating VEGF secretion by exposing fresh cells to β_1 blockers prior to seeding onto control matrices. Our data indicate that blockade of β_1 dramatically increased VEGF secretion relative to the untreated-control condition (Fig. 3.4C, white bars), suggesting that $\alpha_5\beta_1$ interactions with control Fn likely lowered VEGF secretion by stromal cells. We next tested the role of $\alpha_v\beta_3$ in increasing VEGF secretion by exposing new cells to α_v blockers prior to seeding onto tumor-associated matrices. Blockade of α_v decreased VEGF secretion to similar levels as detected in the untreated-control condition (Fig. 3.4C, gray bars). Furthermore, concomitant blocking of β_1 and α_v subunits on both tumor-associated and control matrices restored VEGF secretion to normal levels as seen in untreated-control conditions, suggesting integrin compensation [Hynes, 2002]. Collectively, our data indicate that the presence of unfolded and stiff Fn fibers enhance 3T3-L1 VEGF secretion on tumorassociated matrices by favoring their use of $\alpha_v\beta_3$ over $\alpha_5\beta_1$ integrins. These results are discussed later and are in agreement with previous work by others showing that higher engagement of $\alpha_v\beta_3$ increases VEGF secretion [De et al., 2005].

Because cells respond to altered matrices by modulating their adhesive linkages, we further investigated cell adhesions by monitoring the recruitment of two focal adhesion proteins. Our data reveal differences in both talin and phos-

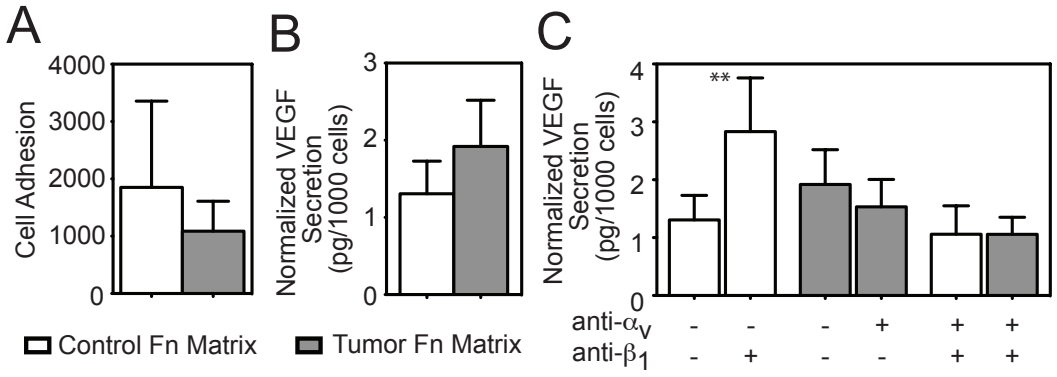

Figure 3.4: Cells adhere to tumor-associated Fn preferentially through α_v integrins with associated increased VEGF secretion. (A) After 4 hours, fewer adherent cells were detected within unfolded and stiff tumor matrices (1088 ± 522 cells) than within control ones (1851 ± 1504 cells) (n = 3/group). Mean ± SD. (B) After 4 hours, new cells secreted higher levels of VEGF when seeded onto tumor-associated Fn (1.9 ± 0.6 pg/1000 cells) than those seeded onto control Fn (1.3 ± 0.42 pg/1000 cells). (C) Cells treated with β_1-integrin blockers secreted significantly higher amounts of VEGF (2.8 ± 0.93 pg/1000 cells; $p < 0.01$) than untreated cells on control matrices, while cells treated with v-integrin blockers secreted slightly lower levels of VEGF (1.5 ± 0.47 pg/1000 cells) than untreated cells on tumor matrices (1.92 ± 0.6 pg/1000 cells) (n = 6/group). Mean ± SD.

phorylated focal adhesion kinase (pFAK [pY397]) distribution among cells re-seeded on control or tumor-associated matrices (SI Fig. 3.9). On control Fn, untreated cells recruited both talin and pFAK to develop fibrillar adhesions (insets: double arrows); instead, cells treated with β_1 blockers grew adhesive ECM clusters comprising mainly talin (SI Fig. 3.9, control). On tumor-associated Fn, untreated cells developed focal contacts comprising both talin and pFAK (insets: arrowheads), while cells treated with α_v blockers began developing fibrillar adhesion located mainly at the cell periphery (insets: double arrows) (SI Fig. 3.9, tumor). Interestingly, cells treated with both integrin blockers developed peripheral fibrillar adhesions on control Fn (insets: double arrows), and

left behind ECM clusters on tumor-associated Fn.

Our findings are in agreement with previous work showing that focal contacts comprise primarily $\alpha_v\beta_3$ integrins whereas fibrillar (or mature) adhesions contain principally $\alpha_5\beta_1$ integrins [Zamir and Geiger, 2001]. These different adhesions are activated through different mechanisms: while $\alpha_v\beta_1$ integrins cluster and recruit adhesion proteins in a contractility-independent manner [Schiller et al., 2013], $\alpha_v\beta_3$ integrins require cell contractility to develop nascent adhesions via talin [Jiang et al., 2003], which regulates $\alpha_v\beta_3$ activation via a conformational change of β_3 reinforcing nascent focal contacts [Wegener et al., 2007, Critchley, 2009, Roca-Cusachs et al., 2013]. Our findings indicate that cells forced to utilize $\alpha_v\beta_3$ integrins on stiff and unfolded tumor-associated matrices recruit higher levels of talin to form large focal contacts, which may also modulate proangiogenic behavior.

3.5 Discussion

The experiments presented herein suggest that breast cancer cell-secreted factors deregulate Fn matrix assembly by stromal cells. Although increased levels of Fn had been previously detected in tumors [Stenman and Vaheri, 1981], our findings indicate that both mechanical and conformational properties of the Fn matrix are altered as overall stiffness and molecular unfolding were simultaneously increased in tumor-associated Fn matrices. Additionally, these Fn alterations were linked to enhanced proangiogenic capability of the surrounding stromal cells with implications for tumor angiogenesis.

More specifically, tumor-conditioned matrices are mechanically different

from control matrices as they exhibit increased stiffness and slower relaxation, indicative of both elasticity and viscosity changes. Furthermore, these matrices are structurally altered across multiple length scales as they are overall: thicker, denser, and composed of thicker fibers that comprise more unfolded Fn molecules. By combining the SFA with FRET, our study provides a detailed picture of the early deposited Fn matrix from the matrix/cellular level to the molecular level. Our results agree with previous work but include new observations with implications on Fn-mediated tumor growth.

At the single fiber level, previous FRET work had shown that strain led to stiffening and unfolding (> 150% strain) in Fn fibers [Klotzsch et al., 2009]. At the matrix level, another FRET study [Chandler et al., 2011] estimated average strain in Fn fibers based on FRET vs. fiber strain calibration and anticipated matrix stiffening. However, no study so far had made a direct correlation between overall matrix stiffness, matrix topology, fiber strain, and molecular conformation of Fn within fibers. To our knowledge, this study reports the first quantitative and direct correlation between Fn matrix stiffness and topology at the matrix/cellular scale with Fn conformations at the molecular scale.

Our findings also underline how dramatic the effect of fixatives is on both the mechanical and structural properties of compliant (0.1 kPa range) and porous materials. Indeed, although the general trends of stiffening and unfolding were maintained for tumor conditioned relative to control matrices, formalin increased rigidity and decreased strain, particularly in control Fn matrices where the random crosslinking of lysines likely resulted in the pinning of dangling Fn fibers in the network.

Our stiffness data indicate lower values for tumor-associated Fn matrices

than for both macroscopic tumors in vivo [Samani et al., 2007] and single Fn fibers [Klotzsch et al., 2009]. These difference can be attributed to (i) the higher porosity of cell-free Fn networks (with enhanced fluid transport) relative to denser tumor tissues, (ii) the presence of both Fn and collagen in mature tumor tissues, and (iii) to the different regime of deformations in individual fibers relative to ECM networks, where the deformation is distributed over a mesh of disordered and connected fibers that respond collectively to strain.

Matrix topology (denser network and thicker fibers) together with molecular unfolding of the initial Fn matrix may also indirectly influence the overall tumor-associated matrix mechanics. On one hand, Fn unfolding has been shown to lead to the subsequent deposition of a more unfolded Fn matrix [Antia et al., 2008]. On the other hand, modified Fn properties might modulate tumor stiffness by altering the deposition of subsequent ECM components. For example, Fn fibers acting as templates for the deposition of collagen [Sottile et al., 2007]. In particular, the binding of collagen I to the gelatin-binding domain of Fn is necessary for the initial codeposition of collagen [Mcdonald et al., 1982]. Because the interaction of Fn with collagen is likely conformation dependent, the unfolded/strained Fn fibers initially generated by 3T3-L1s may dramatically affect collagen fibrillogenesis, either by disrupting the binding site for collagen I or by exposing cryptic sites with enzymatic activity capable of digesting collagen [Schnepel and Tschesche, 2000]. Consequently, Fn unfolding may also indirectly regulate the mechanosignaling of tumorassociated collagen I that ultimately contribute to tumorigenesis [Levental et al., 2009].

In this study, we also report that new (untreated) stromal cells seeded onto

tumor associated matrices exhibit decreased adhesion and enhanced VEGF secretion. Because tumor-associated Fn matrices suffer both conformational and mechanical alterations known to modify cell-matrix interactions, we hypothesized that Fn alterations might serve as a mechanosensor and integrin switch. Our results indicate that the cells responsible for enhanced VEGF secretion detected on tumor-associated matrices (comprising mainly stretched/unfolded Fn fibers) favor the use of $\alpha_v\beta_3$ over $\alpha_5\beta_1$ integrins to interact with Fn. This finding can be explained by differential engagement of either strain-sensitive (e.g., $\alpha_5\beta_1$) or strain-insensitive (e.g., $\alpha_v\beta_3$) integrins with the surrounding matrix. Indeed, the integrin binding FnIII9-III10 sequence of Fn is extremely sensitive to conformational changes resulting from enhanced tension exerted by cells. Earlier reports suggested that the distance between the synergy PHSRN site in FnIII9 and the RGD site in FnIII10 is critical for engagement and activation of integrin $\alpha_5\beta_1$ [Obara et al., 1988, Aota et al., 1991] but has little effect on engagement of integrin $\alpha_v\beta_3$. Therefore the integrin switch measured here on tumor-associated matrices is likely due to strain-induced increased spatial separation between FnIII9 and FnIII10 [Krammer et al., 2002], which inhibits the binding of $\alpha_5\beta_1$ to both sites simultaneously [Pierschbacher and Rouslahti, 1984] and forces cells to utilize more $\alpha_v\beta_3$ to compensate [Petrie et al., 2006]. Our results are in agreement with previous work showing that higher engagement of $\alpha_v\beta_3$ increases VEGF secretion [Wan et al., 2013, De et al., 2005]. Moreover, we see that β_1 blockade of cells seeded on unstretched Fn had a greater effect on VEGF secretion than α_v blockade of cells on tumor-associated (stretched) Fn. This functional difference may be attributed to VEGF receptor availability as VEGF is immobilized to Fn through a $\alpha_5\beta_1$/VEGF-receptor association [Wijelath, 2002] hence inhibiting the accessibility of $\alpha_5\beta_1$ would lead to VEGF release. Another explanation of the

functional difference could be that $\alpha_5\beta_1$ has higher binding affinity (4 nM) to Fn [Takagi et al., 2003] than $\alpha_v\beta_3$ (1.3 μM) [Liu et al., 2010].

Collectively, our results contribute to an improved understanding of the early role of Fn matrix assembly in modulating proangiogenic factor secretion in the breast tumor microenvironment. Future experiments are needed to further clarify the role of Fn in a 3D tissue-like context. Our studies have been performed on 2D Fn-coated mica surfaces, where both substrate rigidity and culture dimensionality can regulate changes in cell behavior. In particular, the mica substrates used in our studies are stiffer than the tumor tissue, which may affect the mechanics and conformation of the Fn matrix. Similarly, the formation of focal adhesions differs in 2D and 3D cell cultures [Fraley et al., 2010] which also potentially modulates the properties of the Fn matrix. Future studies will (i) validate our integrin-modulated VEGF secretion findings in a physiologically relevant 3D matrix [Kloxin et al., 2010] with controlled stiffness and topology, (ii) allow us to discriminate the roles of stiffness and conformation in regulating these processes [Janmey and Weitz, 2004], and (iii) pave the road for targeted anti-VEGF therapies [Cao and Langer, 2010].

3.6 Materials and methods

All materials, methodology, and equipment used herein such as cell lines, substrate preparation, Surface Forces Apparatus, FRET labeling of Fn, cell culture, force curve acquisition, creep testing, immunostaining, FRET data acquisition, analysis of porosity and fiber diameter, cell attachment and VEGF secretion on cell-derived ECMs, and statistics are summarized in SI Materials and Methods.

3.7 Acknowledgements

Victoria Benson & Cory Brown for aid in image analysis and Dr. Juan Carlos Andresen & Shengling Hu for help in coding. Funding by NSF under awards CMMI-1031068 & DMR-1352299 (to DG), NIH/NCI under awards R01 CA185293 & R21CA161532 (to CF and DG) and U54 CA143876 (to CF), CONACYT (to RCAE), and the Cornell Center for Materials Research through Award Number (NSF DMR-1120296).

3.8 Supplemental information

3.8.1 SI Materials and methods

Cell culture

As an in vitro model of cancer-associated stromal cells, we utilized tumor-associated 3T3-L1 pre-adipocytes (ATCC, VA). Tumor soluble factors (TSF) from an aggressive metastatic breast cancer line, MDA-MB-231 cells (ATCC, VA), were collected to mimic paracrine signaling between a tumor and its surrounding microenvironment. After exposing 3T3-L1s to TSF for 3 days, the preconditioned cells were detached and cultured on mica substrates for 24 hours to study early fibronectin mechanics, topology, and conformation. Afterwards, culture systems were decellularized using a modified Cukierman protocol [Castelló-Cros and Cukierman, 2009] and used for parallel SFA and FRET studies. Separate samples to be immunostained were chemically fixed with 10%

neutral buffered formalin.

Substrate preparation

Muscovite mica (S&J Trading, Australia) is a negatively charged, hydrophilic aluminosilicate that cleaves easily along its basal plane. To obtain transparent and uniform thin sections of 2 to 5 μm in thickness, we cleaved mica sheets by hand, yielding a clean, atomically smooth surface. These mica sheets were cut into 1 cm^2 sections and placed on a mica backing sheet. Afterwards, these mica sections were metallized with 55 nm of silver and glued with UV curing glue (E = 1.034 GPa, product 61) (Norland, NJ) under a UV lamp for 50 minutes, with silver side facing down on semi-cylindrical silica surfaces of 10 mm in diameter with a radius of curvature of 20 mm (ESCO Products, NJ), which we call discs. All preparation steps were performed in a laminar flow cabinet to minimize particulate contamination. Customized PDMS wells were used to house the lower silica discs and to contain media during the 24 hours matrix deposition process (see cell culture). The upper discs were prepared identically, kept clean and stored in a desiccator until needed. Each pair of discs (upper and lower discs) was prepared using the same mica section to ensure equal mica thicknesses.

Surface Forces Apparatus

The Surface Forces Apparatus (SFA) (SurForce LLC, CA) is a force measuring technique that uses fringes of equal chromatic order (FECO) to accurately determine the absolute surface separation between two highly reflecting surfaces. The lower disc was mounted on a double cantilever spring, with a measured

spring constant of 980 N/m. The force acting between the surfaces was then obtained. A white light source was directed through two semi-cylindrical surfaces (discs), which have previously been prepared with silvered mica, building an optical interferometer. The light that emerged consists of FECO. These FECO were directed towards the entrance slit of a photo-spectrometer (Princeton Instruments, NJ) and the spectrogram was recorded with a CCD camera (Princeton Instruments, NJ) for further analysis. The acquisition software used was LightField v4.0 (Princeton Instruments, NJ). This technique is extensively described in [Israelachvili, 1973, Israelachvili and McGuiggan, 1990, McGuiggan and Israelachvili, 1990].

FRET Labeling of Fibronectin

AlexaFluor 488 succinimydyl ester and AlexaFluor 546 maleimide (Invitrogen, CA) were used to FRET label Fn as previously described by Baneyx et al.[**?**] and Smith et al.[Smith et al., 2007]. Labeling ratios and Fn concentrations were confirmed using a DU730 UV Vis spectrophotometer (Beckman, IN) at 280 nm, 495 nm, and 556 nm. Soluble calibration of FRET labeled Fn was carried out in guanidine hydrochloride solution, with varying concentrations between 0 and 4M, in order to obtain acceptor/donor intensity ratios (IA/ID) as a function of protein denaturation. Additionally, strain calibration experiments of Fn fibers deposited on PDMS substrate trenches were used to correlate Fn fiber conformation (FRET intensity ratios) with fiber strain, as described in [Klotzsch et al., 2009, Little et al., 2009].

Cell seeding

3T3-L1 (ATCC, VA) pre-adipocytes (passages 4-8) were preconditioned for 3 days in α-MEM culture medium (Control) or α-MEM medium containing normalized tumor soluble factors (TSF). These TSFs were obtained from human MDA-MB-231 breast cancer cells. After this preconditioning period, cells were trypsinized and used for parallel SFA and FRET experiments.

Flat mica sections (culture area: 64-81 mm^2/well) in 24-well plates and mica covered silica discs (culture area: 79.16 mm^2/disc) in PDMS wells were coated with a thin layer of human plasma Fn (Life Technologies, NY) at a concentration of 30 μg/mL in phosphate buffered saline (PBS) and physisorbed at room temperature for 60 minutes to facilitate cell adhesion. After rinsing 3 times with PBS, a concentrated cell solution comprised of $2x10^4$ preconditioned 3T3-L1s (Control or Tumor) was seeded on the mica substrates. After 20 minutes of cell adhesion, 50 μg/mL exogenous Fn in low serum (1% fetal bovine serum (FBS)) was added (400 μL). For FRET experiments, the exogenous Fn consists of 90% unlabeled Fn (unFN) and 10% labeled Fn (Fn-DA). For SFA experiments, only unFN is used.

After culturing at 37°C and 5% CO2 for 24 hours, cultures were decellularized via a modified Cukierman protocol (1) (including deoxycholic acid wash and extra wash steps) and left unfixed in PBS. Further samples were fixed for 1 hour at 4°C, and washed three times with PBS for further immunostaining and morphology studies.

Force curve acquisition

Paired discs were mounted in a crossed cylinder axis configuration, the lower of which contained the ECM and indented with a bare upper disc, as depicted in Fig. 1C. The SFA chamber was filled with 75 mL of warm (37 °C) PBS, to keep both discs immersed and hydrated during the SFA measurements. Before any experiment was carried out, the system was allowed to equilibrate to 37 °C for 1 hour. Then, each sample was probed at 4 different positions along the lower cylinder axis approximately 500 μm apart. Each position was then indented at least 3 consecutive times with increasing load (pressure).

Approach (In) and retraction (Out) measurements were performed at a constant speed of 0.5 μm/min. The system was allowed to equilibrate for 15 minutes between each force run and 30 minutes between each position.

Sequences were acquired at a rate of 3 frames per second and post-processed with Matlab R2012b (MathWorks, MA) to yield force-distance profiles. These profiles were further analyzed to obtain the compressive elastic moduli during approach and retraction, using a contact mechanics model between a sphere and an elastic half-space proposed by Johnson [Johnson, 1985], equation 3.1 (see Results 3.4).

Creep testing

Samples for SFA were prepared and mounted as described in Force curve acquisition, respectively. ECM samples were manually compressed by applying increasing step-loads of approximately 3.7 mN (spring constant, k = 676 N/m), using the SFA fine micrometer. ECMs creep was monitored over 1800 s by fol-

lowing the shift of the FECO fringes.

Immunostaining

ECMs were decellularized and fixed as previously described. These matrices were permeabilized with 0.5% Triton X-100 (Thermo Scientific, IL) in PBS (PBS-X) for 5 minutes, then blocked for non-specific binding with PBS-X containing 1% SuperBlock (Thermo Scientific, IL). After washing twice with PBS-X, the samples were then immunostained overnight at (4 °C) for: Fn using either rabbit or mouse (when co-staining collagen I) antibodies (Sigma-Aldrich, MO), rabbit anti-mouse collagen I (Millipore, MA), mouse anti-talin (Millipore, MA), or rabbit phosphorylated focal adhesion kinase [pY379] (pFAK) (Invitrogen, CA). After the overnight incubation, the samples were washed twice with PBS-X for 5 minutes each, and incubated for 1 hour at room temperature in a PBS-X/1% Super Block solution comprised of the following formulations: DAPI (Life Technologies, NY) (1:5000), Alexa Fluor 568 Phalloidin (1:250), goat anti-rabbit Alexa Fluor 488 (1:100) or goat anti-mouse Alexa Fluor 488 (1:100), goat anti-mouse Alexa Fluor 647 (1:100) (All Alexa Fluors were obtained from Life Technologies, NY). After the secondary antibody incubation, samples were washed twice with PBS-X for 5 minutes, and kept in PBS for confocal microscopy imaging.

FRET data acquisition

Mica substrates were imaged with a Zeiss 710 confocal microscope (Zeiss, Munich, Germany) using the C-apochromat water-immersion 40x/1.2 objective, a pinhole of 2 AU, the 488 nm laser set at 10% power, and pixel dwell time of 6.3

μs.16-bit z-stack images spaced 2 μm apart were acquired. Fn-DA excitations were simultaneously collected for the donor fluorophores in the PMT1 channel (514-526 nm) and for the acceptor fluorophores in the PMT2 channel (566-578 nm), as well as the brightfield channel. These z-stack images were analyzed with a customized Matlab code to generate images with a false color scheme correlating pixels with its FRET intensity ratio (IA/ID) and mean FRET intensity ratios of every z-slice in an image. Individual FRET z-stack images were stacked in ImageJ (NIH) and reconstructed in Volocity (PerkinElmer, Inc., MA) [Smith et al., 2007, Antia et al., 2008, Antia et al., 2006].

Analysis of matrix porosity and fiber diameter

Fn fiber diameters and matrix pore sizes were obtained from immunostained confocal microscope images, analyzed using ImageJ (NIH). To this end, 7 z-stack slices were orthogonally projected. Measurements were taken from the center and periphery. Pore size was analyzed by measuring the average size of the empty space within the projection.

Cell attachment and VEGF secretion on cell-derived matrices

Preconditioned pre-adipocytes were seeded on Fn coated flat mica surfaces for 24 hours as previously described. Samples were decellularized, sterilized with penicillin-streptomycin for 20 minutes, blocked for non-specific binding with PBS containing 1% bovine serum albumin for 20 minutes, and washed twice with PBS. During these incubation steps, untreated pre-adipocytes were trypsinized and suspended in serum free media with various integrin-blocking

antibodies (3 μg/mL) on a shaker at 37°C for 30 minutes. Cells were either left untreated (-β_1/-α_v), treated with only a rat anti-mouse integrin α_v blocker (CD51) (Millipore, MA) (-β_1/+α_v), or treated with only a β_1 blocker (CD29) (BD Biosciences, CA) (+β_1/-α_v). Cells were allowed to attach in serum free media on a shaker at 37°C for 1 hour, before switching to low serum media (1% FBS). After 3 hours (total 4 hours), media was collected to quantify VEGF secretion with a Quantikine ELISA kit (R & D Systems, MN). The samples were then fixed, immunostained, and imaged as previously described. VEGF secretion was normalized by the total number of cells adhered to the cell-derived matrices counted from 2.5x images; cell count was scaled up from three 2.5x objective images comprised of 692 pixels by 520 pixels (≈45% of the total mica substrate surface area).

Statistics

Data were statistically analyzed in GraphPad Prism (GraphPad Software, Inc., CA). Students t-tests or ANOVAs with Tukeys post-hoc tests were performed and statistical significance was determined at $p < 0.05$.

3.8.2 SI Figures

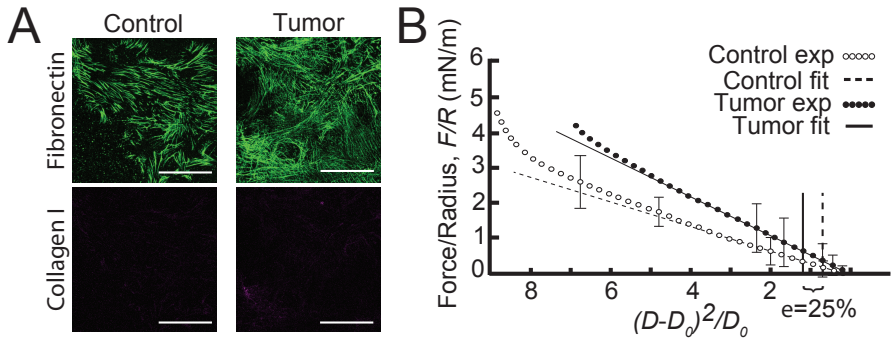

Figure 3.5: ECM composition and linearization of force-distance profiles. (A) Cell-derived ECMs were immunostained simultaneously for both fibronectin and collagen, showing that early tumor-associated ECMs were comprised exclusively of Fn. Scale bars = 50 μm. (B) Linearization of the representative compressive force-distance profiles for control ECMs (experimental ∘, fit – – –) and for tumor ECMs (experimental •, fit– – ––) shown in Fig. 3.11E. Tumor-associated ECMs show a larger linear regime as compared to the control ECMs.

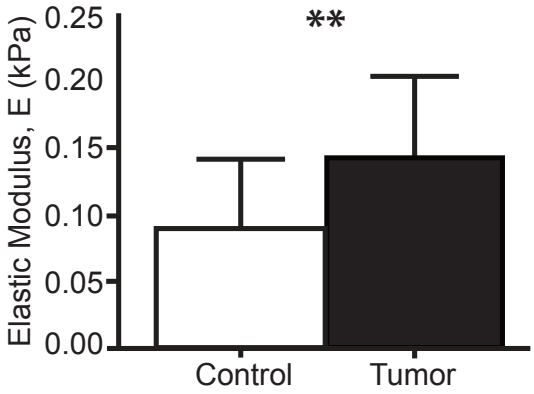

Figure 3.6: Chemical crosslinking increases stiffness. Tumor-associated ECM elastic moduli were measured to be 0.1428 ± 0.06070kPa (n = 20), representing an increase in elastic modulus of 60% compared to the control ECM elastic modulus, measured to be 0.09031 ± 0.05266 kPa (n = 30) ($p < 0.05$).

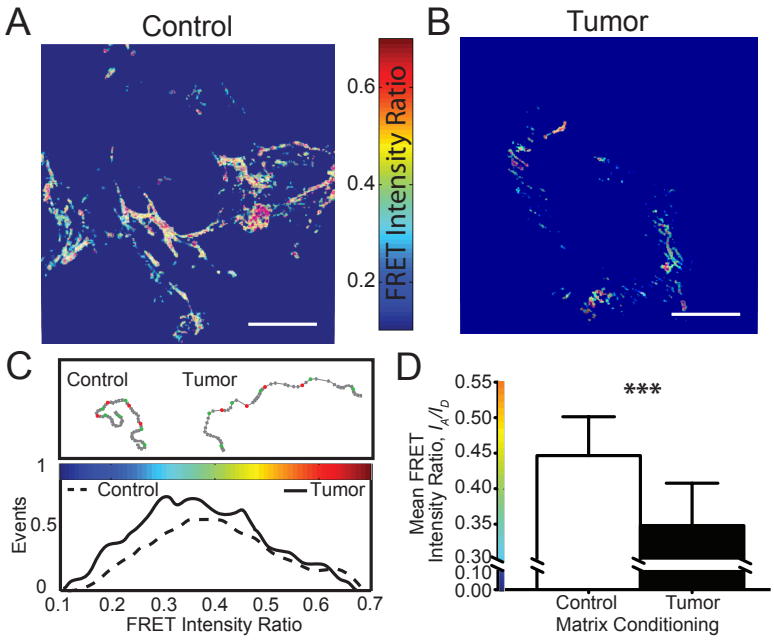

Figure 3.7: Chemical crosslinking relaxes conformation. (A) Control Fn ECMs were comprised of more close-to-compact Fn fibers (high FRET, red/yellow pixels). (B) Tumor-associated Fn ECMs were comprised of more unfolded Fn fibers (low FRET, blue pixels). (C) Representative histograms of FRET ratios displayed. (D) Mean FRET intensity ratios of tumor-associated Fn ECMs (n = 14) were significantly lower than that of control Fn ECMs (n = 18) ($p < 0.0001$). Scale bars = 50 μm.

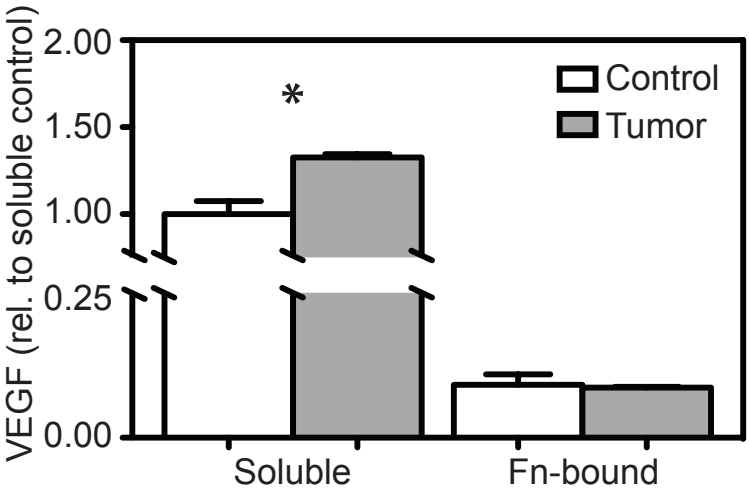

Figure 3.8: Enhanced VEGF secretion. After preconditioned cells deposited Fn matrices for 24 hours, media and decellularized Fn matrix lysates were collected to measure soluble and Fn-bound VEGF, respectively. VEGF values were normalized to cell population, and represented as relative ratios to soluble VEGF detected from control Fn matrix samples. Tumor-associated soluble VEGF secretions were higher than that of control soluble VEGF secretions (n = 2). Tumor-associated Fn-bound VEGF was not different from that of control Fn-bound VEGF (n = 2).

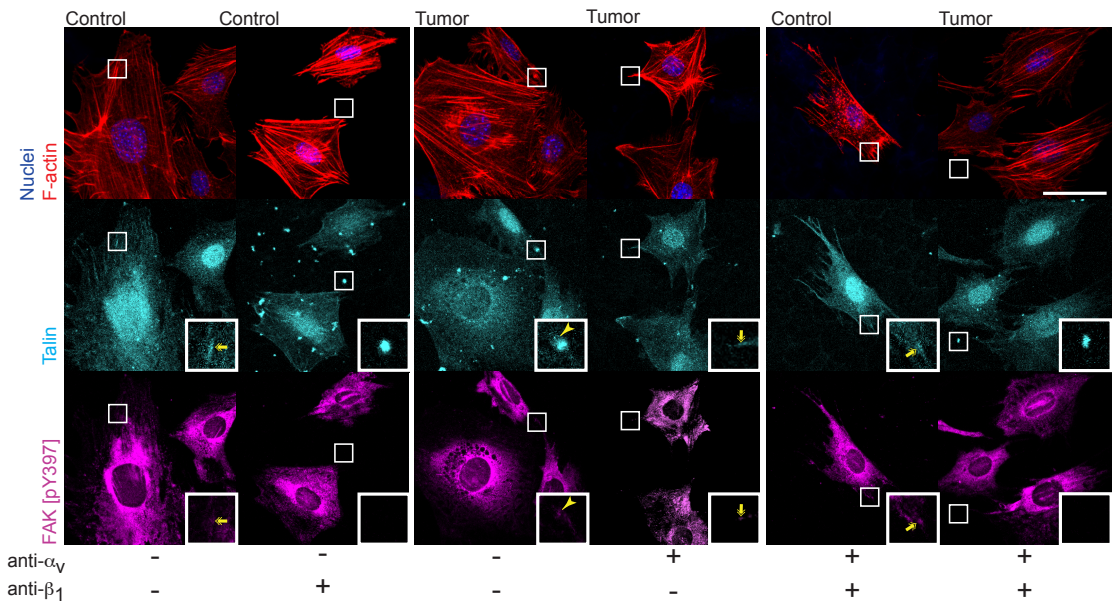

Figure 3.9: Focal adhesion protein recruitment on tumor-associated Fn ECMs associated with development of focal contacts. After 4 hours, untreated cells on control ECMs developed fibrillar adhesions as shown by talin immunostaining (insets: double arrows). Cells treated with β_1-integrin blockers on control ECMs show adhesion clusters comprised talin not associated with cells (insets: ECM cluster). Untreated cells on tumor ECMs appeared to have developed focal contacts comprised both talin and pFAK (insets: large arrowheads). Cells treated with α_v-integrin blockers were able to develop fibrillar adhesions (insets: double arrows). Cells treated with both integrin blockers on control ECMs were also able to develop fibrillar adhesions (insets: double arrows), however treated cells on tumor ECMs left behind adhesion clusters in the surroundings (insets: ECM cluster). Scale bar = 50 μm.

CHAPTER 4

FIBRONECTIN TETHERS SYNOVIAL FLUID COMPONENTS IN THE SUPERFICIAL ZONE OF CARTILAGE

The work presented in this chapter is in preparation for submission: **Roberto C. Andresen Eguiluz**, Fei Wu, Sierra G. Cook, Cory N. Brown, Noah J. Pacifici, Lawrence J. Bonassar, and Delphine Gourdon. Author contributions: R.C.A.E., L.J.B, and D.G. designed research; R.C.A.E., F.W, S.G.C., and C.N.B. performed research; R.C.A.E. and F.W. contributed new reagents/analytic tools; R.C.A.E., F.W., S.G.C., C.N.B., N.J.P., L.J.B., and D.G. analyzed data; and R.C.A.E., S.G.C, L.J.B., and D.G. wrote the paper.

4.1 Abstract

Boundary lubrication occurs under severe loading and/or at slow sliding velocities where layers of molecules separate opposing surfaces and protect them from damage. Fibronectin (Fn) is a glycoprotein present in the superficial zone of articular cartilage; however, its role in boundary lubrication is still unknown. In this chapter, we study the molecular interactions between Fn and lubricin (LUB), hyaluronan (HA), serum albumin (SA), or synovial fluid (SF) solutions, which are known to play an important role in joint lubrication. Using a surface forces apparatus, we investigated the normal and shear interactions between Fn coated mica substrates incubated with different synovial fluid components. We found that Fn tethers LUB and HA, inducing a strong repulsion between the surfaces. Additionally, upon shearing, Fn+LUB remains structurally stable at pressures ≈3 MPa, protecting the underlying mica substrate from wear. Our results have important implications for understanding joint lubrication and diseases such as osteoarthritis.

Keywords: fibronectin, lubricin, wear protection, synovial fluid, surface forces apparatus

4.2 Significance

The goal of this study was to investigate the interactions between Fn and SF components. Using a Surface Forces Apparatus, we have examined their synergistic performance under confinement and sliding conditions. Three important SF components, LUB, HA, and SA were tested and compared to full SF, all incubated on Fn. Our findings indicate that LUB binds to Fn and provides wear protection, similar to what observed with SF. HA and SA bind to Fn as well, but lack the wear protection and lubricating properties of LUB. These results have important implications for our understanding on boundary lubrication and wear protection of articular surfaces, and enhance our knowledge of biotribological interactions that may be exploited for treatments such as osteoarthritis.

4.3 Introduction

In healthy synovial joints, articular cartilage shows excellent lubrication and wear resistance over a person's lifetime. Cartilage surfaces in synovial joints slide on each other with friction coefficients of 0.001-0.05 [Wright and Dowson, 1976, Forster and Fisher, 1996], supporting pressures up to ≈20 MPa [Morrell et al., 2005] under various lubrication modes [McCutchen, 1962, Mow and Lai, 1980, Radin et al., 1970] imposed by extreme gait and locomotion ranges. These tribological properties arise from a com-

bination of complex composition and structure [Wang and Ateshian, 1997] of various proteins present in the joint (see Figure 4.1A). This then leads to reduced friction and enhanced joint protection at different spatial and temporal scales [Mow and Lai, 1980]. In boundary lubrication at direct cartilage-cartilage contact, it is the amorphous outermost layer of the superficial zone of cartilage known as the lamina splendens (LS) [Hughes et al., 2005], that acts as the bearing surface. Also, the LS marks the interface between the cartilage and the SF [M.A. MacConail, 1951, Jurvelin et al., 1996]. The LS contains collagen type II in a hyaline state [Jeffery et al., 1991] and large amounts of the same essential components found in SF (see Table 4.1). Examples of SF components include LUB [Radin et al., 1970], Fn [Balazs, 2009], phospholipids (PL) [Hills, 2002, Hills and Crawford, 2003], HA [Balazs, 2009], and SA [Fan et al., 2012]. There have been many interesting studies on the role of individual components of SF (LUB [Swann et al., 1985, Zappone et al., 2007, Zappone et al., 2008], HA [Greene et al., 2011, Tadmor et al., 2003, Lee et al., 2014], lipids [Yu et al., 2012, Hills and Crawford, 2003]), on the synergistic interactions between two components (HA with LUB [Chang et al., 2009, Das et al., 2013], collagen with LUB [Chang et al., 2013], HA with PL [Liu et al., 2012]), and on SF [Schmidt et al., 2007, Banquy et al., 2014b] itself to understand the lubrication mechanisms in the superficial zone. However, despite much research, the mechanisms behind joint boundary lubrication, in particular the role of Fn, are still unclear.

HA, LUB, SA, and SF have exhibited unique tribological properties in boundary lubrication mode at biological and non-biological interfaces [Jay et al., 1998, Davis et al., 1979, Yu et al., 2012, Greene et al., 2011, Zappone et al., 2007, Heuberger et al., 2005b]. SF was shown to act as an ef-

fective boundary lubricant when confined (i) between opposing articular cartilage surfaces using a variety of test configurations [Schmidt and Sah, 2007, Davis et al., 1979], as well as (ii) between non-biological surfaces [Jay et al., 1998, Davis et al., 1979]. More recently, a tribological study of different species of SF using the SFA demonstrated that proteins and biopolymers when sheared between mica surfaces gradually aggregate to form a homogeneous gel layer resembling the LS [Banquy et al., 2014b]. The lubricating and wear protecting properties of HA have also been assessed at cartilage-cartilage [Radin et al., 1970, Mabuchi et al., 1999] shearing junctions and non-biological interfaces [Jay et al., 1998, Tadmor et al., 2003, Yu et al., 2012, Lee et al., 2014]. Studies agree that HA does not act *per se* as an effective boundary lubricant, but rather exhibits remarkable wear protection properties when grafted (or trapped, as suggested by Greene *et al.* [Greene et al., 2011]) to surfaces [Tadmor et al., 2003, Yu et al., 2012, Lee et al., 2014].

As evidence of the synergistic interactions between HA and LUB, HA wear protection is enhanced and accompanied by a reduction of the friction coefficient when LUB is present [Das et al., 2013], even under extremely high contact pressures. This is unsurprising, since it is known that HA aggregates with LUB to form a protecting cross-linked network [Das et al., 2013]. LUB has been shown to lubricate cartilage against cartilage [Radin et al., 1970, Swann et al., 1977, Greene et al., 2011], cartilage against glass [Swann et al., 1981, Gleghorn et al., 2009] and latex against glass [Jay, 1992], almost as efficiently as SF. Using a SFA, Zappone *et al.* demonstrated that physisorbed LUB forms dense layers and lubricates negatively charged mica with friction coefficients μ = 0.02-0.04 at pressures up to 0.5 MPa, but increasing to μ = 0.2 at higher pressures. These LUB tribological properties are in part

attributed to its molecular architecture. LUB consists of a single mucinous domain (the lubricating domain) separating two globular domains (the binding domains) [Jones et al., 2007]. LUB can bind to various LS components, collagen and HA among them. Interestingly, its highest affinity is for Fn [Elsaid et al., 2005], which is only present in the superficial zone of articular cartilage [Balazs, 2009, Nishida et al., 1995]. SA, which is also in the SF, is known to aid in the lubrication of artificial cartilage and protect against wear between the metal surfaces of implants [Heuberger et al., 2005b, Nakashima et al., 2005]. Similar to LUB, SA combines to build network structures with HA when shearing, modifying the rheological properties of SF.

Fn is a multifunctional glycoprotein which is present in SF [Chevalier, 1993] and in the superficial zone of cartilage, but not in transitional or radial zones (see Figure 4.1 inset 2). This presents the question of whether Fn acts as a tethering molecule for other SF components, such as LUB, HA, or SA. The aim of this work was to (i) investigate whether Fn affects the adsorption of SF components to Fn coated surfaces and (ii) analyze how Fn modifies the tribological behavior of those SF components, in particular the friction coefficient and the protection against wear. Using a SFA we have measured the normal and shear forces, and monitored the thickness of the sheared film together with the onset of damage of the confining Fn-bound surfaces. Fn-bound surfaces were incubated with LUB, HA, bovine SA (BSA), or equine SF (ESF), respectively, to identify which interactions create an effective boundary lubricant and which protect the surfaces against wear. Fn-bound mica substrates incubated with LUB were found to have particularly good lubricating properties, exhibiting coefficients of friction of $\mu = 0.23$ at contact pressures $\approx$3 MPa.

Table 4.1: Components found in SF reported to play a role in joint lubrication and used in this study.

Component	Molecular weight [kDa]	Physiological concentration [mg/ml]	Concentration used [mg/ml]
Hyaluronan, HA	1000	1-4	3
Lubricin, LUB	230	0.05-0.35	0.02
Serum albumin, SA	66	8-11	8
Lipids, PL	0.26	0.137	NA
Glycosaminoglycans, GAGs	250	0.05-0.15	NA
Fibronectin, Fn	440	0.3	0.3

4.4 Materials and Methods

4.4.1 Fibronectin conformation studies

To map the molecular conformation of Fn adsorbed to mica surfaces, two previously published protocols were used [Baneyx et al., 2001, Smith et al., 2007]. AlexaFluor 488 succinimydyl ester and AlexaFluor 546 maleimide (Invitrogen, CA, USA) were used to FRET-label Fn. Labeling ratios and concentrations were determined using a DU730UV-vis spectrophotometer (Beckman, IN, USA) at 280 nm, 495 nm, and 556 nm. Soluble calibration of FRET-labeled Fn (FRET-Fn) was carried out in a guanidine hydrochloride (GdnHCl) solution at concentrations of 0, 2, and 4 M to obtain acceptor/donor intensity ratios (I_A/I_D) as a function of protein denaturation. 100 μl Fn solutions at a concentration of 50 μg/ml containing 10% FRET-Fn were incubated on previously prepared SFA

discs (see next section). Incubated surfaces were stored at 4 °C for 24 hours, then rinsed with phosphate buffered saline (PBS) three times and kept immersed in PBS. Samples were imaged with a Zeiss 710 confocal microscope using a water-immersion 40x objective.

4.4.2 Surface Forces Apparatus

To measure the normal and shear forces between two mica surfaces as a function of film thickness, SFA-Mark III was used (SurForce, LLC, Sta. Barbara, CA, USA). Two freshly cleaved and atomically smooth back-silvered mica (S & J Trading, Australia) sections were glued onto half cylindrical silica discs (R = 1 cm) with UV curing glue (Norland 61, Cranbury, NJ, USA). The discs were mounted in a cross-cylindrical configuration, and the absolute separation distance, D, was measured in real time by MIB. Additionally, MBI was used to quantify the contact diameter and the onset of damage of the shearing surfaces. Before functionalizing the mica surfaces, mica-mica contact in air was determined to obtain the reference distance, $D = 0$. To quantify the normal force, the lower surface was mounted onto a horizontal double cantilever spring (k = 1650 N/m) and displaced at 5 nm/s. To calculate the friction force, the upper surface was mounted onto a vertical double cantilever spring (k = 700 N/m) holding semiconducting strain gauges. Shearing was achieved via a ceramic bimorph slider, and shearing velocities of $V = 0.3\ \mu$m/s, 3 μm/s, and 30 μm/s were used in our experiments. MBI fringes of equal chromatic order were collected with an SP2300 photospectrometer (Princeton Instruments, NJ, USA) with a 600 g/mm grating and 500 nm blaze, digitalized with a ProEM CCD camera (Princeton Instruments, NJ, USA), and visualized using Lightfield v4.0 (Princeton Instru-

ments, NJ, USA). Friction voltages were acquired and quantified with a NI USB-6210 and LabView v8.6 (National Instruments, Austin, TX, USA), respectively.

Similar protocols were carried out for all mica surface functionalization conditions, unless otherwise indicated. First, freshly prepared mica surfaces were incubated with 50 μl of Fn (Sigma-Aldrich, MO, USA) in PBS (0.3 mg/ml) for one hour and rinsed with PBS. After rinsing, 50 μl of BSA at 0.02 mg/ml were added for 30 minutes to block non-specific interactions, and rinsed with PBS. Finally, these Fn-bound mica surfaces were incubated with 50 μl of either ESF (as extracted from equine carpus joint), HA (Lifecore Biomedical, San Diego, CA, USA) in PBS (3 mg/ml), or BSA (Sigma-Aldrich, MO, USA) in PBS (8 mg/ml) for one hour. LUB (Wyeth, PA, USA) samples were incubated with 50 μl solution (0.02 mg/ml) overnight. After the incubation period, samples were rinsed with PBS. Surfaces were sheared in PBS at 25 °C. Surface functionalization steps were carried out with surfaces mounted on the SFA, yielding the same adsorption on both surfaces. All preparation steps were performed in a laminar flow cabinet to prevent particle contamination. All results are reported as mean values ± standard deviation.

All the experiments performed with each fluid were carried out in agreement with the procedures and guidelines provided by the biosafety committee at Cornell University.

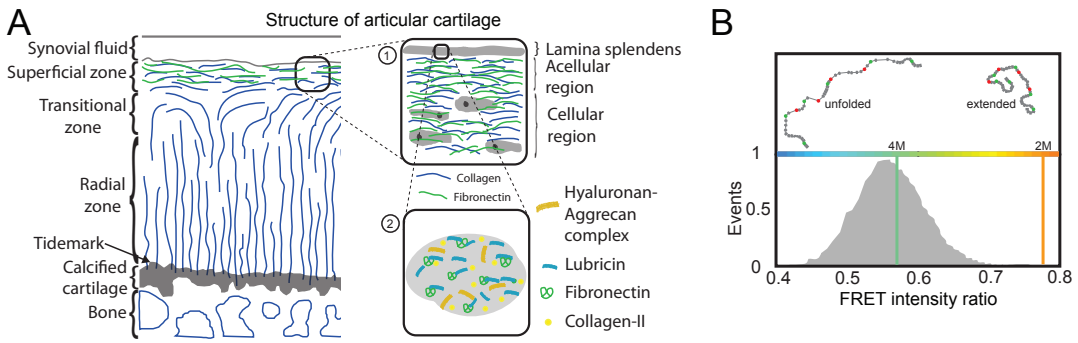

Figure 4.1: (A) Schematics of articular cartilage showing collagen type II fiber orientation as a function of depth. Inset 1: detail of the superficial zone of articular cartilage illustrating the cellular and acellular regions. Inset 2: representation of some relevant biomolecules present in the lamina splendens. (B) FRET intensity ratio frequency histogram of Fn conformations as measured by FRET-Fn adsorbed to curved mica substrates.

4.5 Results

4.5.1 Fibronectin conformation

To investigate the conformation of adsorbed Fn on curved mica, we used FRET-labeled Fn. Donor and acceptor fluorophore signals were collected simultaneously at the center of the curved SFA disc. FRET ratio is defined as acceptor fluorescence over donor fluorescence intensity ratio (I_A/I_D). The FRET ratio histogram [Smith et al., 2007] was used to calculate the average FRET ratio for each field of view (Figure 4.1B). FRET ratio is higher when Fn has a compact conformation and decreases as Fn extends and starts to lose its tertiary/secondary structure. The conformation of Fn adsorbed on curved mica had a relatively low FRET intensity ratio (0.53), indicating that Fn had mostly an unfolded tertiary conformation, as correlated with calibration curves.

4.5.2 Normal interaction forces between fibronectin tethered molecules

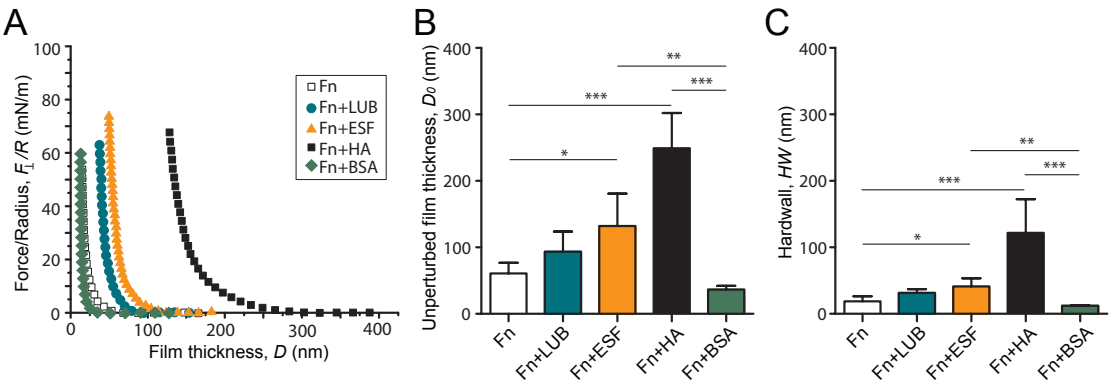

Figure 4.2: (A) Representative curves of the normal force $F_\perp$ normalized by the surface radius of curvature R as a function of the absolute separation distance D between mica surfaces coated with adsorbed Fn (white squares), with adsorbed Fn and LUB (cyan circles), with adsorbed Fn and ESF (orange triangles), with adsorbed Fn and HA (black squares), and with adsorbed Fn and BSA (green diamonds). (B) Bar charts displaying the average values of the unperturbed film thickness D_0 and (C) the average values for the compressed film thickness (hardwalls) HW of Fn films before (white) and after incubation of LUB (cyan), ESF (orange), HA (black), and BSA (green). Values are reported as mean + standard deviation. In all cases, p ¡ 0.05 is indicated by a single star, p ¡ 0.01 by two stars and p ¡ 0.001 by three stars.

To determine whether Fn is able to bind various components of SF, we first coated mica surfaces with Fn and incubated the surfaces in LUB (Fn+LUB), HA (Fn+HA), BSA (Fn+BSA), and ESF (Fn+ESF) respectively. We performed compressive measurements of physisorbed Fn both before and after incubation with either LUB, HA, or BSA all in PBS, or ESF. Figure 4.2A represents normal interaction forces, reported as $F_\perp/R$, $F_\perp$ being the normal force and R the surface radius of curvature between (i) LUB (cyan circles), (ii) ESF (orange triangles), (iii) HA (black squares), and (iv) BSA (green diamonds) all adsorbed to mica

previously coated with Fn. For comparison, a $F_{\perp}/R$ profile of only Fn surfaces is shown (white squares). In all cases, the interaction forces were purely repulsive and no adhesion was measured at the approach/retraction speed of 5 nm/s (quasi-static regime). Unperturbed film thickness (D_0) was extracted from the curves at the onset of repulsion.

Figure 4.2B displays D_0 before (only Fn, white) and after incubation with either LUB, HA, BSA, or ESF, respectively. Fn films showed a D_0 of 61 ± 16 nm. After LUB incubation, D_0 increased to 94 ± 30 nm. A larger increase in D_0 was observed for ESF incubated on Fn films, with an average of 132 ± 49 nm. HA had the largest D_0, 249 ± 53 nm. Interestingly, BSA incubated on Fn yielded a collapsed D_0 even smaller than that of only Fn, 37 ± 7 nm. Together, the changes in D_0 values indicate that Fn tethers the selected SF components (LUB, HA, and BSA) and molecules from ESF after a thorough wash with PBS. For the ESF condition, our study cannot determine the biochemical nature of the molecules that remained bound from ESF. However, it is very likely that LUB, accompanied or combined with other SF components is tethered to the underlying Fn, as further commented in the discussion section of this chapter.

Figure 4.2C shows the average film thicknesses under the highest compressive load (or hardwall, HW) before (only Fn, white) and after incubation of LUB, ESF, HA, or BSA. HW values maintained the same trend as D_0. Fn films showed an average HW value of 19 ± 7 nm. Following LUB incubation, the HW increased to 31 ± 6 nm. A thicker HW was observed for ESF incubated on Fn films, with an average of 41 ± 12 nm. Again, HA showed the largest value, with a HW of 122 ± 51 nm. BSA incubated on Fn resulted in the thinnest HW of all, 12 1 nm. Collectively, the HW values indicate that Fn is not only capable of

tethering the selected SF components and ESF biomolecules, but it also has the properties to retain the biomolecules under confinement and prevent them from being expelled during the repeated compression/decompression cycles.

4.5.3 Effective brush-like behavior

To understand the steric/entropic repulsion film behavior of Fn alone and incubated with LUB, ESF, HA, and BSA, semi-log plots of the force-distance profiles were fitted with the Alexander-de-Gennes (AdG, equation 4.1) model, which describes the behavior of interacting brush-like structures of polymers [Israelachvili, 2011]:

$$\frac{F_{\perp}(D)}{R} = \frac{16\pi kTL}{35s^3}\Big[7\Big(\frac{2L}{D}\Big)^{5/4} + 5\Big(\frac{D}{2L}\Big)^{7/4} - 12\Big] \tag{4.1}$$

where k is the Boltzmann constant, T is temperature, and the fitting parameters L and s are the relaxed brush length and average grafting spacing, respectively.

Fn+LUB, Fn+ESF, Fn+HA and Fn+BSA (Figure 4.3A-D) showed two clear regimes, long range (LR) and short range (SR), both of which were well-fitted by the AdG model. Figure 4.3 compares representative experimental data and the fitted models (red lines), with Fn only as a reference in each panel (white). Fn alone showed the shortest LR and SR "brush" length L, followed by Fn+LUB, Fn+ESF, and finally Fn+HA. Fitting values for L_{LR}, s_{LR}, L_{SR}, and s_{SR} are summarized in Table 4.2. However, for Fn+BSA (Figure 4.3D), despite the collapse of the film (decrease of D_0 and HW relative to Fn alone), the behavior of the

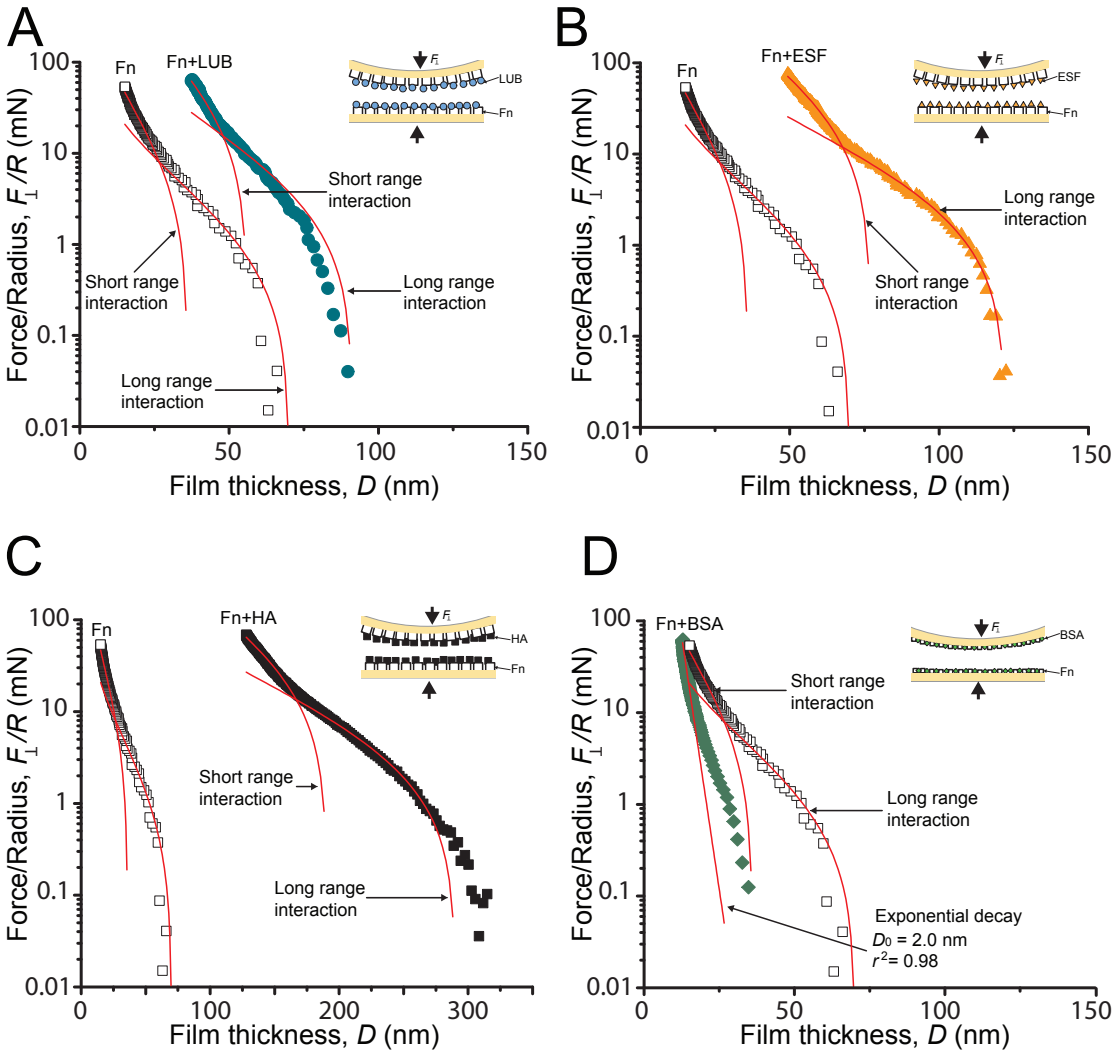

Figure 4.3: Semi-log plots of representative curves of the normal force $F_\perp$ normalized by the surface radius of curvature R as a function of the film thickness D (A) LUB (cyan circles), (B) ESF (orange triangles), (C) HA (black squares), and (D) BSA (green diamonds) adsorbed to Fn. White squares in each panel represent Fn only. Red lines indicate fits to Eq. 4.1 (AdG) or Eq. **??** (exponential decay).

adsorbed proteins were also well fitted by the AdG model.

It is interesting but not surprising that all films showed a brush-like behavior, given that several biological [Zappone et al., 2007, Banquy et al., 2014b, O'Connor et al., 2014] systems have been reported to behave as such. The two regimes (LR and SR) identified in Fn films could be due to the highly organized structure of Fn. In our study, we found that Fn conformation comprised mostly of unfolded Fn molecules, *i.e.* domains type III lost their tertiary structure. However, domains type I and type II are more stable due to the presence of disulfide bonds (absent in domains type III), giving rise to the long range brush like behavior. The short range brush-like behavior could be the manifestation of shorter range forces arising from distorting secondary and primary structures. Fn+LUB, for both ranges, showed a consistent increase in L of 10 nm as compared to the Fn films. It could be that the LUB built loops (as detailed in the discussion section and represented in Figure 4.7) by associating via the N-terminus (forming dimers) and binding to Fn via the C-terminus. The long range brush like behavior would then be the contribution of the loop, while the short range interaction could arise from the contribution of the oligosaccharides that build the side chains of the mucin-like domain of LUB molecules. Also, the L_{LR} value for Fn+LUB is close to half the value of the apparent hydrodynamic radius (R_h = 86 nm) [Zappone et al., 2008] of LUB, which suggests that the LUB molecules are spatially restricted via both globular end domains. For the Fn+ESF film, the analysis becomes complex, given that no a priori knowledge of the components that preferentially bind to Fn is available. Based on binding kinetic studies [Elsaid et al., 2007], we know that LUB binds preferentially to Fn over HA, collagen type I, and collagen type II. Additionally, the concentration of LUB solutions does influence the onset of repulsion D_0 [**?**], shifting to larger

distances with higher LUB concentrations. We can therefore, assume that the long and short range brush-like behaviors of Fn+ESF most likely correspond to LUB molecules (which could be decorated with PL) building loops similar to the LUB dimers. These loops are similar but have shorter anchorage distances, *i.e.* loops with smaller radius of curvature, manifested as larger distances at the onset of interactions. For the case of Fn+HA, the L_{LR} value is close to HA grafted with APTES [Yu et al., 2012], while the L_{SR} would be the contribution of the loops that are forced to build during confinement, changing the configuration from straight molecules to bent ones. Finally, the proposed mechanism for Fn+BSA would be similar to Fn film alone. However, the presence of BSA further unfolds the modules left with tertiary a structure, reducing the brush length contributions, both long and short range, to half of Fn only.

Table 4.2: Brush lengths (L) and average grafting distances (s) for long range (LR) and short range (SR) interactions obtained from Equation 4.1.

Component	L_{LR} [nm]	s_{LR} [nm]	r^2	L_{SR} [nm]	s_{SR} [nm]	r^2
Fn	35	6.0	0.98	18	2.5	0.98
Fn+LUB	46	4.1	0.97	28	1.7	0.98
Fn+ESF	61	5.7	0.99	39	2.0	0.99
Fn+HA	146	5.8	0.99	95	2.5	0.98
Fn+BSA	17	3.8	0.98	9	1.1	0.92
LUB[a]	65	14	0.90			
LUB[b]	115	14	0.89			

[a] at a concentration of 0.064 mg/ml and [b] at a concentration of 0.290 mg/ml, both from reference [Zappone et al., 2007].

4.5.4 Lubrication and wear protection of mica surfaces by fibronectin tethered molecules

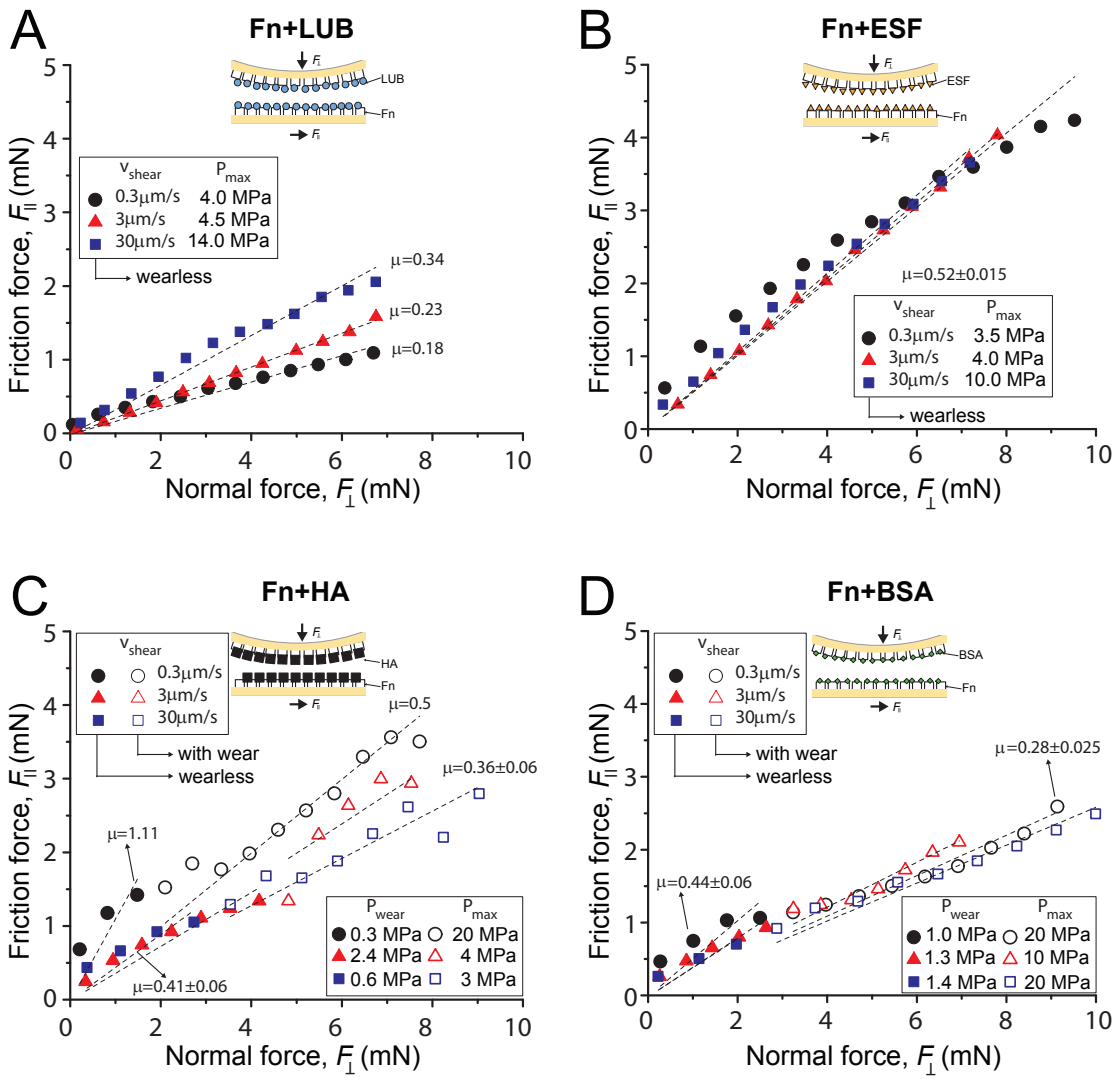

Figure 4.4: Friction force $F_{\parallel}$ as a function of normal force $F_{\perp}$ between (A) mica surfaces with adsorbed Fn and LUB, (B) with adsorbed Fn and ESF, (C) with adsorbed Fn and HA, and (D) with adsorbed Fn and BSA all sheared in PBS. The surfaces were sheared at sliding velocities of $V = 0.3\mu m/s$ (black circles), $V = 3\mu m/s$ (red triangles), and $V = 30\mu m/s$ (blue squares). Open symbols for HA and BSA indicate measurements after the surfaces became damaged with wear.

Next, we asked whether the presence of the Fn layer between the mica and LUB, HA, BSA or ESF facilitates lubrication and protects shearing surfaces from damage. To answer this question, we monitored both the friction forces and the onset of surface damage of the Fn-coated mica surfaces in the presence of LUB, HA, BSA or ESF while shearing in PBS (Figure 4.4), at 25°C using the SFA. Film pressures were obtained from the Derjaguin approximation for a cross-cylinder geometry [Israelachvili, 2011]:

$$P = -\frac{\delta W}{\delta D} = \frac{1}{2\pi R}\left(\frac{\delta F_{\perp}}{\delta D}\right) \tag{4.2}$$

where W is the interaction energy $W = F_{\perp}/2\pi R$, D the film thickness or absolute separation distance, and R the surface radius of curvature.

The friction forces $F_{\parallel}$ measured for Fn+LUB (Figure 4.4A) (i) depended linearly on the applied normal load, $F_{\perp}$, vanishing at $F_{\perp} = 0$ and (ii) were sensitive to shearing velocity V_{shear}. The friction coefficient, μ, defined as $\Delta F_{\parallel}/\Delta F_{\perp}$, was 0.18 at a shearing velocity of V_{shear} = 0.3 μm/s, increasing to 0.23 at V_{shear} = 3 μm/s, and increasing further to 0.34 at V_{shear} = 30 μm/s. It is important to note that Fn+LUB protected the surfaces against wear at all investigated shearing velocities and applied normal loads (pressures up to 14 MPa), well above the physiological range, as no surface damage was ever detected using MBI spectroscopy (as detailed in Figure 5A, E, and I). In contrast, LUB alone has proven to lubricate with very low friction coefficients in a similar setup (μ = 0.04) [Zappone et al., 2007] only when LUB is present in the solution, increasing to similar values (μ = 0.2-0.6) to those as reported here (μ = 0.18-0.34) when only physisorbed to mica. However, the wear protection is drastically enhanced with the underlaying Fn film, delaying the onset of wear from contact pressures

of 0.4 MPa [Zappone et al., 2007] to no damage up to pressures of 14 MPa (see Table 4.3).

Table 4.3: Pressures reported at onset of wear. In brackets max applied pressures without sign of wear.

Component	$P_{wear}[MPa]$			
@ V_{shear} =	0.3 μm/s	3 μm/s	30 μm/s	
Fn+LUB	(4)	(4.5)	(14)	
Fn+ESF	(3.5)	(4)	(10)	
Fn+HA	0.3	2.4	0.6	
Fn+BSA	1	1.3	1.4	
LUB[a]				0.4 (@ V_{shear} = 1 μm/s)
HA[b]				0.4 (@ V_{shear} = 10 μm/s)

[a] from [Zappone et al., 2007] , [b] from [Yu et al., 2012].

As shown in Figure 4.4B, when Fn+ESF coated surfaces were sheared, the measured friction forces $F_{\parallel}$ were (i) found to depend linearly on the applied normal load, $F_{\perp}$, vanishing at $F_{\perp} = 0$ and were (ii) independent of shearing velocities. The average friction coefficient, μ, was 0.52 ± 0.015. Although the Fn+ESF combination exhibited a high coefficient of friction, it protected the surfaces from wear at loads equivalent to contact pressures of 10 MPa.

When surfaces were sheared with Fn+HA, high friction coefficients and early damage were consistently observed (Figure 4.4C). Friction forces were the highest at V_{shear} = 0.3 μm/s with μ = 1.11. The coefficient of friction did not depend linearly on applied load $F_{\perp}$ and did not vanish at$F_{\perp} = 0$. At the intermediate and highest shearing speeds, V_{shear} = 3 μm/s and V_{shear} = 30 μm/s, respectively, the friction forces were very similar, with an average coefficient of

friction of 0.41 ± 0.06, that depended linearly on applied load $F_\perp$ and vanished at $F_\perp = 0$. Unlike Fn+LUB and Fn+ESF, shearing Fn+HA at 0.3 μm/s (lowest shearing velocity) was systematically accompanied by surface wear starting at pressures of ≈0.3 MPa, while wear was triggered at pressures of ≈2.4 MPa for 3 μm/s and ≈0.6 MPa for 30 μm/s. Once wear started, friction coefficients decreased to 0.5 for $V_{shear} = 0.3$ μm/s and to an average of 0.36 ± 0.06 for $V_{shear} = 3$ μm/s and $V_{shear} = 30$ μm/s. The elevated $F_\parallel$ could be due to the entanglement of the HA molecules during shearing, due to poor interpenetration resistance.

For Fn+BSA (Figure 4.4D), the measured friction forces $F_\parallel$ were all found (i) to depend linearly on the applied normal load $F_\perp$, and vanish at $F_\perp = 0$ and (ii) to be weakly sensitive to shearing velocity V_{shear}. The average friction coefficient was measured to be 0.44 ± 0.06. The onset of damage appeared at similar loads for all three velocities, 3 mN, corresponding to pressures of ≈1.2 MPa. These values are comparable to HA studies. After surfaces were damaged, the friction coefficient values decreased to 0.28 ± 0.025. Despite reports indicating that human SA lubricates artificial joints when adsorbed to hydrophilic (ceramic) surfaces[Heuberger et al., 2005a], we did not observe lubrication for low loads with poor wear protection. This is probably due to the binding and exposure of hydrophobic sites, which are less favorably hydrated and therefore provide poorer wear protection as compared to the other tested components.

4.5.5 Surface damage via FECO spectroscopy

The SFA relies on optical interferometry, which allows us to monitor the onset of damage in real time. This can be determined by an alteration in intensity and

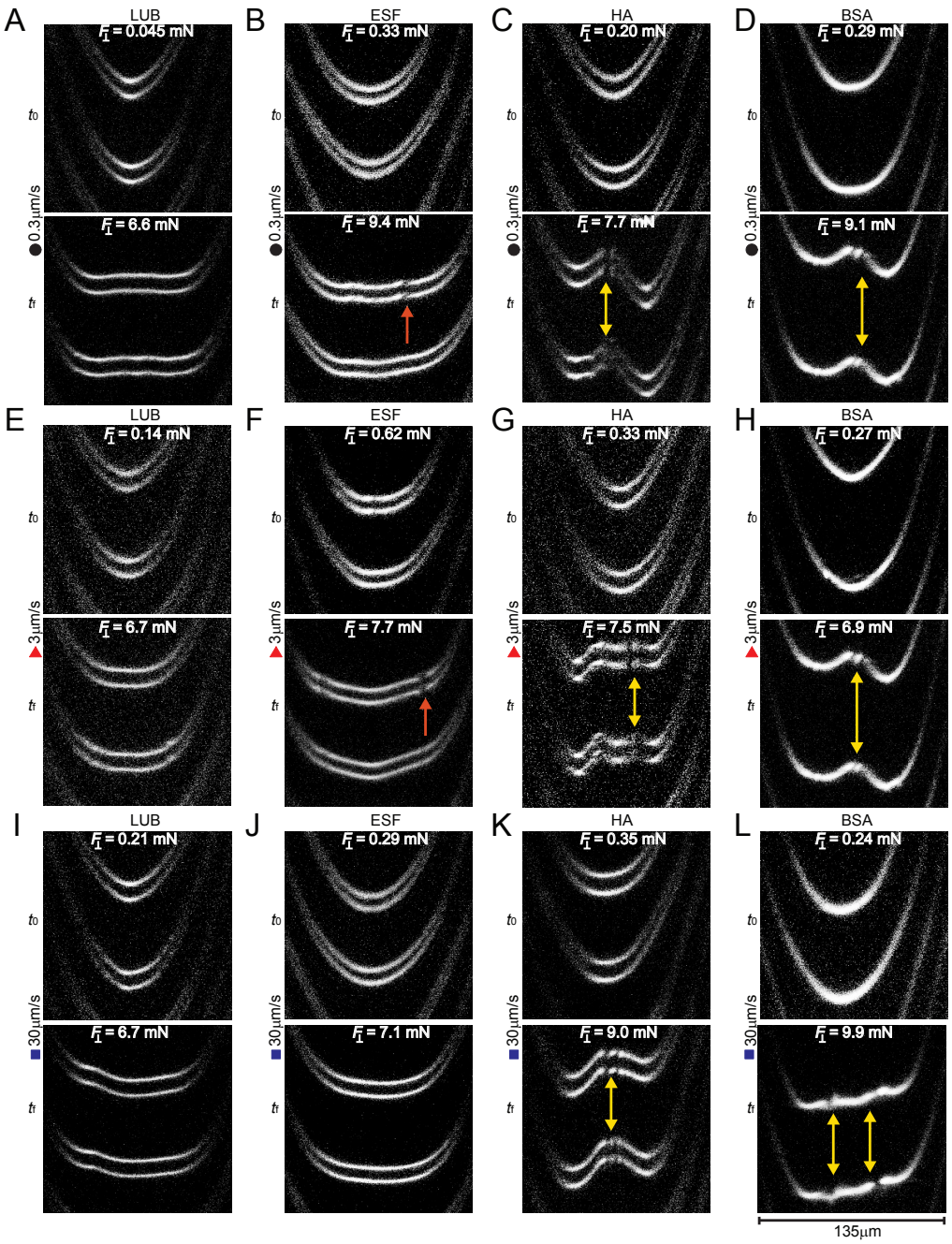

Figure 4.5: Examples of surfaces visualized by MIB of mica substrates (A, E, I) with adsorbed Fn and LUB, (B, F, J) with adsorbed Fn and ESF, (C, G, K) with adsorbed Fn and HA, and (D, H, L) with adsorbed Fn and BSA when shearing started (t_0) and when shearing ended (t_f) at sliding velocities (A, B, C, D) $V = 0.3\mu m/s$, (E, F, G, H) $V = 3\mu m/s$, and (I, J, K, L) $V = 30\mu m/s$. Molecule aggregates without damage is indicated by single sided orange arrows. Damage is indicated by double sided yellow arrows.

contrast of the odd and even fringes; this alteration is a consequence of a change in the refractive index (visible in even MBI fringes) of the confined medium and/or obstruction of the light (odd and even MBI). Figure 5 shows a matrix of images corresponding to the starting and ending shapes of MBI fringes for the four investigated conditions (LUB, ESF, HA, and BSA) and the three shearing velocities ($V_{shear} = 0.3\,\mu$m/s, $V_{shear} = 3\,\mu$m/s, and $V_{shear} = 30\,\mu$m/s). For Fn+LUB, the final MBI fringes remained undamaged, with no signs of wear or material accumulation for the maximal applied pressures of 4 MPa (Figure 4.5A), 4.5 MPa (Figure 4.5E), and 14 MPa (Figure 4.5I). Junctions remained flat for the entire shearing cycles.

Surfaces incubated with Fn+ESF also did not show signs of wear under shearing. The initial and final MBI fringes at maximum applied loads, corresponding to pressures of 3.5 MPa, 4 MPa, and 10 MPa, are shown in Figure 4.5B, F, and J. At low and intermediate shearing speeds, material accumulation at the edges of the junctions were identified. The accumulation is detected as a local change in the refractive index η of the confined medium and is only visible in the even fringes. As described in detail elsewhere [Israelachvili, 1973], even MBI fringes are more sensitive to changes in η. Single red arrows indicate the sites of material accumulation, Figure 4.5B and F. This material accumulation indicates film damage caused by plowing and concentrating agglomerates on the shear junction. Similar observations (shearing in presence of PBS, as opposed to the SF studies) have been reported during shearing of SF under confinement [Banquy et al., 2014b], a plausible mechanism for the formation of the lamina splendens. However, no signs of damage could be identified in the odd MBI fringes or using a microscope objective after shearing. This is indicative of undamaged mica substrate.

For Fn+HA, the onset of damage started at low loads. Shortly before wear became visible by MBI fringes, the surfaces started to deform and damage the film. This gave rise to the formation of debris that eventually incorporated mica flakes. Damage for Fn+HA is indicated by double yellow arrows pointing at both odd and even MBI fringes. The contact shape changed with shearing cycles, as well as wear debris sizes, as described in Figure 4.6. Again, using a microscope objective after shearing, it is revealed that wear was characterized by a single "wear track," corresponding to the distance covered by the wear debris particulates trapped between the junction. These results suggest that Fn only weakly physisorbs HA molecules, strong enough to retain them during compression but not during shearing. The poor wear resistance has been reported to improve when HA molecules are chemically grafted to mica [Yu et al., 2012].

As described previously, Fn+BSA showed early damage on the surfaces. This is indicated by double yellow arrows in Figures 4.5D, H, and L. At low and intermediate shearing speeds, wear debris accumulated at the approximate center of the junction. However, at the highest shearing velocity (Figure 4.5L), two clear regions of wear debris particulate accumulation were formed.

4.5.6 Particulate formation and evolution

For Fn+HA and Fn+BSA, damage of the surfaces was observed during shearing above a certain load, which was accompanied by the release of debris particles. Figure 4.6 shows the $F_{\perp}$ at which a wear debris particulate started to form, and the evolution of the wear debris particulate over the applied $F_{\perp}$ for V_{shear} = 0.3 μm/s (Figure 4.6A), V_{shear} = 3 mum/s (Figure 4.6B), and V_{shear} = 30 mum/s

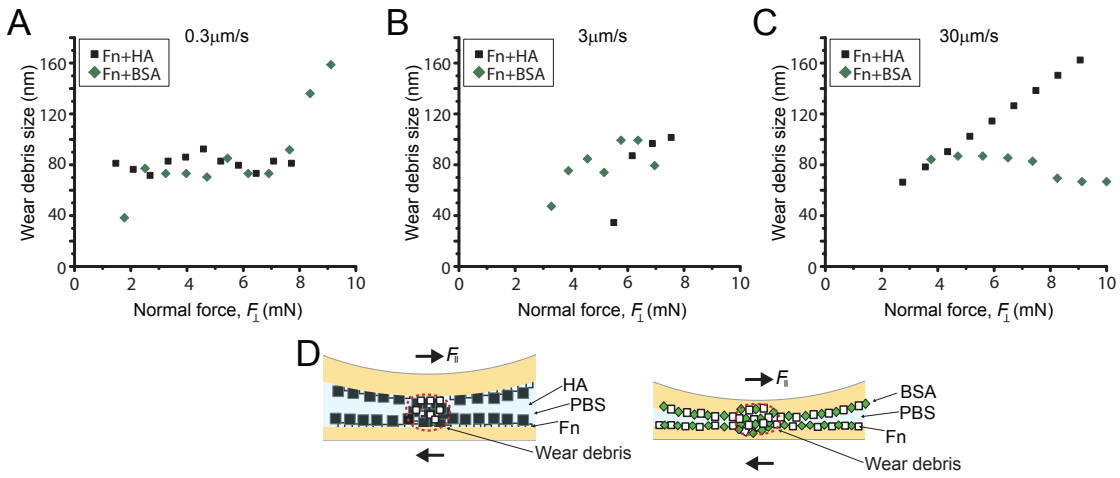

Figure 4.6: Debris size measured as a function of normal force $F_\perp$ at sliding velocities of (A) $V = 0.3\mu m/s$, (B) $V = 3\mu m/s$, and (C) $V = 30\mu m/s$ for mica surfaces with adsorbed Fn and HA (black squares) and with adsorbed Fn and BSA (green diamonds). (D) Schematic representation of Fn+HA and Fn+BSA debris confined between surfaces.

(Figure 4.6C).

At a shearing velocity of V_{shear} = 0.3 *mu*m/s, wear debris formation and evolution for both conditions were very similar. The average wear debris particulate sizes were 80 *pm* 6 nm and 86 *pm* 33 nm for HA and BSA on Fn, respectively. At V_{shear} = 3 *mu*m/s, the wear debris formation started at lower $F_\perp$ for BSA than HA, but both grew to a final size of ≈100 nm. The average wear debris sizes were also very similar, 80 *pm* 31 nm for Fn+HA and 80 ± 18 nm for Fn+BSA. At the highest shearing velocity, V_{shear} = 30 μm/s, for HA, the wear debris kept growing, reaching a final diameter of over 160 nm. Fn+HA average wear debris size was calculated to be 114 ± 32 nm. Fn+BSA wear debris size at V_{shear} = 30 *mu*m/s was similar to those measured at lower velocities, with an average diameter of 78 ± 9 nm. Combined, these results indicate that debris forms agglomerates that act as roller bearings, separating the surfaces and reducing the

coefficients of friction.

4.6 Discussion

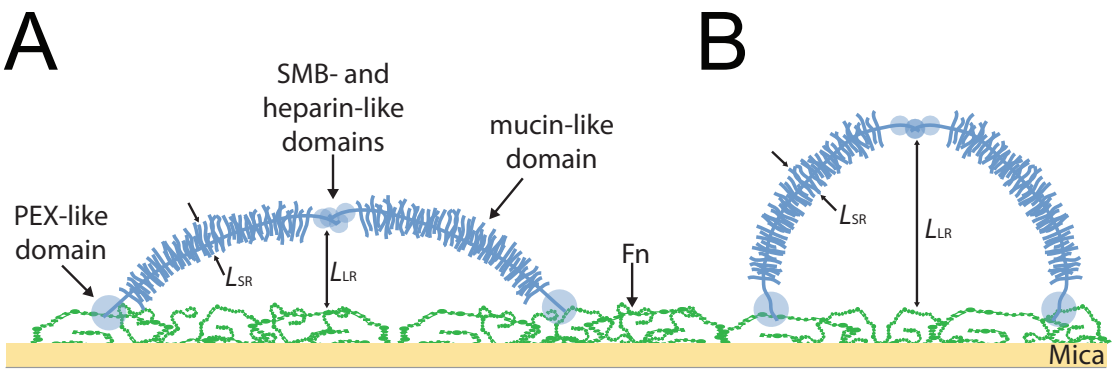

Figure 4.7: Proposed dimer configurations of (A) LUB at low concentrations and (B) LUB at high concentrations (from synovial fluid).

4.6.1 Fn conformation and binding of SF components

Fn is known to adopt a variety of conformations, depending on physical (curvature [Elter et al., 2012], strain [Smith et al., 2007, Klotzsch et al., 2009]) and chemical (pH [Smith et al., 2007], charge [Wan et al., 2012]) factors. These factors which determine the degree of extending or unfolding and exposure of cryptic binding sites for other proteins (and/or cells). Fn was found to adopt a relatively unfolded conformation on curved mica substrates, as indicated by FRET intensity ratios (Figure 4.1B). This means that many of the cryptic binding sites present in Fn are already exposed. However, in the superficial zone of cartilage, Fn is present in its insoluble fibrilar form [Balazs, 2009], so it is very likely that Fn fiber conformation distribution varies as a function of applied strains,

due to compression and/or shearing of the cartilage surfaces. This effect in turn can facilitate binding of critical lubricating molecules (such as LUB, HA and PL) to newly exposed cryptic sites [Klotzsch et al., 2009, Little et al., 2009] responding dynamically, enhancing wear protection and reducing coefficients of friction. Our model uses molecular (soluble) Fn, constraining the possible dynamic ranges of Fn conformations. However, unfolded Fn has exposed heparin (HEP) binding domains at the amino termini (Fn-I 1-5) and close to the carboxyl termini (Fn-III 12-14) [Pankov, 2002]. These in turn could have been used as binding domains by the positively charged somatomedin (SMB) and HEP binding domains present in LUB [Estrella et al., 2010]. But reduction and alkylation are known to reduce the ability of LUB to specifically bind to the cartilage surface [Jones et al., 2007], indicating that LUB utilizes the PEX-like domain (C-terminus) [Jones et al., 2007] to bind to cartilage and the SMB- and heparin-like domain's self-aggregation to build dimers [Jones et al., 2007, Zappone et al., 2007, Zappone et al., 2008]. This opens the question of whether the HEP-like domain is utilized when only Fn is present.

Interestingly, ESF tethered by Fn shows a very similar force-distance profile to that obtained for LUB, but with larger L values (an increase of 15 nm for both, LR and SR) as compared to LUB. We believe that the component that remains bound to the underlying Fn layer when incubated with ESF is LUB. BSA would immediately adsorb to the Fn layer, but given enough time (1 hour in our study), molecules of higher affinity, such as LUB (K_d = 0.12 nM [Elsaid et al., 2007]), would displace BSA. Additionally, LUB is found at concentrations of 0.05-0.2 mg/ml in SF. The higher LUB concentration found in ESF as compared with the LUB concentration used here further enhances binding kinetics. Higher MW molecules (HA) have smaller diffusion constants and would

need to possess a higher binding constant in order to displace LUB. Also, the LUB molecules adsorbed from ESF could be decorated with PL, a mechanism that has been proposed to aid in the transport of PL towards the superficial zone of cartilage [Greene et al., 2011, Das et al., 2013] making the LUB-PL complex stiffer and have a higher MW. Moreover, the brush lengths measured in our studies for LUB and ESF are much smaller than the ones reported for pure LUB adsorbed on mica (L = 65 nm)[Zappone et al., 2007]. We suggest a binding and surface coverage mechanism as shown in Figure 4.7. Pure LUB molecules adsorbed from a low concentration solution have shown shorter interaction distances as compared with higher concentration solutions [Zappone et al., 2007]. Lower concentration LUB solutions would increase the distance between the C-termini, building loops with larger radius of curvature and maximizing surface coverage, which in turn translates into wear protection (and shorter interaction distances, D_0). LUB C-termini distance adsorbed from ESF (higher concentration) would bind with shorter distances, building loops with a smaller radius of curvature with each loop covering a smaller surface area, which would be measured as an increase in the interaction distances, D_0. This proposed mechanism would explain why the brush lengths obtained in our measurements for pure LUB (and LUB from ESF) are shorter than what reported by Zappone *et al.* (see Table 4.2). The L_{SR} (10 - 15 nm) falls into the order of magnitude of LUB molecule diameter [Zappone et al., 2008] which corresponds to twice the size of the oligosaccharides that build the mucinous domain and act as a smaller and shorter range brush. Altogether, the agreement between our experimental data and the AdG model suggests that the aforementioned protein films behave as purely repulsive effective brush layers. However, it is unlikely that the proteins adsorbed on top of Fn have adopted a well-defined brush conformation.

In our study, HA was also effectively tethered by the underlying Fn layer, as consistently confirmed by the long range interaction forces measured. These are consequences of the long linear high MW (relative to the MW of the other SF components studied, see Table 4.1) combined with the high degree of hydration. The binding mechanisms of HA to cartilage surfaces are still under discussion. In our study, the underlying Fn film did not possess the right degree of porosity, and more importantly, the external mechanical stimuli, needed to mechanically trap HA molecules, as proposed for full cartilage [Greene et al., 2011]. This observation favors other mechanisms such as association through some of the many available carboxylic acids of HA for the building of amide bonds with amine groups of Fn.

In contrast, when Fn was incubated with BSA, the change in film thickness came as a collapse, or decrease in the measured distances of both D_0 and HW. We attribute this collapse to the exposure of hydrophobic sites induced by the presence of BSA, which changed the conformation of Fn to a more unfolded one. BSA is known for its high affinity toward hydrophobic sites, and because of this property is used on a regular basis as a blocker for non-specific interactions.

4.6.2 Friction forces, coefficients of friction, and wear protection

Friction forces and wear protection between the different Fn incubated films were varied. For Fn+LUB, coefficients of friction fell into the same range of values as previously reported for LUB alone on mica at high loads [Zappone et al., 2007]. However, contrary to those studies, it is interesting

to remark that no damage ever occurred to the underlying mica substrates or Fn+LUB film. The remarkable wear protection properties exhibited by LUB come from the strong binding that Fn provides for the LUB molecules through the PEX-like domain. This is in addition to good brush-against-brush lubrication provided by the highly hydrated layers surrounding the negatively charged mucin-like domains that minimize brush interpenetration. It is also important to point out that our studies were carried out with low concentrations of LUB (0.02 mg/ml) and prevented wear, suggesting that LUB molecules optimize their binding configuration to maximize surface coverage in the presence of Fn. Several studies have shown that the wear protection and coefficients of friction are sensitive to the concentration of LUB [Zappone et al., 2007, Das et al., 2013, Gleghorn et al., 2009].

Interestingly, Fn+ESF, despite having the highest overall measured friction coefficient of all investigated combinations, showed good wear protection capabilities, similar to what was observed for Fn+LUB films. This reaffirms the fact that coefficients of friction are not directly related to wear and are independent. The confined Fn+ESF film did, however, show more drastic structural changes than those observed for Fn+LUB. MBI spectroscopy inspection revealed a change in molecular rearrangement, as manifested by a change in the η (intensity of the even MBI fringes). This local increase of η was due to the accumulation of Fn+ESF molecules at the edges of the junction as a result of plowing during shear. The increase indicated mild film damage, with maintained protection of the underlying mica substrate. Similar observations have been reported when shearing SF, where gel abrasion and particle formation have been proposed to be mechanisms behind the onset of the LS formation [Banquy et al., 2014b]. Among the macromolecules present in SF, LUB is

the one that has been widely acknowledged to act as a good boundary lubricant. Additionally, Elsaid [Elsaid et al., 2007] has shown that LUB has its highest affinity towards Fn, from among all molecules present in the extracellular matrix of articular cartilage. It is reasonable to assume, therfore, that the main macromolecule tethered by Fn is LUB, most probably forming complexes with PL while modifying LUBs purely mucin behavior, and consequently modifying its biotribological behavior.

In contrast, Fn+HA showed high coefficients of friction, both before and after wear. This comes as no surprise, since it has been proven that HA alone is indeed a deficient boundary lubricant [Lee et al., 2014]. This is probably a consequence of the strongly tethered HA molecules to the underlying Fn film, plus poor interpenetration resistance and therefore the lack of a sharp shearing interface despite its highly hydrated molecules (hydration is a requirement, but not unique condition for good lubricant molecules). The onset of wear due to the large shearing forces, (having a normal (tensile) component) can be caused by the entanglement of HA molecules and easily delaminate the underlying mica substrates [Chen and Israelachvili, 1991].

Finally, BSA in hydrophilic surfaces, such as mica, builds a dense and thick boundary layer. This has been observed in hydrophilic ceramic surfaces, yielding a low coefficient of friction [Heuberger et al., 2005a]. However, in our conditions, mica has been previously saturated with Fn, restricting the availability of the hydrophilic surface. The immediate hydrophobic sites of Fn are easily accessible, making the process more energetically favorable. Furthermore, the adsorbed and denatured proteins are less efficiently hydrated and therefore acting as a poor boundary lubricant.

Finally, it is important to keep present the fact that our model systems utilize two solid and hard surfaces, while natural cartilage and joint lubrication are controlled by several lubrication mechanisms. At high loads and/or low shear velocities, molecules such as those investigated here build a gel layer that act as an effective boundary lubricant maintaining the separation of cartilage surfaces. At higher shear velocities, hydrodynamic lubrication mode plays the most important role [Caligaris and Ateshian, 2009]. Poroelasticity also plays a major role, especially under severe loading conditions or when loads are applied for prolonged periods of time. Our work presented here mimics the superficial zone of articular cartilage, where Fn is present. We demonstrate that the presence of Fn enhances the wear protection of underlying mica substrates, effectively acting as a tethering cartilage component for important boundary lubricating molecules, such as LUB.

4.7 Conclusions

Fibronectin effectively tethers LUB, HA, BSA, and boundary lubricating molecules (possibly LUB) from ESF under confinement and shear, providing wear protection to the underlying mica substrates. Although other cartilage contributions are responsible for the ultra-low coefficients of friction (such as the fluid load support provided by the poro-elastic behavior of the cartilage), our measurements expand the suggestions that none of the main components of synovial joints act alone, but rather contribute synergistically to the lubrication and wear protection of the cartilage surfaces. Additionally, we found that a high friction force does not necessarily correlate with surface damage, and conversely, that a low friction coefficient does not guarantee that no damage will

occur. This may have important implications for the understanding of diseased joints, such as those affected by osteoarthritis, where Fn is up-regulated, LUB down regulated, and HA is cleaved. This dysregulation in joint homeostasis could facilitate binding of more HA or SA and less LUB, given that HA or SA are present at much higher concentrations than LUB. Finally, Fn does appear to have an important tethering role in the superficial zone of articular cartilage, maintaining boundary lubricating molecules and/or molecule-aggregates firmly bound in order to provide surface protection.

4.8 Acknowledgements

Dr. Juan Carlos Andresen for help with coding, Kirk J. Samaroo, Mingchee Tan, Edward Bonnevie for enriching discussions. Funding by NSF under award 1031068 (to DG), NIH/NCI under award 1R21CA161532 (DG), CONACYT (to RCAE), and the Cornell Center for Materials Research through Award Number (NSF DMR-1120296).

CHAPTER 5

LOW FRICTION OF LUBRICIN-MIMICKING BOTTLE-BRUSH POLYMERS INTERACTING WITH FIBRONECTIN

The work presented in this chapter is in prepartion for submission: **Roberto C. Andresen Eguiluz**, Mingchee Tan, Cory N. Brown, Noah J. Pacifici, Lawrence J. Bonassar, David A. Putnam, and Delphine Gourdon. Author contributions: R.C.A.E., M.T., L.J.B, D.A.P.,and D.G. designed research; R.C.A.E., M.T, C.N.B.., and N.J.P. performed research; R.C.A.E. and M.T. contributed new reagents/analytic tools; R.C.A.E., M.T., C.N.B., N.J.P., L.J.B.,D.A.P, and D.G. analyzed data; and R.C.A.E., M.T, and D.G. wrote the paper.

5.1 Abstract

Synthetic biolubricants have been widely investigated as coatings for implants and the treatment of diseases, such as osteoarthritis. However, particularly for osteoarthritis, there have been few effective lubricants. A mucin known as lubricin, found in the synovial fluid, is the glycoprotein responsible for the low friction and known to provide wear protection of cartilage. However, lubricin is expensive to extract, hence a suitable lubricin-mimetic molecule is still to be created. In this study, we use the Surface Forces Apparatus (SFA) to characterize the normal and friction forces of a lubricin-mimetic pAA-PEG copolymer (pAA-62kDa, PEG-2kDa) interacting with fibronectin (Fn), a structural protein found in the superficial zone of cartilage. The normal and the lateral (friction) forces of pAA-PEG polymers were recorded using the SFA, in presence and absence of Fn coating. Our AFM data indicated that the pAA-PEG molecules had an average contour length and a diameter of 72 nm and 10 nm, respectively. Our SFA data

showed that the pAA-PEG polymer was only weakly adsorbed onto (negatively charged) bare mica surfaces but became firmly attached when Fn was added as a polymer linker. All our friction data exhibited (i) low friction coefficients ($\mu \approx 0.25$) up to applied pressures of 3 MPa and (ii) Amonton's like behavior. Together, AFM and SFA have allowed us for molecular and microscopic characterization of the pAA-PEG interactions with surfaces, gaining insight into both the lubrication mechanisms and the interactions of the biomimetic polymer with tissue (Fn). Collectively, these results indicate that our proposed lubricin-mimetic lubricant might be a promising affordable alternative to lubricin.

Keywords: mimetic lubricin, fibronectin, surface forces apparatus, wear.

5.2 Significance

The goal of this study was to investigate the interaction forces between two mica surfaces fully covered by a polymer whose architecture mimics the lubricating protein lubricin, with and without the cartilage component fibronectin. Our findings indicate that the mimetic polymer binds to the Fn coated mica surfaces, but not to the negatively charged bare mica surfaces. When sheared, the system shows low friction forces but early damage in absence of Fn. When Fn is present, wear damage is delayed. Coefficients of friction were independent of the shearing velocities, following an Amontionian behavior. These results indicate that the mimetic polymer brush might be a promising alternative to lubricin for therapeutics.

5.3 Introduction

Currently, there are many clinical needs for efficient biolubricants - applications including contact lenses, joint treatments, and arthroplasties. For clinical needs, biolubricants must be viable in the aqueous, protein rich and saline environment of the human body. Some technologies have been developed, such as dimethylpolysiloxane silicone water-based lubricants and hyaluronan formulations, to tackle these difficulties. However, these technologies are limited to low load bearing systems or are only efficient for a short period of time [Rutjes et al., 2012]. Efficient biolubricants must be engineered to withstand the loading (pressure) ranges, sliding speeds, contact areas, and shearing distances found in synovial joints. These mechanical characteristics of synovial joints give rise to fast changing biolubrication modes, from boundary to elasto-hydrodynamic lubrication [Swann et al., 1974, Roberts et al., 1982]. These dynamic ranges easily damage the underlying surfaces without proper lubrication. Nature has developed an efficient solution to overcome fast changing sliding speeds with proper lubrication and robust wear protection. A mucin known as lubricin (LUB), found in synovial fluid [Radin et al., 1970, Swann et al., 1981], is accountable for the exceptional frictional properties of articular cartilage. Cartilage-on-cartilage interfaces have been shown to have friction coefficients as low as 0.001 [Wright and Dowson, 1976, Morrell et al., 2005]. The lubrication property arises from the complex structure of the protein [Swann et al., 1985], resembling a bottle-brush. LUB binds through its carboxyl-terminus to cartilage [Jones et al., 2007], building a brush-like layer of loops, tails and associated tails (aggregating through the amino-terminus) [Zappone et al., 2007, Zappone et al., 2008]. Additionally, LUB can bind to a variety of extracellu-

lar matrix (ECM) components, including collagen [Chang et al., 2013] (COL) and hyaluronan [Das et al., 2013] (HA). Interestingly, its highest affinity is for fibronectin [Elsaid et al., 2007] (Fn), a prominent fibrillar protein of the ECM found in the superficial zone of cartilage [Balazs, 2009], *i.e.* at the interface between cartilage and synovial fluid.

Inspired by natural lubricants with bottle-brush architecture, a range of mimetic analogues have been explored [Banquy et al., 2014a, Perry et al., 2009, Yan et al., 2004, Iruthayaraj et al., 2008, Krivorotova et al., 2010]. All studies agree with the fact that the bottle-brush architecture efficiently counteracts chain interpenetration between opposing surfaces coated with such molecules. This steric repulsive behavior is desirable for achieving low friction forces and is partially a result of the high degree of hydration, which effectively swells and stretches the brushes. However, hydration itself is not enough. Synthetic bottle-brush polymers must be strongly anchored to the surfaces via their backbone [Yan et al., 2004, Pettersson et al., 2008] or anchored by their extremities [Banquy et al., 2014a]. This can be achieved either by strong covalent binding [Yan et al., 2004] or by electrostatic interactions [Huang et al., 2001, Banquy et al., 2014a]. In bottle-brush copolymers with PEG side chains, grafting density [Perry et al., 2009] and length of extended side chains [Pettersson et al., 2008] in the interfacial regions are also crucial in mediating lubrication. Despite the low friction coefficients measured in the aforementioned systems, PEG-copolymers have not been widely investigated as water based biolubricants but more as protective coatings such as anti-fouling [Fan et al., 2006, Heuberger et al., 2005a, Lee et al., 1990]. Moreover, while the interactions of LUB with COL [Chang et al., 2013] and HA [Das et al., 2013, Chang et al., 2009, Greene et al., 2011] at the superficial zone of

cartilage are well understood, there have not been any studies investigating the interactions between LUB and Fn, a crucial aspect of the superficial zone.

In this study, we designed and synthesized a polymer mimicking the structure of LUB (mimLUB) possessing bottle-brush architecture with a thiol terminal as the tethering moiety, mimicking the carboxyl-terminus of LUB. The mimLUB polymer was composed of a long and flexible poly(acrylic acid, pAA) backbone with grafted poly(ethylene glycol, PEG) as side chains. Additionally, pAA as well as PEG polymers have shown to have the desired immunological responses, similar to those seen in other biocompatible materials [Yim et al., 2009]. The aim of this work was to characterize the tribological properties of mimLUB on two model surfaces at the molecular scale. Using a Surface Forces Apparatus (SFA) we have measured the normal and friction forces between mimLub layers adsorbed either onto bare mica or onto Fn-bound mica. Adsorbed mimLUB affected the frictional response and wear of Fn-bound mica substrates at physiological relevant pressures and pH.

5.4 Materials and methods

5.4.1 mimLub synthesis

Acrylic acid (AA, 99.5%) stabilized with 200 ppm 4-methoxyphenol, methanol (99.8%) and sodium borate buffer were obtained from VWR (Radnor, PA, USA). 4,4 azobis (4-cyanopentanoic acid) (A-CPA) and 4-cyano-4-(phenylcarbonothioylthio)pentanoic acid (CPA-DB) (> 97% HPLC) was obtained from Sigma-Aldrich (St. Louis, MO, USA). Methoxy-poly(ethylene

glycol)-amine powder (PEG-NH2) was obtained from Jenkem Technologies (Beijing, PRC) and 4-(4,6-dimethoxy-1,3,5-triazin-2-yl)-4-methylmorpholinium chloride
(DMTMM) was from TCI America (Portland, OR, USA). All chemicals were used as received unless otherwise specified.

Synthesis and characterization of poly(acrylic acid) backbone (pAA).

Synthesis: Polyacrylic acid was synthesized by RAFT polymerization of acrylic acid (AA), using A-CPA as initiator (I) and CPA-DB as chain transfer agent (CTA) under anhydrous, airtight and dark conditions in methanol. AA concentration was maintained at ~ 3.8 mM, while [AA]:[I]:[CTA] was 762:0.25:1. The general reaction scheme was as follows: AA was added to a flame dried 5 ml brown ampule with one flea magnet, to which CPA-DB dissolved in 2.9 ml of nitrogen-purged methanol was added, followed by addition of A-CPA dissolved in 0.7 ml of nitrogen-purged methanol. Nitrogen gas was bubbled through the reaction mixture after the addition of each reagent for several minutes to prevent oxygen gas influx. After the last nitrogen purge the reaction ampule was flame sealed, placed in a 60°C oil bath to initiate polymerization and allowed to stir for 48 hours. Upon the completion of the reaction the ampule neck was broken to expose the reactants to air and the solution was cooled in ice to stop the polymerization. The solution was diluted with DI water, dialyzed against deionized water for 3 days, and then lyophilized to obtain a white, waxy powder. Characterization: proton nuclear magnetic resonance (1H NMR) (INOVA 400 MHz, D2O, ppm): δ 1.5-2.0 (pAA-CH2-), δ 2.25-2.75 (pAA-CH-). Molecular weight determined by Waters gel permeation chromatography (GPC)

system using poly(methacrylic acid) standards and phosphate buffered saline (pH 7.4) as the mobile phase at 30°C.

Synthesis and characterization of pAA-*g*-PEG polymer brushes.

The pAA-*graft*-PEG (pAA-*g*-PEG) copolymer was synthesized by polymer analogous conjugation of monoamine-functionalized PEG to the pAA backbone using DMTMM as coupling agent. pAA was dissolved in 0.1 M borate buffer (pH 8.5) at 3.3 mg/ml, while [AA]:[DMTMM]:[PEG] was 1:2:2. The general reaction was as follows: pAA and 2000 Mn PEG-amine were dissolved in 3 ml borate buffer in a 10 ml flask with magnetic stir bar. DMTMM dissolved in 0.6 ml borate buffer was added drop-wise into the flask with the final pH adjusted to 6-7 using 1 N HCl. Each conjugation reaction was conducted for 24 hours at room temperature, dialyzed against deionized water for 3 days and lyophilized to obtain a white powder. The assigned nomenclature for the polymer brushes are given as pAA(a)-*g*-PEG(b), where a and b are the molecular weights of pAA and PEG respectively, and *g* is the grafting ratio defined as the moles of PEG grafted to the pAA backbone divided by the moles of AA monomers in the pAA backbone. Molecular weight was characterized by multi-angle laser light scattering size exclusion chromatography (MALLS/SEC) performed at the Biophysics Resource of Keck Facility at Yale University.

5.4.2 Preparation of mimLub and fibronectin solutions

mimLUB with an average molecular weight of 1400 kDa was dissolved in phosphate buffered saline (PBS) solution containing 120 mM NaCl, 10 mM phospate

salt, 2.7 mM KCl, pH 7.4 (PBS from EMD, Billerica, USA) with final concentration of 3 mg/ml. The solution was sonicated for 30 minutes to completely dissolve mimLUB in the PBS solution, prepared using 18MΩ Milli-Q water (Millipore Corporation, Billerica, MA, USA). Fn solution of 1 mg/ml in PBS was obtained from Sigma-Aldrich (St. Louis, Missouri, USA). Lower concentration aliquots at 0.3 mg/ml were prepared and stored at $-80\,^{\circ}C$, and thaw when needed. All glassware used in the preparation was cleaned with ethanol and rinsed with DI.

5.4.3 Atomic force microscopy

Atomic force microscopy (AFM) measurements were performed in air using a commercial AFM (MFP-3D, Asylum, Sta. Barbara, CA, USA). SiO_2 probes monuted on k = 42 N/m levers with radius of curvature of 9 nm (AC160TS, Olympus, USA) were used for intermittent contact mode imaging. Images were taken over a range of 500 x 500 nm, at a frequency of 1 Hz and 1536 x 1536 pixels for maximal resolution. Image analysis was performed in Gwyddion (Czech Metrology Institute) and ImageJ (NIH). AFM samples consisted of freshly cleaved mica substrate, spin-coated at 2000 rpm with 100 μl of mimLub in DI solution at 0.3 mg/ml for one minute and left 4-5 hours for complete drying.

5.4.4 Surface Forces Apparatus

To measure the normal and shear forces between two mica surfaces as a function of surface separation (film thickness), the surface forces apparatus (SFA) Mark III was used (SurForce, LLC, Sta. Barbara, CA, USA). Two freshly cleaved back-silvered mica (S&J Trading, Australia) sections were glued onto half cylindrical silica discs with UV curing glue (Norlan 61, Cranbury, NJ, USA). Discs having a radius of curvature of R $\approx$ 2 cm were used for normal force measurements while discs having a radius of curvature of R $\approx$ 1 cm were used for shear force measurements. These discs were mounted in a cross-cylindrical configuration and the absolute separation distance, D, was measured in real time by multiple beam interferometry (MBI). Additionally, MBI was also used to quantify the contact diameter and the onset of damage of the shearing surfaces. Before functionalizing the mica surfaces, mica-mica contact in air was determined to obtain the reference distance, $D = 0$. To quantify the normal force, the lower surface was mounted onto a horizontal double cantilever spring (k = 590 N/m for normal forces characterization, and k = 1650 N/m for simultaneous normal and lateral forces studies) and displaced at $\approx$5 nm/s. To calculate the friction force, the upper surface was mounted onto a vertical double cantilever spring (k = 700 N/m) holding strain gauges. Shearing was achieved via a ceramic bimorph slider, and shearing velocites of V $\approx$ 0.3 μm/s, 3 μm/s, and 30 μm/s were used in our experiments. MBI fringes of equal chromatic order were collected with a SP2300 photospectrometer (Princeton Instruments, NJ, USA) with a 600 g/mm grating and 500 nm blaze, digitalized with a ProEM CCD camera (Princeton Instruments, NJ, USA), and visualized using Lightfield v4.0 (Princeton Instruments, NJ, USA). Friction voltages were acquired and quantified with a NI USB-6210 and LabView v8.6 (National Instruments, Austin, TX, USA), re-

spectively. Two protocols were carried out for mica surface functionalization. (i) mimLUB adsorbed on bare mica and (ii) mimLUB adsorbed on Fn-bound mica. For (i), freshly prepared mica surfaces were incubated with 50 μl mimLUB solutions at 3 mg/ml for one hour and rinsed with PBS. For (ii), freshly prepared mica surfaces were first incubated with 50 μl of Fn solution (0.3 mg/ml) for one hour and rinsed with PBS. After rinsing, 50 μl of bovine serum albumin (BSA) at 0.02 mg/ml were added for 30 min to block non-specific interactions, and rinsed with PBS. Finally, these Fn-bound mica surfaces were incubated with 50 μl mimLUB solutions at 3 mg/ml for one hour and rinsed with PBS. In addition, we used two different experimental conditions. Surfaces were sheared either in PBS or in mimLUB (3 mg/ml) solution. All surface functionalization steps were carried out with surfaces mounted on the SFA, yielding same adsorption on both surfaces. All steps were performed in a laminar flow cabinet to prevent particle contamination.

5.5 Results

5.5.1 Molecular characterization of mimLUB

We designed a polymer mimic of lubricin which molecular architecture is depicted in Figure 5.1A. The polymer was named mimLUB (pAA-g-PEG) because it resembles the architecture of native LUB. The mimLUB polymer possess a long central region with bottle-brush architecture composed of a flexible pAA backbone decorated with PEG side-chains. To determine the dimensions of single polymer molecules, we incubated freshly cleaved mica surfaces in a dilute

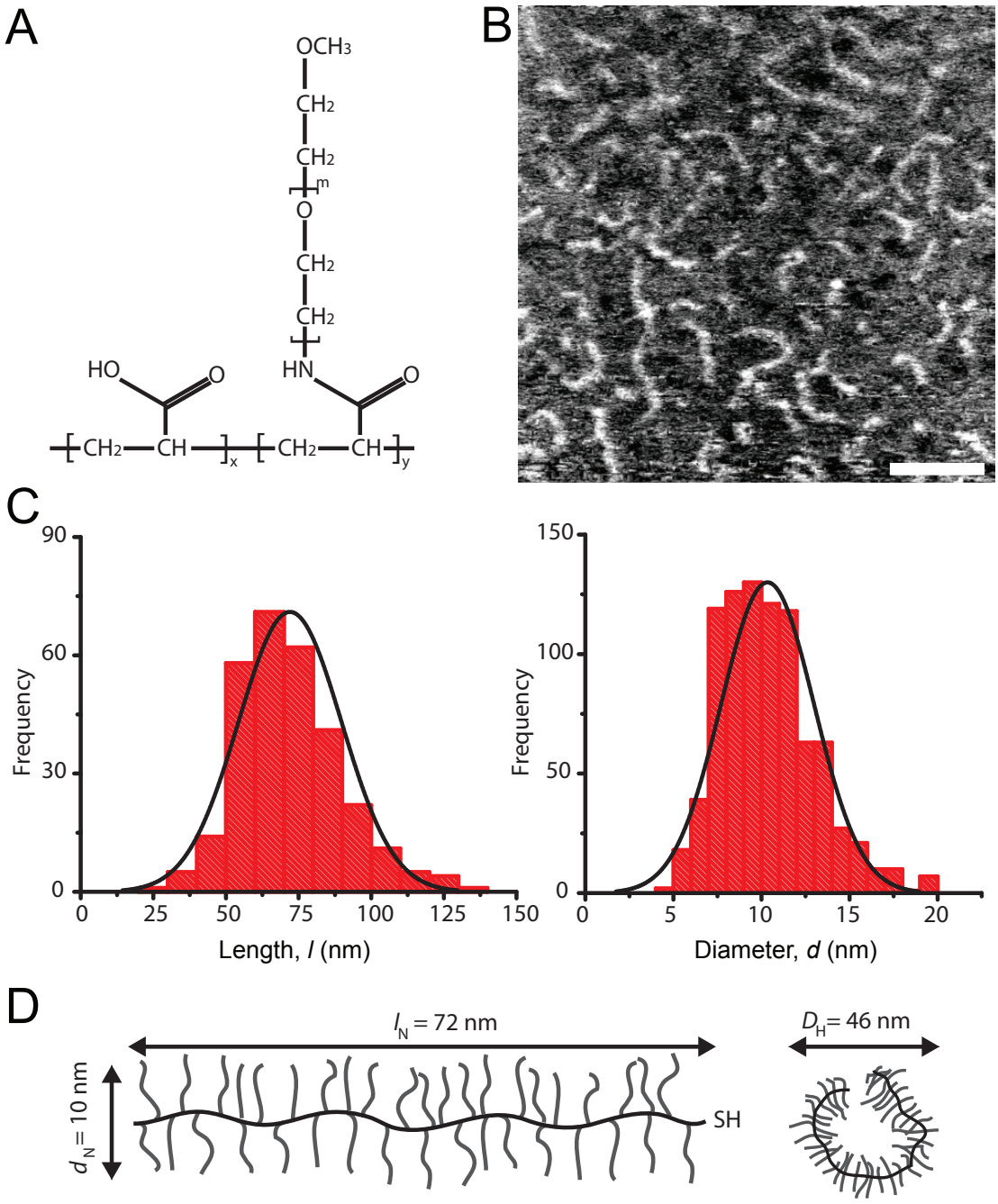

Figure 5.1: (A) Molecular structure of the pAA-PEG bottle-brush polymer mimLUB, with x~185 y~650, m~45, and MW ≈ 1400 kDa, (B) Tapping mode AFM height micrograph in air of the polymer chains adsorbed on a freshly cleaved mica surface from a solution at 300 μg/ml, scale bar = 50 nm, (C) number-average contour length l_N and number-average molecular diameter d_N, and (D) schematic representation of the mimLUB with l_N, d_N and hydrodynamic diameter D_H.

mimLUB solution (at 0.3 mg/ml) for 1 hour. After rinsing 3 times and drying, individual polymer chains were imaged in air using atomic force microscopy (AFM) in intermittent contact mode. As shown in Figure 5.1B, the molecules exhibit worm-like morphology. mimLUB molecules imaged via AFM, average contour length l_N and average diameter d_N (frequency histograms for l_N and d_N are displayed in Figure 5.1C) were 72 ± 18 nm and 10 ± 2.6 nm, respectively. The hydrodynamic diameter, D_H, quantified via dynamic light scattering, was 46 nm. All these measured molecular dimensions are summarized in Figure 5.1D. Additionally, the percent conjugation calculated from average molecular weight MW was 83%, the measured length polydispersity index PDI obtained from GPC-MALLS was MW/MN=1.3, and MW was 1400 kDa.

5.5.2 Role of fibronectin in normal interaction forces of mica surfaces across mimLUB

To determine whether the presence of an intermediate Fn layer between the mica substrate and the mimLUB alters the interaction force profile of the polymer, we first performed compressive measurements of mimLUB (in presence and absence of Fn) in phosphate buffer saline (PBS) at 25 °C using the SFA. Figure 5.2 shows the normal interaction forces, reported as $F_\perp/R$, $F_\perp$ being the normal force and R the surface curvature, between (i) mimLUB films directly adsorbed to mica surfaces and (ii) mimLUB films adsorbed to mica previously coated with Fn. In both cases, the interaction forces were purely repulsive (no measurable adhesion) and no hysteresis was observed at the approach/retraction speed of 5 nm/s (quasi-static regime). In absence of Fn, (Figure 5.2A) long-

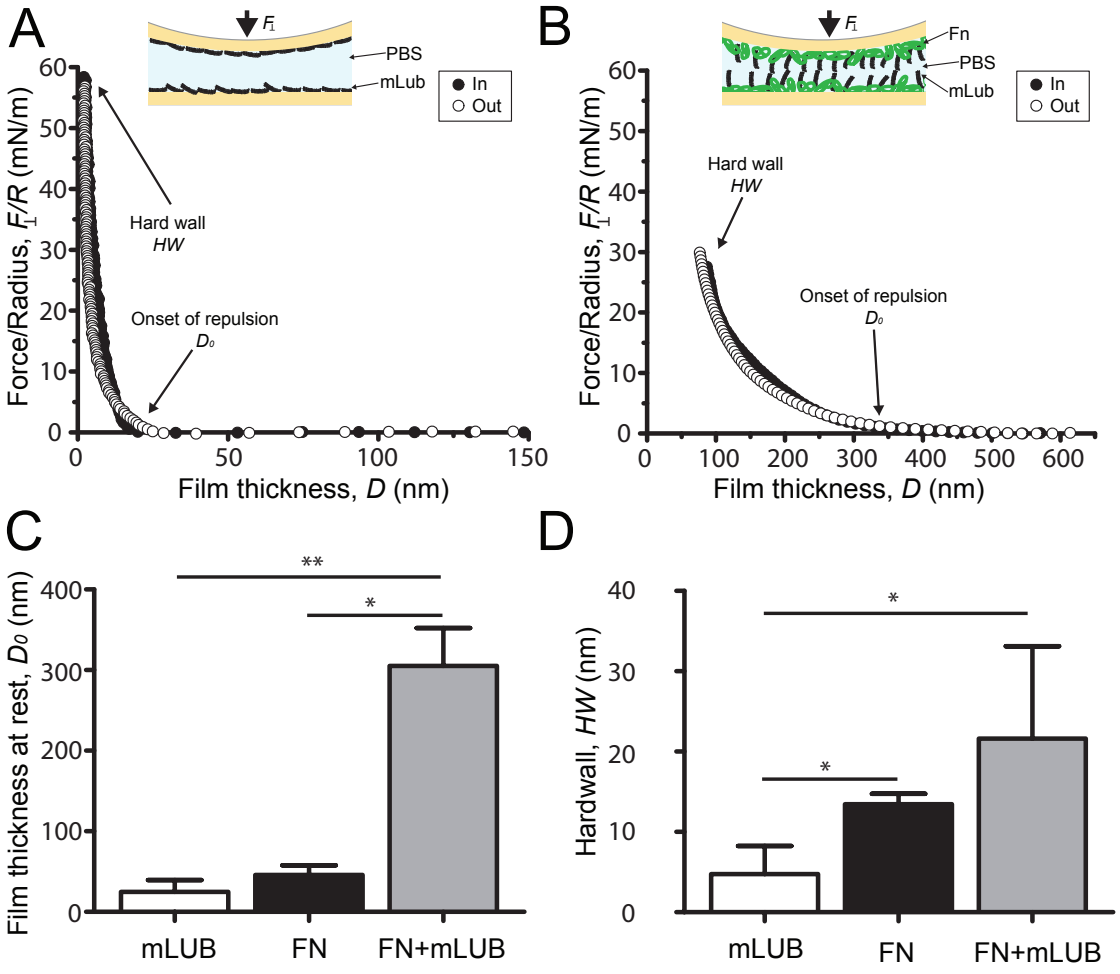

Figure 5.2: Normal force $F_\perp$ normalized by the surface radius of curvature R between mimLub molecules adsorbed on mica surfaces (A) and between two physisorbed Fn layers (B) on mica surfaces with mimLUB as a function of the mica-mica separation distance (film thickness), D. Forces on approach are shown by solid circles and on separation by open circles. Bar charts displaying the average value for film thickness at rest D_0 (C) and average value for the HW (D) for mimLUB adsorbed on mica (white), Fn only (black), and Fn+mimLUB (gray). Average + standard deviation reported. Values reported as mean + standard deviation. In all cases, $p < 0.05$ is indicated by a single star and $p < 0.01$ by two stars.

range interaction forces starting at 35 nm were systematically detected. The final mimLUB film thickness was 5 nm under a pressure of 0.5 MPa. In presence of Fn (Figure 5.2B), long-range interaction forces starting at 500 nm were detected. The final Fn+mimLUB film thicknesswas ≈85 nm under a pressure of 0.25 MPa. Note that prior to incubation with mimLUB (Fn film only), short-range interaction forces starting at 80 nm were detected, and the intermediate Fn film thickness was ≈40 nm at 0.25 MPa. These results suggest that Fn not only binds mimLUB molecules, but is also capable of maintaining them under confinement and prevents them from being expelled by the pressure. Additionally, the underlying Fn film is probably altering the preferred binding configuration of the molecules, given that the interaction forces start at much higher distances comparable to the contour length of the mimLUB molecules.

5.5.3 Role of fibronectin in lubrication and wear protection of mica surfaces by mimLUB

Whether the presence of an intermediate Fn layer between the mica and the mimLUB improved the lubrication and wear protection at the shearing junction was also investigated. To determine this, both the friction forces and the onset of surface damage were measured between the mica surfaces coated with mimLUB films (in presence and absence of Fn) and sheared either in PBS (Figure 5.3) or in dilute mimLUB medium (Figure 5.4), at 25 °C using the SFA.

In PBS, the lubrication properties of the polymer were found to be sensitive to the presence of Fn (Figure 5.3). As shown in Figure 5.3A, when mimLUB-coated surfaces (no Fn) were sheared, the measured friction forces $F_{\|}$, were si-

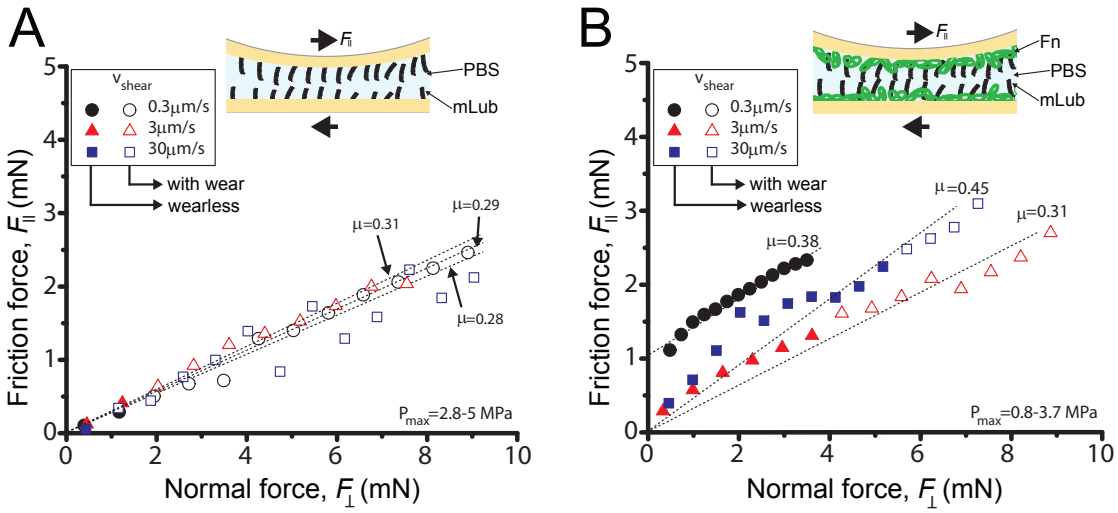

Figure 5.3: Friction force $F_{||}$ as a function of normal force $F_{\perp}$ between mica surfaces with adsorbed mimLub (A) and with physisorbed Fn layers with mimLub (B), both in PBS. The surfaces were sheared at sliding velocities of $V = 0.3\mu m/s$ (black circles), $V = 3\mu m/s$ (red triangles), and $V = 30\mu m/s$ (blue squares). Open symbols indicate measurements after the surfaces became damaged (with wear).

milar at all three shearing velocities and found to depend linearly on the applied normal load, $F_{\perp}$, vanishing at $F_{\perp} = 0$. The average friction coefficient μ, defined as $\Delta F_{||}/\Delta F_{\perp}$, was equal to 0.29 ± 0.01 and nearly identical for all speeds, at pressures up to 5 MPa. Importantly, shearing mimLUB in absence of Fn was systematically accompanied by (almost immediate) surface wear, triggered at extremely low loads ($F_{\perp} < 1$ mN) under all three sliding speed conditions. On the contrary, the friction forces measured on mimLUB in presence of Fn (Figure 5.3B) were sensitive to shearing velocity, did not depend linearly on the applied load $F_{\perp}$, and did not vanish at $F_{\perp} = 0$, particularly at the intermediate sliding speed (V = 3 μm/s). The average friction coefficients μ (estimated from the linear portion of the friction curves), ranged from 0.31 ± 0.01 (V = 3 m/s) to 0.38 ± 0.01 (V = 0.3 μm/s). Interestingly, shearing mimLUB in presence of Fn at V

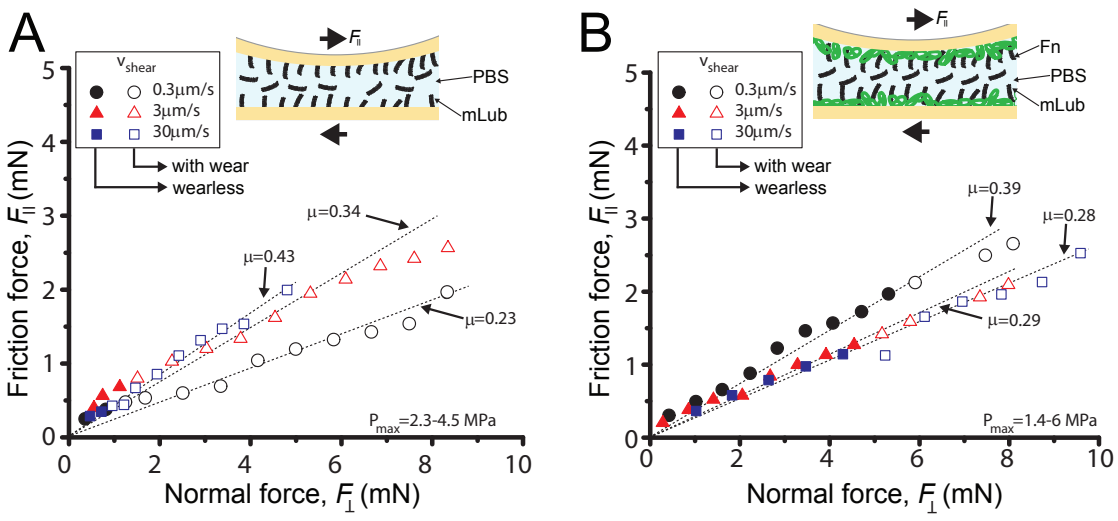

Figure 5.4: Friction forces $F_{||}$ as a function of the normal force $F_{\perp}$ between mica surfaces with adsorbed mimLub (A) and with physisorbed Fn layers with mimLub (B) in PBS with free mimLub ($C_{mimLub} = 3mg/ml$) in the solution. The surfaces were sheared at sliding velocities of $V = 0.3\mu m/s$ (black circles), $V = 3\mu m/s$ (red triangles), and $V = 30\mu m/s$ (blue squares). Open symbols indicate measurements after the surfaces became damaged (with wear).

= 0.3 μm/s (lowest shearing speed) was never accompanied by surface wear up to pressures of 0.8 MPa, while wear was triggered only at loads of 3.6 mN and 5 mN (corresponding to pressures of 1.5 MPa and 1.7 MPa, well into the physiological range [Morrell et al., 2005]) at speeds of V = 3 μm/s and 30 μm/s, respectively.

When sheared in mimLUB media (3 mg/ml) instead of PBS, the tribological properties of the polymer were found to be even more sensitive to the presence of Fn (Figure 5.4). Although all measured friction forces depended linearly on the applied normal load $F_{\perp}$ (vanishing at $F_{\perp} = 0$) at all sliding speeds, and exhibited similar friction coefficients, the presence of Fn had a drastic effect on surface protection. As shown in Figure 5.4A, when mimLUB-coated mica sur-

faces (no Fn) were sheared in mimLUB media, the average friction coefficients μ, were found to increase slightly with sliding speed, ranging from 0.23 ± 0.01 (V = 0.3 μm/s) to 0.43 ± 0.01 (V = 30 μm/s). Here too, the absence of Fn led to surface wear that was systematically observed at extremely low loads ($F_\perp$ ¡ 1 mN), under all three sliding speeds conditions. Shearing in presence of Fn had little effect on the measured friction coefficients μ, ranging from 0.28-0.29 ± 0.01 (V = 3 μm/s and 30 μm/s) to 0.39 ± 0.01 (V = 0.3 μm/s), however, it drastically deferred surface damage that was triggered only for $F_\perp > 4.5$ mN, i.e. for pressures above 1.3 MPa, well into the physiological range.

5.5.4 Role of fibronectin on mimLUB confinement and overall film viscosity

To understand the role of Fn on the confinement of mimLUB molecules in the shearing junction and to estimate overall film viscosity, the film thickness was monitored during shearing in absence and presence of Fn, at both low (Figure 5.5A and B) and high (Figure 5.5C and D) shearing velocities.

The shear viscosity of the confined film is given by [Luengo et al., 1997]:

$$\eta = \frac{5F_{\|}}{16\pi RVlog\frac{2R}{D}} \tag{5.1}$$

where R is the curvature of the surfaces, V the shearing velocity, D the average film thickness and $F_{\|}$ the maximal shear force. The results show (Figures 5.6A and 5.6B) a monotonic dependence with respect to the shear rate, which corresponds to shear thickening of the films. When shearing in presence PBS,

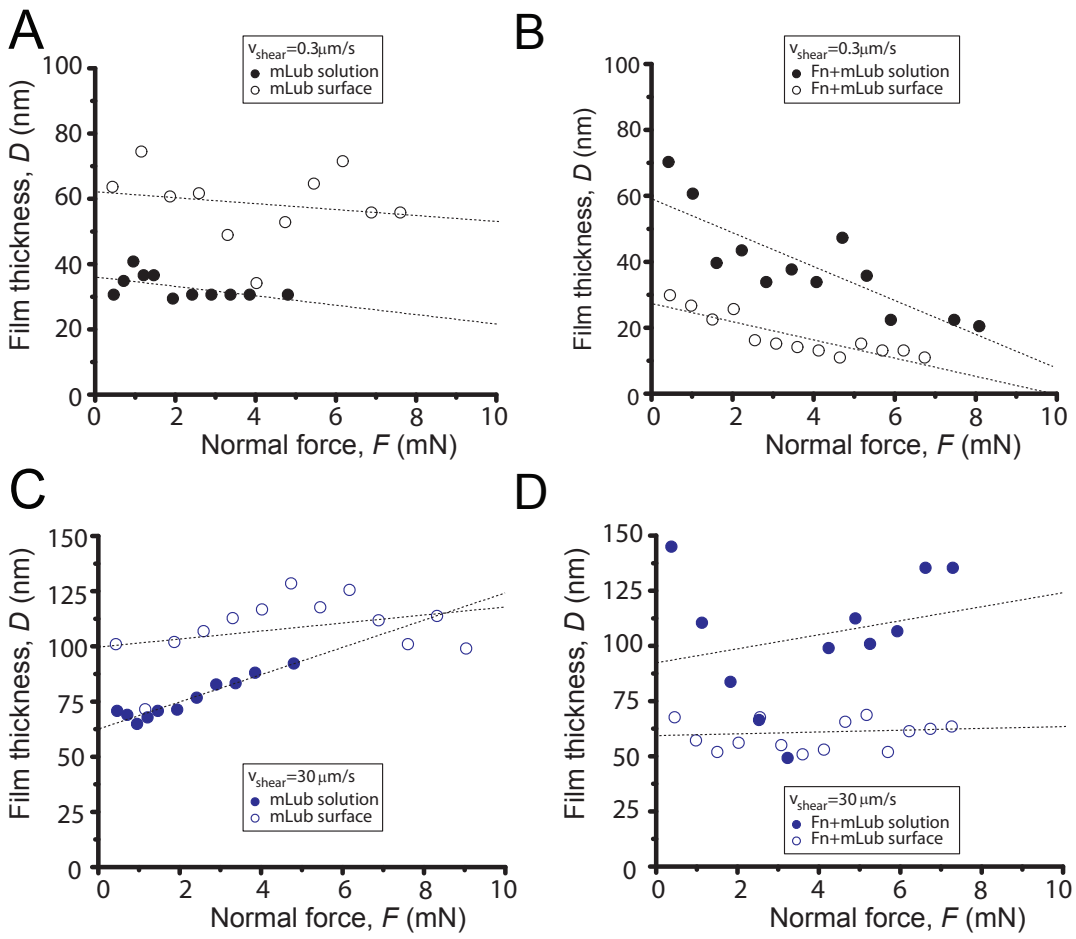

Figure 5.5: Film thickness D measured as a function of normal force $F_\perp$ at sliding velocities of $V = 0.3\mu m/s$ (A-B) and $V = 30\mu m/s$ (C-D).

the viscosity η was found to be very similar to the the viscosity η when seared in mimLUB media (3 mg/ml), for all three investigated shearing velocities. However, the overall viscosity for each shearing velocity was found to be higher for surfaces sheared in presence of Fn (25%, 35%, and 60% for 0.3 μm/s, 3 μm/s, and 30 μm/s, respectively).

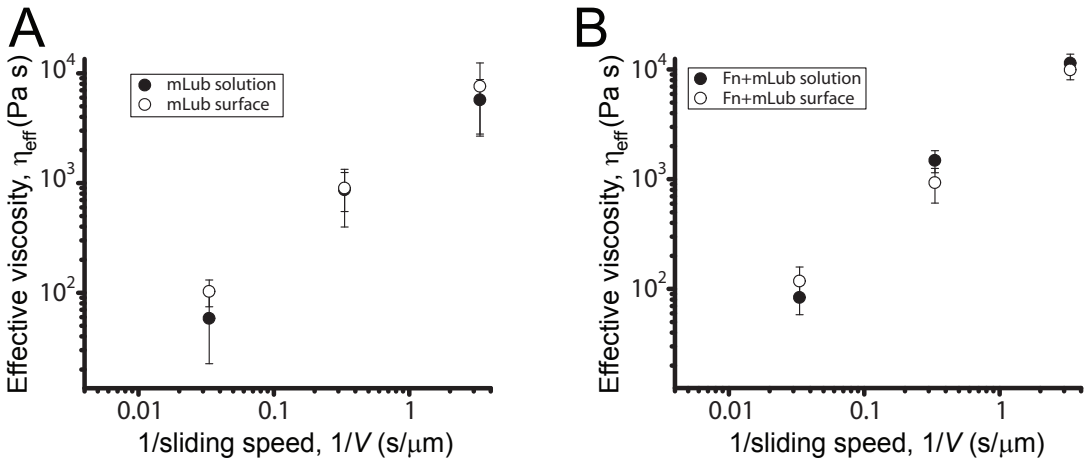

Figure 5.6: Experimental effective viscosity of the confined solutions between the surfaces. Results showing that the viscosity of the confined film is inversely proportional to sliding speed, without Fn (A) and with Fn (B) adsorbed to mica surfaces.

5.6 Discussion

Imaging of the mimLUB single molecules was facilitated by the PEG side chains. Some of the side chains were tightly adsorbed to the mica substrate, while others were desorbed and aggregated on top of the pAA backbone. The adsorbed side chains helped to isolate the various macromolecules, while the desorbed side chains enhanced the topographic contrast between the mica substrate and the macromolecule, yielding a delineated mimLUB molecule. Furthermore, strong steric repulsion between the adsorbed side chains forced the partial extension of the pAA backbone [Sheiko and Möller, 2001]. The measured l_N (72 nm) was very close to the calculated value of the fully extended pAA backbone, 101 nm, based on CC bond length and C-C-C angle. However, the measured d_N (10 nm) was three times smaller than the calculated value, 30 nm, based on C-C, C-O bond lengths and C-C-C and C-O-C angles. The measured d_N value was still within the same order of magnitude and suggests that the PEG side chains

were not fully stretched.

For both testing conditions of mimLUB either adsorbed onto bare mica or adsorbed onto Fn-bound mica, electrostatic interactions were expected to be hindered by the ionic strength of the PBS buffer solution, with an estimated Debye length λ_D smaller than 1 nm [Tadmor et al., 2002b]. However, this did appear to be the case, therefore it is safe to assume that the long range repulsive forces observed in Figure 5.2A and Figure 5.2B are purely of steric origin and not ionic.

During the experiment with bare mica and absorbed mimLUB a repulsive exponential behavior began at 35 nm when the surfaces began contact, as would be expected for an electrostatic double layer interaction. This distance corresponds to a film thickness t_{LR} of approximately two molecular diameters d_N and a final HW value of ≈5 nm, which corresponds to one half of the measured polymer brush diameter. This can be interpreted as an expulsion of mimLUB molecules upon confinement, where only one mimLUB molecule thick layer remained trapped and highly compressed. In this configuration, mimLUB molecules are weakly physisorbed and can easily be removed by the shear forces applied by the fluid flowing away from the confinement zone. However, when mimLUB was adsorbed onto an underlying Fn film, long range interaction forces and HW values increased considerably. The long range interaction started at ≈300 nm (onset of repulsion of Fn only started at ≈45 nm) and HW at ≈20 nm. This long range interaction value suggests that the mimLUB molecules are firmly bound to the underlying Fn film, and pointing perpendicular to the underlaying substrate. mimLUB molecules could be binding to the underlying Fn film via disulfide bonds, likely to happen with Fn cysteins present in Fn. HW

values further confirm that mimLUB molecules remain at the junction upon confinement. The difference in HW between bare Fn and Fn incubated with mimLUB suggest that the mimLUB molecules that were originally pointing straight up have been bent, probably building a polymer loop that lacks the capability of interacting with Fn with its other naked end-domain, even after strong compression (pressure ≈0.5 MPa). This mimLUB feature could indeed prevent the building of bridges between opposing surfaces, since no measurable adhesion was ever detected with mimLUB incubated in Fn films. The highly hydrated PEG side chains are most probably giving rise to strong steric repulsion and aiding in maintaining a hydration shield that prevents molecular interpenetration.

SFA measurements suggest that mimLUB l_N is ≈125 nm, which in fact is very close to the theoretical value and almost twice as long as the measured values via AFM. The difference can be a consequence of the highly hydration of the PEG side chains decorating the pAA backbone, forcing it to be in a fully stretched configuration, a condition that is not fulfilled during AFM dry imaging.

When shearing mimLUB adsorbed on bare mica, either in PBS or free floating in solution, no lubrication and wear protection was detected. When mimLUB free floating molecules were present, the onset of wear was slightly delayed. This condition only reaffirms the fact that mimLUB molecules are only weakly physisorbed onto the negatively charged mica substrate. In addition, wear debris is almost immediately released, building aggregates that act as small bearings that aid in maintain the surfaces sliding against each other with low shearing forces, corresponding to friction coefficients of the order of ≈0.25,

typical values found in damaged sliding systems. This lack in lubrication is a consequence of the poor binding capabilities of the mimLUB to the underlying mica substrate. When shearing Fn+mimLUB incubated surfaces, wear protection was consistently observed up to pressures 5 MPa. This confirms the fact that a boundary lubricant needs to remain bound to the protecting surface. Additionally, PEG side chains are highly hydrated, creating a sharp interface (at least until damage begins) which prevents interpenetration and keeps the shearing junction sliding smoothly.

5.7 Conclusion

We propose a lubricant whose molecular architecture is inspired in boundary molecule that is naturally present in synovial fluid, and can be used for treatment of damaged cartilage surfaces or artificial joints, such as the knee or hip. When mimLUB alone, wear protection and lubrication was observed, however, when combined with Fn, mimLUB lubricates and protects the surfaces until reaching a critical normal load. This is due to the fact of remaining firmly attached to the protecting surface. These results reaffirm findings that a boundary lubricant needs to remain bound to the protecting surface. In addition, functionalizing mimLUB molecules with a positively end-domain, such as poly-L-lysine could drastically enhance the tethering properties of the mimLUB molecules to negatively charged surfaces, which are commonly found in biological systems, such as the cartilage surface. Further, exploring mimLUB polymers with different backbone and side-chain sizes, functionalization of the binding end domain with different peptides or functional groups, together with varying grafting rations could yield lubricating molecules with specific applications which could

be easily designed in the laboratory.

5.8 Acknowledgements

Kirk J. Samaroo & Eddward Bonnevie for enriching discussions. Funding by NSF under award 1031068 (to DG), NIH/NCI under award 1R21CA161532 (DG), CONACYT (to RCAE), and the Cornell Center for Materials Research through Award Number (NSF DMR-1120296). SEC was performed at the Biophysics Resource of Keck Facility at Yale University. The SEC-LS/UV/RI instrumentation was supported by NIH Award Number 1S10RR023748-01. The content of this paper is solely the responsibility of the authors and does not necessarily represent the official views of the National Institutes of Health.

CHAPTER 6

CONCLUSIONS

6.1 Summary

Fn is present in various tissues at different concentrations, conformations, and distributions, and it regulates many fundamental biological processes. Fn is one of the primary components secreted and assembled in an ECM. Its assembly and remodelling are ubiquitous in living systems. The way in which Fn is initially synthesized and deposited determines its biological performance. When assembly is dysregulated, the biological response is usually manifested as disease. For example, adipocytes in adipose tissue can acquire cancer-associated fibroblastic features in response to tumor-derived cues, thus participating in dysregulated ECM deposition leading to enhanced angiogenesis, enhancing tumor growth. In boundary lubrication of articular cartilage, it is critical to protect and maintain the articular ECM (cartilage) surface as functional. This is achieved by a delicate balance between biomechanical and biochemical cues, including surface active boundary lubricating molecule concentrations. If this balance is not maintained, the development of OA can occur. This dissertation presents investigations on the role of Fn in the mediation of ECM stiffness and boundary lubrication in the context of breast tumor growth and joint lubrication, respectively. Chapter 3 investigates the correlation between ECM stiffness, topology, Fn molecular conformation and the ECM dysregulation on cell adhesion and VEGF secretion. Chapter 4 examines the ability of Fn to tether LUB, HA, SA, and SF to cartilage, in order to provide lubrication and wear protection, while chapter 5 examines the lubrication and wear protection ability of a mimetic LUB. The chapter pre-

sented here reports the main findings of the thesis and lists potential future experiments to complement the research.

The studies presented in Chapter 3 showed that when exposed to breast tumor soluble factors (extracted from MDA-MB231 cell line), adipose stromal cell, assembled an ECM with Fn upregulation. This upregulation consisted of a thicker and denser matrix, with thicker diameter Fn fibers, and with Fn conformation within fibrils more unfolded and with a narrower distribution, than when compared to ECMs assembled by unexposed adipose stromal cells. Combined, upregulated properties increased the ECM overall stiffness. Reseeding ECMs with unexposed adipose stromal cells showed that cellular adhesion decreased, while VEGF secretion increased for stiffer matrices comprised of thicker fibers, denser network, and more unfolded Fn. VEGF secretion is a crucial hallmark of cancer, since it is required for angiogenesis hence tumor vascularization. These results are an important contribution for the understanding of tumor development and vascularization. Additionally, they also provide new insights into the structure-mechanics relationship of protein networks by enhancing the knowledge of cell-matrix mechanobiological interactions. The latter may be exploited for other biomaterials-based applications including advanced tissue engineering approaches.

The studies presented in Chapter 4 demonstrated that Fn effectively tethers LUB (and maybe PL) to cartilage, remaining tightly bound among all SF components. We used Fn bound mica substrates as an *in vitro* model of cartilage superficial zone's Fn. Molecular film structural changes were consistently measured for Fn+SF components under confinement. Interestingly, all films were well described by a polymer brush model, showing a long and a short range

interaction regime. This behavior is well suited to load bearing, as opposed to other configurations. Remarkably, from the selected molecular components, only pure LUB and LUB molecules that remained bound from SF showed lubrication and wear protection capabilities. We know that LUB possesses a bottle-brush molecular architecture, which has been proposed as a key signature for boundary lubricants. This is in addition to selective binding domains, which allow LUB molecules to remain attached to the underlying surface. Dimensional similarities between the measured films and normal interaction profiles for LUB and SF suggest that the components that remained attached from the latter consist of LUB molecules, possibly decorated with other components present in SF, such as PL or other glycosaminoglycans or glycoproteins. As far as we know, this is the first study that explores the synergistic interactions of Fn with SF components under confinement and shear. Our results suggest that Fn, which is present only in the superficial zone of articular cartilage, plays an important role in tethering boundary lubricating molecules to the surface of articular cartilage, assisting in the protection and lubrication of diarthrodial joints at pressures up to 14 MPa.

The studies presented in Chapter 5 demonstrate that a mimetic LUB (mimLUB), inspired by the bottle-brush architecture of native LUB, is capable of differentially modifying the coefficient of friction and of providing wear protection when incubated on Fn saturated mica surfaces and sheared. The mimLUB molecules were not capable of protecting negatively-charged bare mica surfaces, due in part to the mimLUB's inability to remain bound upon confinement. The lubricating properties are probably a consequence of the combined effects of binding capabilities (to the underlying Fn film) and the high hydration properties of the decorating side chains, consisting of polyethylene glycol.

These findings demonstrate that the proposed mimLUB may be a feasible alternative to treating lack of lubrication and damaged cartilage, two conditions present in joint diseases such as OA.

In combination, the studies reported within this dissertation confirm our hypothesis that Fn is a multifunctional glycoprotein involved in the regulation of two very different but equally important biological environments. Fn conformation and its role in modulating matrix stiffness have been directly correlated at the molecular and cellular scales for the first time. Our findings also demonstrate Fn's capability to effectively tether lubricating molecules and aid in joint lubrication. Our results shed light on LUB-Fn synergistic mechanisms that could contribute to creating functional tissue engineering techniques.

6.2 Future directions

While this dissertation provides key answers to some fundamental questions regarding Fn's role in tumor development and joint lubrication, the number of open questions that arise from the research performed is high. Specifically, Fn is only one of many molecules that are involved in regulating the complex machinery that is the human body. In order to understand the collective interactions in which Fn is involved in more depth, the following paragraphs present some possible future research projects that could continue shedding light on the roles of Fn in tumorigenesis and joint lubrication.

6.2.1 Cell type generalization and 3-D studies

While the results of the studies presented so far are specifically for mouse preadypocites, the model system utilized herein is well suited to evaluate how other cell types present in the breast stroma assemble a Fn matrix when exposed to tumor-conditioned media. Among these cells are fibroblasts, endothelial cells, and immune cells such as macrophages, or even tumor cells, which may also respond to Fn conformational changes. Altered ECM mechanics, composition, and topology for some of the aforementioned cell types are worth evaluating in future studies.

Our experimental setup studies cell-matrix interactions in a *2-D* environment. However, signaling in response to dysregulated Fn matrix conformations, mechanics, topology, and composition can vary in a *3-D* culture environment. Therefore, utilization of 3-D scaffolds is strongly encouraged. The aforementioned suggestions combined, could lead to a generalization of cellular behavior in tumor development, which would have broad implications, not only for the fundamental understanding of tumor development, but for the field of tissue engineering.

6.2.2 Conformation-dependent binding of lubricin to fibronectin

Since the binding activity of Fn to other molecules is to some extent conformational dependent, investigation of the binding kinetics of LUB upon Fn conformations is important to further identify Fn-LUB binding domains. These can

be approached by using FRET to characterize the molecular conformation of Fn fibers. By stretching (straining) Fn fibers, cryptic binding sites on Fn are exposed because of partial unfolding of the weakest Fn type III modules. FRET-labeled Fn can be used as a ruler for mapping molecular conformations and local strains on manually-extruded Fn fibers from a high concentration solution. The manually extruded Fn fibers will be deposited on top of micro-patterned elastic PDMS substrates, which can be stretched in the focal plane of a confocal microscope in the presence of LUB labeled with a third, longer wave emitting fluorophore. Images of fluorescent LUB can be acquired simultaneously to later be colocalized with the underlying FRET-labeled Fn fibers. Preliminary results following the aforementioned approach are presented in Appendix C.

Binding kinetics experiments can be repeated after treating extruded Fn fibers with peptides known to bind to specific Fn domains, such as PUR4 peptides. These would block cell binding domains on Fn (domains III_{8-10}). Alternatively, HEP could be used to block domains I_{1-5} and III_{12-14} and further test the hypothesis that LUB utilizes the HEP-like domain to bind to Fn.

Since LUB is in a natural competitive state when present in SF with many other glycoproteins and proteglycans, we propose an approach based on the previously described method. Single labeled Fn fibers can be extruded as previously explained and strained in a confocal microscope stage in the presence of the labeled LUB. In this experiment, a third competing single labeled molecule, such as HA, can be added to the LUB solution. Images of LUB and HA can be acquired simultaneously to later be colocalized with the underlying single-labeled Fn fiber. With this approach, competing sites or synergy sites could be identified, followed by, again, peptide, HEP, or Fn fragments treated before per-

forming the binding experiments.

6.2.3 Bi- and multi-synovial fluid component shear experiments on fibronectin films

Since Fn-LUB binding studies are relevant for understanding the role of Fn in joint lubrication, shear experiments using the Surface Forces Apparatus will be needed to complement the picture. In addition to LUB, aggrecans are known to associate with HA, building a brush structure. Among our findings is the fact that Fn tethers HA but does not provide wear protection when sheared. By adding LUB or aggrecan in increasing concentrations to Fn-bound HA, a plot dose-coefficient of friction response could be obtained, in order to determine (by approximate calculations) the number of LUB/aggrecan molecules per HA molecule needed in order to ”switch” HA to a lubricating and wear-protecting condition.

Similarly, the SFA studies could be complemented by exposing the underlying Fn film to peptides, such as PUR4, HEP, or larger Fn fragments, in order to block possible LUB binding domains and further explore the binding mechanisms of LUB to the underlying surfaces. One advantage of the SFA is that samples can be ”treated” *in situ*. That is, the SFA allows the addition of solutions such as enzymes in real time to explore effects of molecular cleavage on the wear protection and friction behavior of the lubricating molecules.

6.2.4 Tweaking mimetic polymer brushes and exposing them to real biological systems

While the studies documented here on mimetic LUB polymer brushes deal with only one configuration, *i.e.* fixed backbone - sidechain - grafting density, architectural parameters such as backbone size, sidechain length, grafting density, and binding terminal are synthesis parameters that our collaborators have exploited. However, how the polymer brush design parameters affect lubrication and wear protection have not yet been tested for lubrication. The tribological characterization can be performed by means of SFA shearing experiments according to what was described in Chapter 5. Different binding domains can be functionalized at the end domain of the polymer brushes in order to optimize and force selective binding of the polymers to tissue components, enhancing surface attachment and possibly providing better wear protection. In addition, in our studies concentrations used were based on weight concentrations rather than molar concentrations. The latter could provide a better one-to one comparison of lubricating performance when directly compared to LUB.

Finally, if the mimetic LUB polymer brush is to be a possible treatment for damaged joints, its tribological performance in the presence of SF components must be addressed. A direct approach would be, for example, to test tribological performances of OA synovial fluid and compare them to tribological performance of healthy SF. Experiments would culminate by adding the mimetic LUB polymer brush to OA synovial fluid by monitoring the changes, if any, of its tribological performance.

APPENDIX A

APENDIX: COLLABORATIVE PROJECTS

In addition to the work presented so far as the main content of the thesis, I have been and am involved in a number of collaborative projects. Since these projects are not primarily my own work, they are here presented with the abstracts.

A.1 Past collaborations

A.1.1 Implanted adipose progenitor cells as physicochemical regulators of breast cancer

Work by Emily M. Chandler, Bo Ri Seo, Joseph P.Califano, **Roberto C. Andresen Eguiluz**, Jason S. Lee, Christine J. Yoon, David T. Tims, James X. Wang, Le Cheng, Sunish Mohanan, Mark R. Buckley, itai Cohen, Alexander Yu Nikitin, Rebecca M. Williams, Delphine Gourdon, Cynthia A. Reinhart-King, and Claudia Fischbach has been published in *Proc Natl Acad Sci U S A*. 2012 Jun 19;109(25):9786-91.

Abstract

Multipotent adipose-derived stem cells (ASCs) are increasingly used for regenerative purposes such as soft tissue reconstruction following mastectomy; however, the ability of tumors to commandeer ASC functions to advance tumor progression is not well understood. Through the integration of physical sci-

ences and oncology approaches we investigated the capability of tumor-derived chemical and mechanical cues to enhance ASC-mediated contributions to tumor stroma formation. Our results indicate that soluble factors from breast cancer cells inhibit adipogenic differentiation while increasing proliferation, proangiogenic factor secretion, and myofibroblastic differentiation of ASCs. This altered ASC phenotype led to varied extracellular matrix (ECM) deposition and contraction thereby enhancing tissue stiffness, a characteristic feature of breast tumors. Increased stiffness, in turn, facilitated changes in ASC behavior similar to those observed with tumor-derived chemical cues. Orthotopic mouse studies further confirmed the pathological relevance of ASCs in tumor progression and stiffness in vivo. In summary, altered ASC behavior can promote tumorigenesis and, thus, their implementation for regenerative therapy should be carefully considered in patients previously treated for cancer.

A.1.2 Controlling Adhesion and Elasticity of Mytilus edulis Foot Protein-1 Films via DOPA-DOPA Crosslinking

Work by Rebecca M. Schur, **Roberto C. Andresen Eguiluz**, Heather K. Schopper, and Delphine Gourdon, *in preparation*

Abstract

Adhesive proteins from marine mussels have long been studied for their potential biomedical and environmental applications. Mytilus edulis foot protein-1 (mefp-1) forms the protective outer layer which coats the mussels adhe-

sive construct. This protein has demonstrated remarkable adhesive and mechanical properties which are mediated by 3,4-dihydroxyphenylalanine (DOPA) residues and their unique ability to form both covalent and metal coordination crosslinks. In this study, AFM force spectroscopy was used to investigate the effects of crosslink formation on the adhesion and elasticity of mefp-1 films adsorbed onto mica substrates at pH 5.5 to a spherical silica bead. The natural crosslinking interactions of mefp-1 were mimicked in vitro by adding Fe^{3+}, a cation which forms octahedral complexes with three DOPA groups. Covalent diDOPA linkages were produced following the addition of $NaIO_4$, an oxidizing agent, to the mefp-1 films. In the absence of crosslinkers, mefp-1 demonstrated (i) high adhesion, (ii) an ability to spontaneously bridge an opposing surface, and (iii) long-range adhesion due to extensible mefp-1 chains at the surface of the film. With the addition of Fe^{3+} and $NaIO_4$, cohesion and elastic modulus of the protein films increased and adhesion was significantly reduced. Crosslinking removed the spontaneous bridging previously observed. Only Fe^{3+} crosslinks allowed adhesion to be maintained over a long range. The ability to manipulate adhesion and elasticity of mefp-1 through crosslinks will be used in the future development of coatings and interfaces with tunable properties.

A.2 Current collaborations

A.2.1 Obesity-dependent changes of interstitial ECM mechanics and their role in breast tumorigenesis

Work by Bo Ri Seo, Jacqueline Gonzalez, P. Bhardwaj, **Roberto C. Andresen Eguiluz**, Karin Wang, H. Sha, S. Mohanan, Rebecca M. Williams, L. T. Vahdat, L. Qi, O. Reizes, A. J. Dannenberg, Delphine Gourdon, Claudia Fischbach, *in preparation*.

Abstract

Obesity and extracellular matrix (ECM) stiffness are considered independent risk and prognostic factors for breast cancer. Whether they are functionally linked is uncertain. Here, we investigated the hypothesis that obesity enhances local myofibroblast content in mammary adipose tissue and that these stromal changes increase malignant potential via enhancing interstitial ECM stiffness. Indeed, mammary fat of both diet- and genetically-induced mouse models of obesity were enriched for myofibroblasts and stiffness-promoting ECM components. These differences were related to varied adipose stromal cell (ASC) characteristics as ASCs isolated from obese mice contained more myofibroblasts and deposited denser and stiffer ECMs relative to ASCs from lean control mice. Accordingly, decellularized matrices from obese ASCs stimulated mechanosignaling and thereby the malignant potential of breast cancer cells. Finally, the clinical relevance and translational potential of our findings were supported by analysis of patient specimens and the observation that caloric restriction in

a mouse model reduces myofibroblast content in mammary fat. Collectively, these findings suggest that obesity-induced interstitial fibrosis promotes breast tumorigenesis via the alteration of mammary ECM mechanics with important implications for anti-cancer therapies and adipose tissue-based reconstructive approaches following mastectomy.

APPENDIX B

APENDIX: MATLAB CODES FOR ELASTIC MODULI EXTRACTION

This program processes force-distance profiles and outputs onset of interaction D_0, elastic modulus E, percentage of strain used in the calculations ϵ, force-distance profile with fitted data, linearized force-distance profiles (F vs. $\frac{(D_0-D)^2}{D_0}$) by minimizing the error. The strain regime used for the fit can be hard-coded, as well as the strain increase, $\Delta\epsilon$. This code was developed by Dr. Juan Carlos Andresen.

```
function finalList = getAllFiles(dirName,pattern)

  dirData = dir(dirName);%# Get the data for the current directory
  dirIndex = [dirData.isdir];%# Find the index for directories
  fileList = {dirData(~dirIndex).name}';%'# Get a list of the files
  if ~isempty(fileList)
    fileList = cellfun(@(x) fullfile(dirName,x),...%# Prepend path to files
                       fileList,'UniformOutput',false);
  end
  subDirs = {dirData(dirIndex).name};%# Get a list of the subdirectories
  validIndex = ~ismember(subDirs,{'.','..'});%# Find index of subdirectories
  %#   that are not '.' or '..'
  for iDir = find(validIndex)%# Loop over valid subdirectories
    nextDir = fullfile(dirName,subDirs{iDir});%# Get the subdirectory path
    fileList = [fileList; getAllFiles(nextDir)];%# Recursively call getAllFiles
  end
  finalList={};
  for idx = 1:numel(fileList)
      if not(isempty(findstr(fileList{idx},'xlsx')))
          &findstr(fileList{idx},pattern)
```

```
            finalList{end+1}=fileList{idx};
        end
    end
    finalList=finalList';
end


function out = juan(pattern,outputFileName)
%get file list of *.xlsx files with filename pattern
%output file name is the name of the file where all the data will
%be stored ADDITIONALLY to the standart output file which is the
%name of the XLXS file but with the .csv extension

%We write the header of the data of the output file name, in this case
%the file is allways opened to append additional data. We never loose
%data.
OFILE=fopen(outputFileName,'a');
fprintf(OFILE,'#Filename\tSheet Nr.\tE\tD0\tPercent of fitted data
relative to D0\tError of data to fit\n');
fclose(OFILE);

%get all files with extension xlsx in the current directory and
%filenames that match the given pattern
files=getAllFiles('.',pattern);
%Go over all files that match the pattern
for idx=1:numel(files)
    %Get Excel Sheet Number from fileName
    fileName=files{idx};
    [~,sheet]=xlsfinfo(fileName);
    sheetTotalNumber=numel(sheet);
    %Open the data file, here the filename is 'hardcoded' as the name of
    %the original xlsx file with an other extention. The file is always
```

```
%rewritten such that previous data in the file is lost.
FILE=fopen(strrep(fileName,'.xlsx',strcat('.csv')),'w');
fprintf(FILE,'#Filename\tSheet Nr.\tE\tD0\tPercent of fitted data
relative to D0\tError of data to fit\n');
fclose(FILE);
%Go over all excel sheets
for sheetNumber= 1:sheetTotalNumber
    fprintf('\nAnalyzing sheet nr. %d\n',sheetNumber);
    clearvars temp;
    %Read data from xlsx file
    data = xlsread(fileName,sheetNumber);
    %Catch errors, if the sheet file is empty it is skipped
    if(isempty(data))
        warning('No data in sheet %d of file %s, skipping sheet',...
            sheetNumber,fileName);
        pause;
        continue;
    end
    %Determine the minimum and maximum of the data read
    ymin = min(data(:,2)); ymax = max(data(:,2));
    %We hard code 40 steps to analyze the "best" fit. This can be
    %chenged if needed
    for i = 1:1
        %Again the percent range we look at is hard coded, it can be
        %changed if needed
        percent=0.10 + 0.001*i;
        %If it is In or Out determines if the first value is the
        %smallest or the largest, as we look for D0 as the first
        %value that crosses y=0 we need to know if it is In or Out
        %and pick the right D0. This is done here.
        if data(1,2)<data(length(data),2)
            D0=data(find(data<0,1,'last')-length(data),1);
```

```
else
    temp(1,:)=fliplr(data(:,1)');
    temp(2,:)=fliplr(data(:,2)');
    data=temp';
    D0=data(find(data<0,1,'last')-length(data),1);
    data
end
%If D0 is empty, means that the data does not cross the y=0
%axis. Therefore we cannot determine D0 and the data set is
%skipped. We break the loop and set the boolean variable to
%false to continue; the next loop.
if isempty(D0)
    DoesCrossZero=false;
    break;
else
    DoesCrossZero=true;
end
%l is the actual fitting range defined by the percentage
%hard coded above and D0
l=D0-D0*percent;
%keeps data that satifies the wanted conditions defined by
%D0 and the hard coded percentage
fdata = data(data(:,1)>l&data(:,1)<D0,:);
%performs linear fit for slope, where y = F/R,
%x = (D-D0)^2/D0, y = mx
clearvars x;
x = (fdata(:,1)-D0).^2/D0;
slope = x(:)\fdata(:,2);
err= sum( sqrt( (fdata(:,2) - slope* x).^2 ) )/length(x);
E=slope;
%Stores the values of this run in result
result(i,2)=E;
```

```
    result(i,3)=err;
    result(i,1)=percent*100;
end
%Catching errors: If the data did not cross in the previous
%inner loop this loops continues; and the data set is skipped.
%If you do not want to press any key each time you can comment
%the pause command
if not(DoesCrossZero)
    warning('Data in file %s and sheet %d\n do not cross Zero,
    skipping file,\npress any button to continue'...
        ,fileName,sheetNumber);
    pause;
    continue;
else
    fprintf('Plotting data from file\n%s \nand
    sheed %d out of %d',...
        fileName,sheetNumber,sheetTotalNumber);
end
%Store best value E as min of all the possible %
E=min(result(:,2));
%Plot of the evolution of E and error as a function of the %
%included in the fit
close all; figure('Units', 'pixels','Position', [100 100 500 375]);
semilogy(result(:,1),result(:,2),'-b');
hold on;
[minval,ind] = min(result(:,2));
[Y,Z] = ind2sub([size(result(:,2),1) size(result(:,2),2)],ind);
percent=result(Y,1);
semilogy(result(:,1),result(:,3),'-r');
plot (percent*[1 1],[min(result(:,3)),max(result(:,2))],'-g');
hold on;
l={};
```

```
xlabel('Indentation % from D_0');
ylabel('E / Error');
l{1}=sprintf('E_{min}=%1.3f and
Indentation=D_{0}*%% =%1.2f*%1.2f%%=%1.2f',...
    min(result(:,2)),D0,percent/100,percent*D0/100);
l{2}=sprintf('Error=|(f(x_i)-Y_i)|/N = %1.4f',result(Y,3));
legend(l);
hold off;
%Save the generated plot into the file
saveas(gcf,strrep(fileName,'.xlsx',strcat('_sheet_nr_',...
    num2str(sheetNumber),'_Error.pdf')),'pdf');
%Plot of the best fit with the original data
figure;
plot(data(:,1),data(:,2));
hold on;
x_values = linspace(data(1,1),data(end,1),100);
y_values = (x_values-D0).^2/D0*E;
plot(x_values,y_values,'-r');
plot( D0 * [1 1], [-0.1 4],'-g');
%axis([20 35 -0.1 4]);
xlabel('D');
ylabel('F/R');
l ={'Original data (Y_i)'};
l{2} = sprintf('D_{0}=%1.3f E=%1.3f Percent:%1.1f%%',D0,E,percent);
legend(l);
%Save the generated plot into the file
saveas(gcf,strrep(fileName,'.xlsx',strcat('_sheet_nr_',...
    num2str(sheetNumber),'_Data.pdf')),'pdf');
hold off;
%Plot of the best fit with the original data in linear
%representation and the range where it should be linear from 0
%to D1=((D0-percent*D0)-D0)^2/D0=percent^2*D0
```

```
figure;
%Here we just set the minus for the values that are negative
%since it gets lost when squaring
x=data(:,1);
for i = 1:numel(x)
    if data(i,1)<=D0
        x(i)=(data(i,1)-D0)^2/D0;
    else
        x(i)=-(data(i,1)-D0)^2/D0;
    end
end
plot(x,data(:,2));
hold on;
x_values = linspace(x(1,1),x(end,1),100);
y_values = x_values*E;
Dl=(percent/100).^2*D0;
plot(Dl*[1 1],[min(y_values) max(y_values)],'-g')
plot(x_values,y_values,'-r');
%axis([-0.5 2.5 -1 4.5]);
xlabel('(D-D_0)^2/D_0');
ylabel('F/R');
l ={'Original data'};
l{2} = sprintf('D_{0}=%1.3f E=%1.3f Percent:%1.1f%%',D0,E,percent);
legend(l);
%Save the generated plot into the file
saveas(gcf,strrep(fileName,'.xlsx',strcat('_sheet_nr_',...
    num2str(sheetNumber),'_DataLin.pdf')),'pdf');
hold off;
%Write data file with default naming
FILE=fopen(strrep(fileName,'.xlsx',strcat('.csv')),'a+');
fprintf(FILE,'%s\t%d\t%0f\t%0f\t%0f\t%0f',fileName,sheetNumber,...
    E,D0,percent);
```

```
        fprintf(FILE,'\n');
        fclose(FILE);
        %Write data file with given nameing
        OFILE=fopen(outputFileName,'a');
        fprintf(OFILE,'%s\t%d\t%0f\t%0f\t%0f\t%0f',fileName,sheetNumber,...
            E,D0,percent);
        fprintf(OFILE,'\n');
        fclose(OFILE);
        %Clear the variables used to avoid size not matching when
        %overriding them.
        clearvars data,result,x,slope,D0,err,E,fdata,slope;
        fprintf('Sheet nr. %d finished.\n',sheetNumber);


    end
end
```

APPENDIX C

APENDIX: FN STRAIN-INDUCED UNFOLDING APPEARS TO PROMOTE LUB AND PAA-*G*-PEG BINDING

In addition to the work presented so far as the main content of the thesis, I have been involved in strain-binding studies of labeled Fn-fibers exposed to labeled LUB and labeled mimLUB, following similar protocols published by Klotzsch *et al.* [Klotzsch et al., 2009].

To test whether LUB binds to Fn in a strain dependent manner, we extruded Fn fibers (10% of the Fn was single labeled with Alexa Fluor 488) from a 0.3 mg/ml solution and deposited across microfabricated trenches on an elastic PDMS substrate. Fn fibers were then passivated in a BSA solution (0.02 mg/ml) for 30 minutes. We then stretched single Fn fibers in the focal plane of a confocal microscope in presence of LUB ($0.2 mg/ml$) labeled with a longer wavelength emitting fluorophore, Alexa Fluor 633. Signals of labeled-Fn and labeled-LUB were acquired simultaneously and the intensity ration (IR) calculated. Using the same protocol, we characterized the binding behavior of a pAA-*g*-PEG polymer (105 kDa - 5 kDa) fluorescently labeled with Alexa Fluor 594.

C.1 Materials and methods

C.1.1 Microfabrication of master mold

A photosensitive Cr mask plate was directly patterned using a DWL 2000 (Heidelberg Instruments, Germany). The patterned mask was then used to expose Si-wafers containing a permanent epoxy negative photoresist.

N-type Si-wafers were used as substrates and prepared following standard photolithographic techniques. A permanent epoxy negative photoresist (SU-8 2000, MicroChem, MA) was spin coated at 500 rpm for 10 seconds with an acceleration of 100 rpm/s, followed by a spin at 2000 rpm for 30 seconds with an acceleration of 300 rpm/s. Once spin coating was finished, edge bid was removed with acetone. Immediately after edge bid removal, Si-wafers were soft baked using a hot plate at 95°C for 4 minutes, before exposure. Using a long pass filter to eliminate UV-radiation below 350 nm, Si-wafers were exposed with high intensity UV light with an exposure dose of 150 mJ/cm^2 (ABM Contact Aligner, CA), followed by a post exposure bake at 95°C for 5 minutes. At this stage, Si-wafers were immersed in acetone accompanied by gentle agitation of the solution during 5 minutes. This step that developed the latent image. After obtaining the image, Si-wafers were rinsed twice with isopropyl alcohol and finished with a hard bake at 150°C for 5 minutes. All aforementioned parameters were optimized for each newly opened SU-8 photoresist bottle. However, the given parameters were (and may be) used as starting values.

C.1.2 PDMS patterning and preparation

PDMS was prepared using a standard Sylgard® 184 silicon elastomer kit (Corning, NY). Freshly prepared PDMS mixture was stored at −20°C for 24 hours and allowed to degas. A silicon wafer containing the patterns (negative of the trenches) was mounted on a spinning disc at 2000 rpm and treated with a siliconizing reagent (Sigmacote®, Sigma-Aldrich, MO) by pouring 1-2 ml over the spinning wafer. This step prevented PDMS from sticking to the Si-wafer, making the peeling process easier. Following the degasing and drying of the

wafer, PDMS was poured over the Si-wafer (≈2 gr.), and cured at 60°C for at least 1 hour. Once these steps were completed, the patterned PDMS elastomer was carefully peeled and further treated. PDMS substrates patterned with 50 μm wide trenches were hydrophilized with oxygen plasma for 1 minute at medium intensity (Harrick Plasma, NY), followed by silanization with a 1% (3-aminopropyl)triethoxysilane (3-APTES) solution during 15 minutes. This step was finalized by thoroughly rinsing with Milli-Q water, then inked with glutaraldehyde and left to dry for 30 minutes, and finished with another Milli-Q water wash before Fn was extruded and deposited. This process ensured covalent attachment of the manually extruded and deposited Fn fibers to the underlying PDMS substrate, minimizing slippage during straining.

C.2 Preliminary strain-binding results

C.2.1 LUB binds to Fn in a strain dependent manner

Using the approach detailed in Materials and methods (section C.1), the strain-binding behavior of a 633-labeled LUB to 488-labeled Fn was investigated. PDMS patterned with 50μm wide trenches were functionalized as previously described. Manually extruded and deposited Fn fibers across PDMS containing microfabricated trenches were strained in the focal plane of a confocal microscope with a homemade uniaxial strain device. Fibers were immersed in PBS solution containing free floating labeled LUB (0.2 mg/ml) for 30 minutes, and the interactions as a function of strain were measured. After each straining step, fibers were left 30 minutes at constant strain to allow LUB to interact with

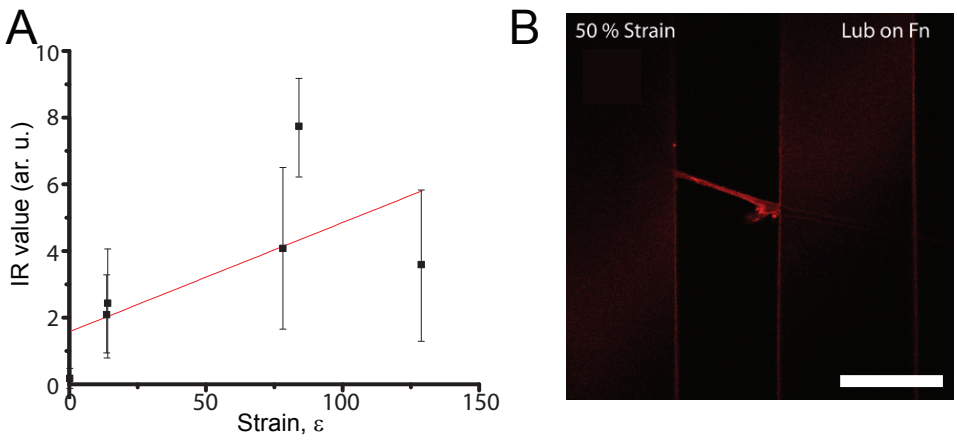

Figure C.1: (A) Plot of 633 labeled LUB strain-dependent binding to Fn fibers using the relative intensity ratio (IR value) of Alexa-633 to Alexa-488 as a function of strain. (B) Image of 633 labeled Lub additive binding at 14% strain. Scale bar = 50μm.

Fn. Figure C.1A shows the relationship between the strain of Fn fibers and the binding of free LUB. A positive trend is observed indicating strain-dependent binding behavior. This increased binding was observed in the images, as aggregation around the fiber (see figure C.1B). Strain trials were conducted up to 127% microscopic strain.

C.2.2 pAA-*g*-PEG binds to Fn in a strain dependent manner

In previous preliminary studies, pAA-*g*-PEG polymers were determined to interact with Fn if some degree of denaturation was present. As the amount of polymer interacting with Fn can depend on the degree of Fn III unfolding, strain-binding behaviour of a 594-labeled pAA-*g*-PEG to 488-labeled Fn was investigated. Figure C.2A depicts the relationship observed in the experimental set between the strain of the Fn fiber and the binding of free pAA-*g*-PEG. A fairly strong positive trend is observed indicating strain-dependent binding

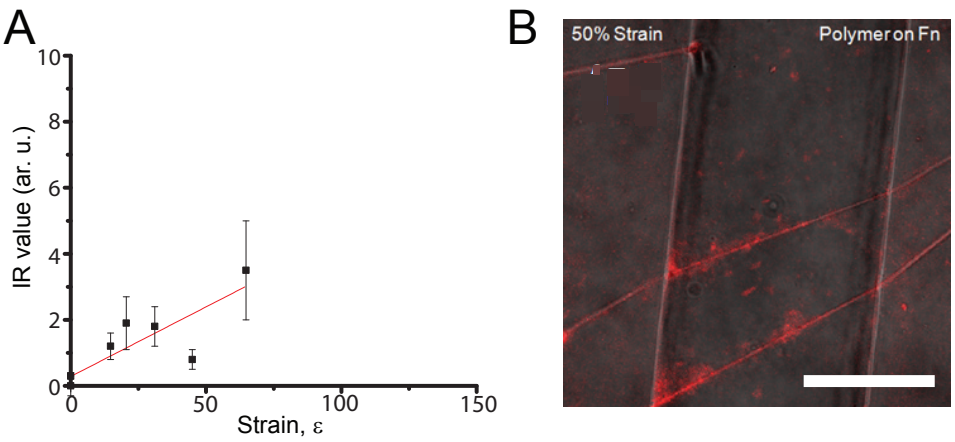

Figure C.2: (A) Plot of a 4 mg/ml solution of 105 kDa-5 kDa pAA-PEG polymer binding in a strain-dependent manner to Fn fibers. Measurements were done using the relative intensity ratio (IR value) of Alexa-594 to Alexa-488 as a function of strain. (B) Image of 594-labeled B-Lub polymer additive binding at 14% macroscopic strain. Scale bar = 50μm.

behavior. This increased binding was visually observed in the images as aggregation around the fiber from a previously uniform distribution within the solution, figure C.2B. Strain trials were conducted up to 150% macroscopic strain; however, microscopic strain analysis indicated lower true strain values of the fibers, which likely lie in the linear regime of uncoiling Fn.

BIBLIOGRAPHY

[Akiyama et al., 1995] Akiyama, S. K., Olden, K., and Yamada, K. M. (1995). Fibronectin and integrins in invasion and metastasis. *Cancer and Metastasis Reviews*, 14(3):173–189.

[Altroff et al., 2003] Altroff, H., Choulier, L., and Mardon, H. J. (2003). Synergistic activity of the ninth and tenth FIII domains of human fibronectin depends upon structural stability. *Journal of Biological Chemistry*, 278(1):491–497.

[Anderson, 2001] Anderson, J. M. (2001). Biological responses to materials. *Annual Review of Materials Research*, 31:81–110.

[Antia et al., 2008] Antia, M., Baneyx, G., Kubow, K. E., and Vogel, V. (2008). Fibronectin in aging extracellular matrix fibrils is progressively unfolded by cells and elicits an enhanced rigidity response. *Faraday Discussions*, 139:229.

[Antia et al., 2006] Antia, M., Islas, L. D., Boness, D. a., Baneyx, G., and Vogel, V. (2006). Single molecule fluorescence studies of surface-adsorbed fibronectin. *Biomaterials*, 27(5):679–90.

[Aota et al., 1991] Aota, S., Nagai, T., and Yamada, K. M. (1991). Characterization of regions of fibronectin besides the arginine-glycine-aspartic acid sequence required for adhesive function of the cell-binding domain using site-directed mutagenesis. *The Journal of Biological Chemistry*, 266(24):15938–43.

[Assoian and Klein, 2008] Assoian, R. K. and Klein, E. a. (2008). Growth control by intracellular tension and extracellular stiffness. *Trends in Cell Biology*, 18(7):347–52.

[Bailey, 2001] Bailey, a. (2001). Molecular mechanisms of ageing in connective tissues. *Mechanisms of Ageing and Development*, 122(7):735–755.

[Balazs, 2009] Balazs, E. a. (2009). The role of hyaluronan in the structure and function of the biomatrix of connective tissues. *Structural Chemistry*, 20(2):233–243.

[Baneyx et al., 2001] Baneyx, G., Baugh, L., and Vogel, V. (2001). Coexisting conformations of fibronectin in cell culture imaged using fluorescence resonance energy transfer. *Proceedings of the National Academy of Sciences of the United States of America*, 98(25):14464–8.

[Banquy et al., 2014a] Banquy, X., Burdyska, J., Lee, D. W., Matyjaszewski, K., and Israelachvili, J. (2014a). Bioinspired bottle-brush polymer exhibits low friction and Amontons-like behavior. *Journal of the American Chemical Society*, 136(17):6199–202.

[Banquy et al., 2014b] Banquy, X., Lee, D. W., Das, S., Hogan, J., and Israelachvili, J. N. (2014b). Shear-induced aggregation of mammalian synovial fluid components under boundary lubrication conditions. *Advanced Functional Materials*, pages n/a–n/a.

[Bhushan, 2013] Bhushan, B. (2013). *Introduction to Tribology*. John Wiley & Sons.

[Bissell and Hines, 2011] Bissell, M. J. and Hines, W. C. (2011). Why don't we get more cancer? A proposed role of the microenvironment in restraining cancer progression. *Nature Medicine*, 17(3):320–9.

[Bissell and Radisky, 2001] Bissell, M. J. and Radisky, D. (2001). Putting tumors in context. *Nature Reviews Cancer*, 1:46–54.

[Brittain and Minko, 2007] Brittain, W. and Minko, S. (2007). A structural definition of polymer brushes. *Journal of Polymer Science Part A: Polymer Chemistry*, 45:3505–3512.

[Butcher et al., 2009] Butcher, D. T., Alliston, T., and Weaver, V. M. (2009). A tense situation: forcing tumour progression. *Nature Reviews. Cancer*, 9(2):108–22.

[Caino et al., 2013] Caino, M. C., Chae, Y. C., Vaira, V., Ferrero, S., Nosotti, M., Martin, N. M., Weeraratna, A., Connell, M. O., Jernigan, D., Fatatis, A., Languino, L. R., Bosari, S., and Altieri, D. C. (2013). Metabolic stress regulates cytoskeletal dynamics and metastasis of cancer cells. *Journal of Clinical Investigation*, 123(7):2907–2920.

[Caligaris and Ateshian, 2009] Caligaris, M. and Ateshian, G. A. (2009). Effects of Sustained Interstitial Fluid Pressurization Under Migrating Contact Area, and Boundary Lubrication by Synovial Fluid, on Cartilage Friction. *Osteoarthritis Cartilage*, 16(10):1220–1227.

[Calvo et al., 2013] Calvo, F., Ege, N., Grande-Garcia, A., Hooper, S., Jenkins, R. P., Chaudhry, S. I., Harrington, K., Williamson, P., Moeendarbary, E., Charras, G., and Sahai, E. (2013). Mechanotransduction and YAP-dependent matrix remodelling is required for the generation and maintenance of cancer-associated fibroblasts. *Nature Cell Biology*, 15(6):637–46.

[Cao and Langer, 2010] Cao, Y. and Langer, R. (2010). Optimizing the delivery of cancer drugs that block angiogenesis. *Science Translational Medicine*, 2(15):15ps3.

[Castelló-Cros and Cukierman, 2009] Castelló-Cros, R. and Cukierman, E. (2009). Stromagenesis during tumorigenesis: characterization of tumor-associated fibroblasts and stroma-derived 3D matrices. *Methods in Molecular Biology*, 522:275–305.

[Chandler et al., 2011] Chandler, E. M., Saunders, M. P., Yoon, C. J., Gourdon, D., and Fischbach, C. (2011). Adipose progenitor cells increase fibronectin matrix strain and unfolding in breast tumors. *Physical Biology*, 8(1):015008.

[Chandler et al., 2012] Chandler, E. M., Seo, B. R., Califano, J. P., Andresen Eguiluz, R. C., Lee, J. S., Yoon, C. J., Tims, D. T., Wang, J. X., Cheng, L., Mohanan, S., Buckley, M. R., Cohen, I., Nikitin, A. Y., Williams, R. M., Gourdon, D., Reinhart-King, C. a., and Fischbach, C. (2012). Implanted adipose progenitor cells as physicochemical regulators of breast cancer. *Proceedings of the National Academy of Sciences of the United States of America*, 109(25):9786–9791.

[Chang et al., 2009] Chang, D. P., Abu-lail, N. I., Coles, J. M., Guilak, F., Gregory, D., and Zauscher, S. (2009). Friction force microscopy of lubricin and hyaluronic acid between hydrophobic and hydrophilic surfaces. *Soft Matter*, 5(18):3438–3445.

[Chang et al., 2013] Chang, D. P., Guilak, F., Jay, G. D., and Zauscher, S. (2013). Interaction of lubricin with type II collagen surfaces: adsorption, friction, and normal forces. *Journal of Biomechanics*, pages 1–8.

[Chen et al., 2009] Chen, M., Briscoe, W. H., Armes, S. P., and Klein, J. (2009). Lubrication at physiological pressures by polyzwitterionic brushes. *Science*, 323(5922):1698–701.

[Chen and Israelachvili, 1991] Chen, Y. L. and Israelachvili, J. N. (1991). New Mechanism of Cavitation Damage. *Science*, 252(5009):1157–1160.

[Chevalier, 1993] Chevalier, X. (1993). Fibronectin, cartilage, and osteoarthritis. *Seminars in Arthritis and Rheumatism*, 22(5):307–18.

[Cinti, 2012] Cinti, S. (2012). The adipose organ at a glance. *Disease Models & Mechanisms*, 5(5):588–94.

[Coles et al., 2010] Coles, J. M., Zhang, L., Blum, J. J., Warman, M. L., Jay, G. D., Guilak, F., and Zauscher, S. (2010). Loss of cartilage structure, stiffness, and frictional properties in mice lacking PRG4. *Arthritis and Rheumatism*, 62(6):1666–74.

[Cox and Erler, 2011] Cox, T. R. and Erler, J. T. (2011). Remodeling and homeostasis of the extracellular matrix: implications for fibrotic diseases and cancer. *Disease Models & Mechanisms*, 4(2):165–78.

[Critchley, 2009] Critchley, D. R. (2009). Biochemical and structural properties of the integrin-associated cytoskeletal protein talin. *Annual Review of Biophysics*, 38:235–54.

[Curran and Keely, 2013] Curran, C. S. and Keely, P. J. (2013). Breast tumor and stromal cell responses to TGF-β and hypoxia in matrix deposition. *Matrix Biology*, 32(2):95–105.

[Dahl et al., 1985] Dahl, L. B., Dahl, I. M., Engström-Laurent, a., and Granath, K. (1985). Concentration and molecular weight of sodium hyaluronate in synovial fluid from patients with rheumatoid arthritis and other arthropathies. *Annals of the Rheumatic Diseases*, 44(12):817–22.

[Das et al., 2013] Das, S., Banquy, X., Zappone, B., Greene, G. W., Jay, G. D., and Israelachvili, J. N. (2013). Synergistic interactions between grafted hyaluronic acid and lubricin provide enhanced wear protection and lubrication. *Biomacromolecules*, 14:16691677.

[Davis et al., 1979] Davis, W., Lee, S., and Sokoloff, L. (1979). A proposed model of boundary lubrication by synovial fluid: structuring of boundary water. *Journal of Biomechanical Engineering*, 101(3):185–192.

[De et al., 2005] De, S., Razorenova, O., McCabe, N. P., O'Toole, T., Qin, J., and Byzova, T. V. (2005). VEGF-integrin interplay controls tumor growth and vascularization. *Proceedings of the National Academy of Sciences of the United States of America*, 102(21):7589–94.

[De Wever et al., 2008] De Wever, O., Demetter, P., Mareel, M., and Bracke, M. (2008). Stromal myofibroblasts are drivers of invasive cancer growth. *International Journal of Cancer*, 123(10):2229–38.

[Dedinaite, 2012] Dedinaite, A. (2012). Biomimetic lubrication. *Soft Matter*, 8(2):273.

[Dickinson et al., 1994] Dickinson, R. B., Guido, S., and Tranquillo, R. T. (1994). Biased cell migration of fibroblasts exhibiting contact guidance in oriented collagen gels. *Annals of Biomedical Engineering*, 22(4):342–56.

[Dong et al., 2009] Dong, R., Lindau, M., and Ober, C. K. (2009). Dissociation behavior of weak polyelectrolyte brushes on a planar surface. *Langmuir*, 25(8):4774–9.

[Egeblad et al., 2010] Egeblad, M., Rasch, M. G., and Weaver, V. M. (2010). Dynamic interplay between the collagen scaffold and tumor evolution. *Current Opinion in Cell Biology*, 22(5):697–706.

[Elsaid et al., 2007] Elsaid, K., Chichester, C., and Jay, G. (2007). Lubricin purified from bovine synovial fluid and from articular cartilage exhibit similar binding affinities to cartilage matrix proteins. *Transactions of the Orthopaedic Research Society*, 32:551.

[Elsaid et al., 2005] Elsaid, K. a., Jay, G. D., Warman, M. L., Rhee, D. K., and Chichester, C. O. (2005). Association of articular cartilage degradation and loss of boundary-lubricating ability of synovial fluid following injury and inflammatory arthritis. *Arthritis and Rheumatism*, 52(6):1746–55.

[Elter et al., 2012] Elter, P., Lange, R., and Beck, U. (2012). Atomic force microscopy studies of the influence of convex and concave nanostructures on the adsorption of fibronectin. *Colloids and Surfaces. B, Biointerfaces*, 89:139–46.

[Engler et al., 2006] Engler, A. J., Sen, S., Sweeney, H. L., and Discher, D. E. (2006). Matrix elasticity directs stem cell lineage specification. *Cell*, 126(4):677–89.

[Estrella et al., 2010] Estrella, R. P., Whitelock, J. M., Packer, N. H., and Karlsson, N. G. (2010). The glycosylation of human synovial lubricin: implications for its role in inflammation. *The Biochemical Journal*, 429(2):359–67.

[Eyre et al., 2004] Eyre, D. R., Pietka, T., Weis, M. A., and Wu, J.-J. (2004). Covalent cross-linking of the NC1 domain of collagen type IX to collagen type II in cartilage. *The Journal of Biological Chemistry*, 279(4):2568–74.

[Fan et al., 2012] Fan, J., Myant, C., Underwood, R., and Cann, P. (2012). Synovial fluid lubrication of artificial joints: protein film formation and composition. *Faraday Discussions*, 156:69.

[Fan et al., 2006] Fan, X., Lin, L., and Messersmith, P. B. (2006). Cell fouling resistance of polymer brushes grafted from ti substrates by surface-initiated polymerization: effect of ethylene glycol side chain length. *Biomacromolecules*, 7(8):2443–8.

[Fischbach et al., 2009] Fischbach, C., Joon, H., Hsiong, S. X., Evangelista, M. B., Yuen, W., and Mooney, D. J. (2009). Cancer cell angiogenic capability is regulated by 3D culture and integrin engagement. *Proceedings of the National Academy of Sciences of the United States of America*, 106(2):399–404.

[Forster and Fisher, 1996] Forster, H. and Fisher, J. (1996). The influence of loading time and lubricant on the friction of articular cartilage. *Proceedings of the Institution of Mechanical Engineers*, 210:109–119.

[Fraley et al., 2010] Fraley, S. I., Feng, Y., Krishnamurthy, R., Kim, D.-H., Celedon, A., Longmore, G. D., and Wirtz, D. (2010). A distinctive role for focal adhesion proteins in three-dimensional cell motility. *Nature Cell Biology*, 12(6):598–604.

[Friedland et al., 2009] Friedland, J. C., Lee, M. H., and Boettiger, D. (2009). Mechanically activated integrin switch controls alpha5 beta1 function. *Science*, 323(January):642–644.

[Geiger, 2001] Geiger, B. (2001). Cell biology. Encounters in space. *Science*, 294(5547):1661–3.

[Gleghorn et al., 2009] Gleghorn, J. P., Jones, A. R. C., Flannery, C. R., and Bonassar, L. J. (2009). Boundary mode lubrication of articular cartilage by recombinant human lubricin. *Journal of Orthopaedic Research*, 27(6):771–7.

[Gourdon et al., 2008] Gourdon, D., Lin, Q., Oroudjev, E., Hansma, H., Golan, Y., Arad, S., and Israelachvili, J. (2008). Adhesion and stable low friction provided by a subnanometer-thick monolayer of a natural polysaccharide. *Langmuir*, 24(4):1534–40.

[Grant et al., 1997] Grant, R. P., Spitzfaden, C., Altroff, H., Campbell, I. D., and Mardon, H. J. (1997). Structural requirements for biological activity of the ninth and tenth FIII domains of human fibronectin. *Journal of Biological Chemistry*, 272(10):6159–6166.

[Greene et al., 2011] Greene, G. W., Banquy, X., Woog, D., Lowrey, D. D., Yu, J., and Israelachvili, J. N. (2011). Adaptive mechanically controlled lubrication

mechanism found in articular joints. *Proceedings of the National Academy of Sciences of the United States of America*.

[Hartung et al., 2008] Hartung, W., Drobek, T., Lee, S., Zürcher, S., and Spencer, N. D. (2008). The influence of anchoring-group structure on the lubricating properties of brush-forming graft copolymers in an aqueous medium. *Tribology Letters*, 31(2):119–128.

[Heuberger et al., 2005a] Heuberger, M., Drobek, T., and Spencer, N. D. (2005a). Interaction forces and morphology of a protein-resistant poly(ethylene glycol) layer. *Biophysical Journal*, 88(1):495–504.

[Heuberger et al., 2005b] Heuberger, M. P., Widmer, M. R., Zobeley, E., Glockshuber, R., and Spencer, N. D. (2005b). Protein-mediated boundary lubrication in arthroplasty. *Biomaterials*, 26(10):1165–73.

[Hills and Crawford, 2003] Hills, B. and Crawford, R. (2003). Normal and prosthetic synovial joints are lubricated by surface-active phospholipid. *The Journal of Arthroplasty*, 18(4):499–505.

[Hills, 2002] Hills, B. A. (2002). Surface-active phospholipid : a Pandora s box of clinical Part II . Barrier and lubricating properties. *Internal Medicine Journal*, 32:242–251.

[Horkay et al., 2008] Horkay, F., Basser, P. J., Hecht, A.-M., and Geissler, E. (2008). Gel-like behavior in aggrecan assemblies. *The Journal of Chemical Physics*, 128(13):135103.

[Huang et al., 2001] Huang, N.-p., Michel, R., Voros, J., Textor, M., Hofer, R., Rossi, A., Elbert, D. L., Hubbell, J. A., and Spencer, N. D. (2001). Poly (L -lysine) - g -poly (ethylene glycol) Layers on Metal Oxide Surfaces: Surface-Analytical Characterization and Resistance to Serum and Fibrinogen Adsorption. *Langmuir*, 17(6):489–498.

[Hughes et al., 2005] Hughes, L. C., Archer, C. W., and ap Gwynn, I. (2005). The ultrastructure of mouse articular cartilage: collagen orientation and implications for tissue functionality. A polarised light and scanning electron microscope study and review. *European Cells & Materials*, 9(0):68–84.

[Hunziker, 2010] Hunziker, E. B. (2010). *Regenerative medicine and biomaterials for the repair of connective tissues*. Cambridge University Press.

[Hynes, 2002] Hynes, R. O. (2002). A reevaluation of integrins as regulators of angiogenesis. *Nature Medicine*, 8(9):918–21.

[Ingber, 2003] Ingber, D. E. (2003). Tensegrity I. Cell structure and hierarchical systems biology. *Journal of Cell Science*, 116(7):1157–1173.

[Iruthayaraj et al., 2008] Iruthayaraj, J., Olanya, G., and Claesson, P. M. (2008). Viscoelastic properties of adsorbed bottle-brush polymer layers studied by quartz crystal microbalance - dissipation measurements. *Journal of Physical Chemistry A*, 112:15028–15036.

[Israelachvili, 1973] Israelachvili, J. (1973). Thin film studies using multiple-beam interferometry. *Journal of Colloid and Interface Science*, 44(2):259–272.

[Israelachvili, 2011] Israelachvili, J. N. (2011). *Intermolecular and Surface Forces*. Amsterdam: Academic Press and Elsevier.

[Israelachvili and McGuiggan, 1990] Israelachvili, J. N. and McGuiggan, P. M. (1990). Adhesion and short-range forces between surfaces. Part I: New apparatus for surface force measurements. *Journal of Materials Research*, 5(10):2223–2231.

[Janmey and Weitz, 2004] Janmey, P. a. and Weitz, D. a. (2004). Dealing with mechanics: mechanisms of force transduction in cells. *Trends in Biochemical Sciences*, 29(7):364–70.

[Jay, 1992] Jay, G. (1992). Characterization of a bovine synovial fluid lubricating factor. I. Chemical, surface activity and lubricating properties. *Connective Tissue Research*, 1–2(28):71–88.

[Jay, 2004] Jay, G. (2004). Lubricin and surfacing of articular joints. *Opinion in Orthopaedics*, 15:355–359.

[Jay et al., 1998] Jay, G. D., Haberstroh, K., and Cha, C. J. (1998). Comparison of the boundary-lubricating ability of bovine synovial fluid, lubricin, and Healon. *Journal of Biomedical Materials Research*, 40(3):414–8.

[Jay et al., 2007] Jay, G. D., Torres, J. R., Rhee, D. K., Helminen, H. J., Hytinnen, M. M., Cha, C.-J., Elsaid, K., Kim, K.-S., Cui, Y., and Warman, M. L. (2007). Association between friction and wear in diarthrodial joints lacking lubricin. *Arthritis and Rheumatism*, 56(11):3662–9.

[Jeffery et al., 1991] Jeffery, A., Blunn, G., Archer, C., and Bentley, G. (1991). Three-dimensional collagen architecture in bovine articular cartilage. *Journal of Bone and Joint Surgery*, 73(5):795–801.

[Jiang et al., 2003] Jiang, G., Giannone, G., Critchley, D. R., Fukumoto, E., and Sheetz, M. P. (2003). Two-piconewton slip bond between fibronectin and the cytoskeleton depends on talin. *Nature*, 424(July):334–337.

[Johnson, 1985] Johnson, K. L. (1985). *Contact Mechanics*. Cambridge University Press.

[Jones et al., 2007] Jones, A. R. C., Gleghorn, J. P., Hughes, C. E., Fitz, L. J., Zollner, R., Wainwright, S. D., Caterson, B., Morris, E. A., Bonassar, L. J., and Flannery, C. R. (2007). Binding and localization of recombinant lubricin to articular cartilage surfaces. *Journal of Orthopaedic Research*, 12(March):10–12.

[Jurvelin et al., 1996] Jurvelin, J. S., Müller, D. J., Wong, M., Studer, D., Engel, a., and Hunziker, E. B. (1996). Surface and subsurface morphology of bovine humeral articular cartilage as assessed by atomic force and transmission electron microscopy. *Journal of Structural Biology*, 117(1):45–54.

[Kadler et al., 2008] Kadler, K. E., Hill, A., and Canty-Laird, E. G. (2008). Collagen fibrillogenesis: fibronectin, integrins, and minor collagens as organizers and nucleators. *Current Opinion in Cell Biology*, 20(5):495–501.

[Kampf et al., 2004] Kampf, N., Raviv, U., and Klein, J. (2004). Normal and shear forces between adsorbed and gelled layers of chitosan, a naturally occurring cationic polyelectrolyte. *Macromolecules*, 37(3):1134–1142.

[Karnoub et al., 2007] Karnoub, A. E., Dash, A. B., Vo, A. P., Sullivan, A., Brooks, M. W., Bell, G. W., Richardson, A. L., Polyak, K., Tubo, R., and Weinberg, R. a. (2007). Mesenchymal stem cells within tumour stroma promote breast cancer metastasis. *Nature*, 449(7162):557–63.

[Kempson, 1982] Kempson, G. E. (1982). Relationship between the tensile properties of articular cartilage from the human knee and age. *Annals of the Rheumatic Diseases*, 41(5):508–11.

[Kirchner and Marshall, 2006] Kirchner, M. and Marshall, D. (2006). A double-blind randomized controlled trail comparing alternate forms of high molecular weight hyaluronan for the treatment of osteoarthritis of the knee. *Osteo Arthritis and Cartilage*, 14:154–162.

[Klein et al., 1993] Klein, J., Kamiyama, Y., Yoshizawa, H., Israelachvili, J. N., Fredrickson, G. H., Pincus, P., and Fetters, L. J. (1993). Lubrication forces between surfaces bearing polymer brushes. *Macromolecules*, 26(21):5552–5560.

[Klotzsch et al., 2009] Klotzsch, E., Smith, M. L., Kubow, K. E., Muntwyler, S., Little, W. C., Beyeler, F., Gourdon, D., Nelson, B. J., and Vogel, V. (2009). Fibronectin forms the most extensible biological fibers displaying switchable force-exposed cryptic binding sites. *Proceedings of the National Academy of Sciences of the United States of America*, 106(43):18267–72.

[Kloxin et al., 2010] Kloxin, A. M., Kloxin, C. J., Bowman, C. N., and Anseth, K. S. (2010). Mechanical properties of cellularly responsive hydrogels and their experimental determination. *Advanced Materials*, 22(31):3484–94.

[Krammer et al., 2002] Krammer, A., Craig, D., Thomas, W. E., Schulten, K., and Vogel, V. (2002). A structural model for force regulated integrin binding to fibronectin's RGD-synergy site. *Matrix Biology*, 21:139–147.

[Krammer et al., 1999] Krammer, A., Lu, H., Isralewitz, B., Schulten, K., and Vogel, V. (1999). Forced unfolding of the fibronectin type III module reveals a tensile molecular recognition switch. *Proceedings of the National Academy of Sciences of the United States of America*, 96(February):1351–1356.

[Krishnan et al., 2004] Krishnan, R., Caligaris, M., Mauck, R. L., Hung, C. T., Costa, K. D., and Ateshian, G. a. (2004). Removal of the superficial zone of bovine articular cartilage does not increase its frictional coefficient. *Osteoarthritis and Cartilage*, 12(12):947–55.

[Krivorotova et al., 2010] Krivorotova, T., Makuska, R., Naderi, a., Claesson, P., and Dedinaite, a. (2010). Synthesis and interfacial properties of novel cationic polyelectrolytes with brush-on-brush structure of poly(ethylene oxide) side chains. *European Polymer Journal*, 46(2):171–180.

[Kumar and Weaver, 2009] Kumar, S. and Weaver, V. M. (2009). Mechanics, malignancy, and metastasis: the force journey of a tumor cell. *Cancer Metastasis Reviews*, 28(1-2):113–27.

[Laurent et al., 1996] Laurent, T., Laurent, U., and Fraser, J. (1996). The structure and function of hyaluronan: an overview. *Immunology and Cell Biology*, 74:A1–A7.

[Leahy et al., 1996] Leahy, D. J., Aukhil, I., and Erickson, H. P. (1996). 2.0 A crys-

tal structure of a four-domain segment of human fibronectin encompassing the RGD loop and synergy region. *Cell*, 84(1):155–64.

[Lee et al., 2014] Lee, D. W., Banquy, X., Das, S., Cadirov, N., Jay, G., and Israelachvili, J. (2014). Effects of molecular weight of grafted hyaluronic acid on wear initiation. *Acta Biomaterialia*, 10(5):1817–23.

[Lee et al., 1990] Lee, J. H., Kopeckova, P., Kopecek, J., and Andrade, J. D. (1990). Surface properties of copolymers of alkyl methacrylates with methoxy (polyethylene oxide) methacrylates and their application as protein-resistant coatings. *Biomaterials*, 11(7):455–64.

[Levental et al., 2009] Levental, K. R., Yu, H., Kass, L., Lakins, J. N., Erler, J. T., Fong, S. F. T., Csiszar, K., Giaccia, A., Yamauchi, M., Gasser, D. L., and Weaver, V. M. (2009). Matrix crosslinking forces tumor progression by enhancing integrin signaling. *Cell*, 139(5):891–906.

[Liberelle and Giasson, 2008] Liberelle, B. and Giasson, S. (2008). Friction and normal interaction forces between irreversible attached weakly charged polymer brushes. *Langmuir*, 24:1550–1559.

[Little et al., 2009] Little, W. C., Schwartlander, R., Smith, M. L., Gourdon, D., and Vogel, V. (2009). Stretched extracellular matrix proteins turn fouling and are functionally rescued by the chaperones albumin and casein. *Nano Letters*, 9(12):4158–67.

[Liu et al., 2012] Liu, C., Wang, M., An, J., Thormann, E., and Ddinait, A. (2012). Hyaluronan and phospholipids in boundary lubrication. *Soft Matter*, 8(40):10241.

[Liu et al., 2010] Liu, Y., Pan, Y., and Xu, Y. (2010). Binding investigation of integrin alphavbeta3 with its inhibitors by SPR technology and molecular docking simulation. *Journal of Biomolecular Screening*, 15(2):131–7.

[López-Otín and Diamandis, 1998] López-Otín, C. and Diamandis, E. P. (1998). Breast and prostate cancer: an analysis of common epidemiological, genetic, and biochemical features. *Endocrine Reviews*, 19(4):365–96.

[Loret and Simões, 2004] Loret, B. and Simões, F. M. (2004). Articular cartilage with intra- and extrafibrillar waters: a chemo-mechanical model. *Mechanics of Materials*, 36(5-6):515–541.

[Lu et al., 2012] Lu, P., Weaver, V. M., and Werb, Z. (2012). The extracellular matrix: a dynamic niche in cancer progression. *The Journal of Cell Biology*, 196(4):395–406.

[Luengo et al., 1997] Luengo, G., Tsuchiya, M., Heuberger, M., and Israelachvili, J. (1997). Thin film rheology and tribology of chocolate. *Journal of Food Science*, 62(4):767–812.

[M.A. MacConail, 1951] M.A. MacConail (1951). The movements of bones and joints. *The Journal of Bone and Joint Surgery*, 33B(2):251–257.

[Mabuchi et al., 1999] Mabuchi, K., Obara, T., Ikegami, K., Yamaguchi, T., and Kanayama, T. (1999). Molecular weight independence of the effect of additive hyaluronic acid on the lubricating characteristics in synovial joints with experimental deterioration. *Clinical Biomechanics*, 14(5):352–6.

[Mammoto et al., 2009] Mammoto, A., Connor, K. M., Mammoto, T., Yung, C. W., Huh, D., Aderman, C. M., Mostoslavsky, G., Smith, L. E. H., and Ingber, D. E. (2009). A mechanosensitive transcriptional mechanism that controls angiogenesis. *Nature*, 457(7233):1103–8.

[Mao and Schwarzbauer, 2005] Mao, Y. and Schwarzbauer, J. E. (2005). Fibronectin fibrillogenesis, a cell-mediated matrix assembly process. *Matrix Biology*, 24(6):389–99.

[Martin and Buckwalter, 2002] Martin, J. A. and Buckwalter, J. A. (2002). Aging , articular cartilage chondrocyte senescence and osteoarthritis. *Biogerontology*, 3:257–264.

[Martin et al., 1997] Martin, J. a., Ellerbroek, S. M., and Buckwalter, J. a. (1997). Age-related decline in chondrocyte response to insulin-like growth factor-I: the role of growth factor binding proteins. *Journal of Orthopaedic Research*, 15(4):491–8.

[Martino et al., 2011] Martino, M. M., Tortelli, F., Mochizuki, M., Traub, S., Ben-David, D., Kuhn, G. a., Müller, R., Livne, E., Eming, S. a., and Hubbell, J. a. (2011). Engineering the growth factor microenvironment with fibronectin domains to promote wound and bone tissue healing. *Science Translational Medicine*, 3(100):100ra89.

[McCutchen, 1962] McCutchen, C. W. (1962). The frictional properties of animal joints. *Wear*, 5:1–17.

[Mcdonald et al., 1982] Mcdonald, J. A., Kelley, D. G., and Broekelmann, T. J. (1982). Role of fibronectin in collagen deposition: Fab ′ to the gelatin-binding domain of fibronectin inhibits both fibronectin and collagen organization in fibroblast extracellular matrix. *Journal of Cell Biology*, 92:485–492.

[McGuiggan and Israelachvili, 1990] McGuiggan, P. M. and Israelachvili, J. N. (1990). Adhesion and short-range forces between surfaces. Part II: Effects of surface lattice mismatch. *Journal of Materials Research*, 5(10):2232–2243.

[Midwood et al., 2004] Midwood, K. S., Williams, L. V., and Schwarzbauer, J. E. (2004). Tissue repair and the dynamics of the extracellular matrix. *The International Journal of Biochemistry & Cell Biology*, 36(6):1031–7.

[Mishra et al., 2008] Mishra, P. J., Mishra, P. J., Humeniuk, R., Medina, D. J., Alexe, G., Mesirov, J. P., Ganesan, S., Glod, J. W., and Banerjee, D. (2008). Carcinoma-associated fibroblast-like differentiation of human mesenchymal stem cells. *Cancer Research*, 68(11):4331–9.

[Morrell et al., 2005] Morrell, K. C., Hodge, W. A., Krebs, D. E., and Mann, R. W. (2005). Corroboration of in vivo cartilage pressures with implications for synovial joint tribology and osteoarthritis causation. *Proceedings of the National Academy of Sciences of the United States of America*, 102(41):14819–24.

[Mott and Werb, 2004] Mott, J. D. and Werb, Z. (2004). Regulation of matrix biology by matrix metalloproteinases. *Current Opinion in Cell Biology*, 16(5):558–64.

[Mow et al., 1984] Mow, V., Holmes, M., and Lai, W. (1984). Fluid transport and mechanical properties of articular cartilage: a review. *Journal of Biomechanics*, 17:377–394.

[Mow et al., 1993] Mow, V. C., Ateshian, G. A., and Spilker, R. L. (1993). Biomechanics of diarthrodial joints : a review of twenty years of progress. *Journal of Biomechanical Engineering*, pages 460–467.

[Mow and Lai, 1980] Mow, V. C. and Lai, M. (1980). Recent developments in synovial joint biomechanics. *SIAM Review*, 22(3):275–317.

[Nakashima et al., 2005] Nakashima, K., Sawae, Y., and Murakami, T. (2005). Study on wear reduction mechanisms of artificial cartilage by synergistic protein boundary film formation. *JSME International journal*, 48(4):555–561.

[Nishida et al., 1995] Nishida, K., Inoue, H., and Murakami, T. (1995). Immunohistochemical demonstration of fibronectin in the most superficial layer of normal rabbit articular cartilage. *Annals of the Rheumatic Diseases*, 54(12):995–8.

[Obara et al., 1988] Obara, M., Kang, M. S., and Yamada, K. M. (1988). Site-directed mutagenesis of the cell-binding domain of human fibronectin : separable , synergistic sites mediate adhesive function. *Cell*, 53:649–657.

[O'Connor et al., 2014] O'Connor, S., Gaddis, R., Anderson, E., Camesano, T. a., and Burnham, N. a. (2014). A high throughput matlab program for automated forcecurve processing using the Adg polymer model. *Journal of Microbiological Methods*.

[Pankov, 2002] Pankov, R. (2002). Fibronectin at a glance. *Journal of Cell Science*, 115(20):3861–3863.

[Park et al., 2011] Park, J., Euhus, D. M., and Scherer, P. E. (2011). Paracrine and endocrine effects of adipose tissue on cancer development and progression. *Endocrine Reviews*, 32(4):550–70.

[Paszek et al., 2005] Paszek, M. J., Zahir, N., Johnson, K. R., Lakins, J. N., Rozenberg, G. I., Gefen, A., Reinhart-King, C. a., Margulies, S. S., Dembo, M., Boettiger, D., Hammer, D. a., and Weaver, V. M. (2005). Tensional homeostasis and the malignant phenotype. *Cancer Cell*, 8(3):241–54.

[Perry et al., 2009] Perry, S. S., Yan, X., Limpoco, F. T., Lee, S., Müller, M., and Spencer, N. D. (2009). Tribological properties of poly(L-lysine)-graft-poly(ethylene glycol) films: influence of polymer architecture and adsorbed conformation. *ACS Applied Materials & Interfaces*, 1(6):1224–30.

[Petrie et al., 2006] Petrie, T. a., Capadona, J. R., Reyes, C. D., and García, A. J. (2006). Integrin specificity and enhanced cellular activities associated with surfaces presenting a recombinant fibronectin fragment compared to RGD supports. *Biomaterials*, 27(31):5459–70.

[Pettersson et al., 2008] Pettersson, T., Naderi, A., Makuska, R., and Claesson, P. M. (2008). Lubrication properties of bottle-brush polyelectrolytes: an AFM study on the effect of side chain and charge density. *Langmuir*, 24(7):3336–47.

[Pickford et al., 1997] Pickford, a. R., Potts, J. R., Bright, J. R., Phan, I., and Campbell, I. D. (1997). Solution structure of a type 2 module from fibronectin:

implications for the structure and function of the gelatin-binding domain. *Structure*, 5(3):359–70.

[Pierschbacher and Rouslahti, 1984] Pierschbacher, M. D. and Rouslahti, E. (1984). Cell attachment activity of fibronectin can be duplicated by small synthetic fragments of the molecule. *Nature*, 309:30–33.

[Pollard, 2004] Pollard, J. W. (2004). Tumour-educated macrophages promote tumour progression and metastasis. *Nature Reviews Cancer*, 4:71–78.

[Polyak, 2007] Polyak, K. (2007). Science in medicine Breast cancer : origins and evolution. *Journal of Clinical Investigation*, 117:3155–3163.

[Potts and Campbell, 1996] Potts, J. R. and Campbell, I. D. (1996). Structure and function of fibronectin modules. *Matrix Biology*, 15(5):313–20; discussion 321.

[Radin et al., 1970] Radin, E. L., Swann, D. A., and Weisser, P. A. (1970). Separation of a hyaluronate-free lubricating fraction from synovial fluid. *Nature*, 22:377–378.

[Raviv et al., 2003] Raviv, U., Giasson, S., Kampf, N., Gohy, J.-F., Jérôme, R., and Klein, J. (2003). Lubrication by charged polymers. *Nature*, 425(6954):163–5.

[Rhee et al., 2005] Rhee, D. K., Marcelino, J., Baker, M., Gong, Y., Smits, P., Lefebvre, V., Jay, G. D., Stewart, M., Wang, H., Warman, M. L., and Carpten, J. D. (2005). The secreted glycoprotein lubricin protects cartilage surfaces and inhibits synovial cell overgrowth. *The Journal of Clinical Investigation*, 115(3):622–31.

[Roberts et al., 1982] Roberts, B. J., Unsworth, a., and Mian, N. (1982). Modes of lubrication in human hip joints. *Annals of the Rheumatic Diseases*, 41(3):217–24.

[Robinson et al., 1991] Robinson, S. D., Silberstein, G. B., Roberts, A. B., Flanders, K. C., and Daniel, C. W. (1991). Regulated expression and growth inhibitory effects of transforming growth factor-beta isoforms in mouse mammary gland development. *Development*, 113(3):867–878.

[Roca-Cusachs et al., 2013] Roca-Cusachs, P., del Rio, A., Puklin-Faucher, E., Gauthier, N. C., Biais, N., and Sheetz, M. P. (2013). Integrin-dependent force transmission to the extracellular matrix by α-actinin triggers adhesion maturation. *Proceedings of the National Academy of Sciences of the United States of America*, 110(15):E1361–70.

[Ruoslahti, 1988] Ruoslahti, E. (1988). Fibronectin and its receptors. *Annual Review of Physical Chemistry*, 57:375–413.

[Rutjes et al., 2012] Rutjes, A. W., Jueni, P., da Costa, B. R., Trelle, S., Nueesch, E., and Reichenbach, S. (2012). Viscosupplementation for osteoarthritis of the knee. *Annals of Internal Medicine*, 157:180–191.

[Sakai et al., 2003] Sakai, T., Larsen, M., and Yamada, K. M. (2003). Fibronectin requirement in branching morphogenesis. *Nature*, 423:876–881.

[Samani et al., 2007] Samani, A., Zubovits, J., and Plewes, D. (2007). Elastic moduli of normal and pathological human breast tissues: an inversion-technique-based investigation of 169 samples. *Physics in Medicine and Biology*, 52(6):1565–76.

[Schaefer et al., 2004] Schaefer, D., Wendt, D., Moretti, M., Jakob, M., Jay, G., Herberer, M., and Martin, I. (2004). Lubricin reduces cartilage-cartilage integration. *Biorheology*, 41:503–508.

[Schiller et al., 2013] Schiller, H. B., Hermann, M.-R., Polleux, J., Vignaud, T., Zanivan, S., Friedel, C. C., Sun, Z., Raducanu, A., Gottschalk, K.-E., Théry, M., Mann, M., and Fässler, R. (2013). β1- and αv-class integrins cooperate to regulate myosin II during rigidity sensing of fibronectin-based microenvironments. *Nature Cell Biology*, 15(6):625–36.

[Schmidt et al., 2007] Schmidt, T. a., Gastelum, N. S., Nguyen, Q. T., Schumacher, B. L., and Sah, R. L. (2007). Boundary lubrication of articular cartilage: role of synovial fluid constituents. *Arthritis and Rheumatism*, 56(3):882–91.

[Schmidt and Sah, 2007] Schmidt, T. a. and Sah, R. L. (2007). Effect of synovial fluid on boundary lubrication of articular cartilage. *Osteoarthritis and Cartilage*, 15(1):35–47.

[Schnepel and Tschesche, 2000] Schnepel, J. and Tschesche, H. (2000). The proteolytic activity of the recombinant cryptic human fibronectin type IV collagenase from E. coli expression. *Journal of Protein Chemistry*, 19(8):685–92.

[Seong et al., 2013] Seong, J., Tajik, A., Sun, J., Guan, J.-L., Humphries, M. J., Craig, S. E., Shekaran, A., García, A. J., Lu, S., Lin, M. Z., Wang, N., and Wang, Y. (2013). Distinct biophysical mechanisms of focal adhesion kinase mechanoactivation by different extracellular matrix proteins. *Proceedings of*

the National Academy of Sciences of the United States of America, 110(48):19372–7.

[Sheiko and Möller, 2001] Sheiko, S. S. and Möller, M. (2001). Visualization of macromolecules–a first step to manipulation and controlled response. *Chemical Reviews*, 101(12):4099–124.

[Singh et al., 2010] Singh, P., Carraher, C., and Schwarzbauer, J. E. (2010). Assembly of fibronectin extracellular matrix. *Annual Review of Cell and Developmental Biology*, 26:397–419.

[Sinkus et al., 2005] Sinkus, R., Tanter, M., Catheline, S., Lorenzen, J., Kuhl, C., Sondermann, E., and Fink, M. (2005). Imaging anisotropic and viscous properties of breast tissue by magnetic resonance-elastography. *Magnetic Resonance in Medicine*, 53(2):372–87.

[Smith et al., 2007] Smith, M. L., Gourdon, D., Little, W. C., Kubow, K. E., Eguiluz, R. A., Luna-Morris, S., and Vogel, V. (2007). Force-induced unfolding of fibronectin in the extracellular matrix of living cells. *PLoS Biology*, 5(10):e268.

[Sofat et al., 2012] Sofat, N., Robertson, S. D., and Wait, R. (2012). Fibronectin III 13-14 domains induce joint damage via Toll-like receptor 4 activation and synergize with interleukin-1 and tumour necrosis factor. *Journal of Innate Immunity*, 4(1):69–79.

[Sørlie et al., 2006] Sørlie, T., Wang, Y., Xiao, C., Johnsen, H., Naume, B. r., Samaha, R. R., and Bø rresen Dale, A.-L. (2006). Distinct molecular mechanisms underlying clinically relevant subtypes of breast cancer: gene expression analyses across three different platforms. *BMC Genomics*, 7:127.

[Sottile and Hocking, 2002] Sottile, J. and Hocking, D. C. (2002). Fibronectin polymerization regulates the composition and stability of extracellular matrix fibrils and cell-matrix adhesions. *Molecular Biology of the Cell*, 13(10):3546–59.

[Sottile et al., 2007] Sottile, J., Shi, F., Rublyevska, I., Chiang, H.-Y., Lust, J., and Chandler, J. (2007). Fibronectin-dependent collagen I deposition modulates the cell response to fibronectin. *American Journal of Physiology. Cell Physiology*, 293(6):C1934–46.

[Spaeth et al., 2009] Spaeth, E. L., Dembinski, J. L., Sasser, a. K., Watson, K., Klopp, A., Hall, B., Andreeff, M., and Marini, F. (2009). Mesenchymal stem

cell transition to tumor-associated fibroblasts contributes to fibrovascular network expansion and tumor progression. *PloS one*, 4(4):e4992.

[Stenman and Vaheri, 1981] Stenman, S. and Vaheri, A. (1981). Fibronectin in human solid tumors. *International Journal of Cancer*, 27:427–435.

[Swann et al., 1974] Swann, D. a., Radin, E. L., Nazimiec, M., Weisser, P. a., Curran, N., and Lewinnek, G. (1974). Role of hyaluronic acid in joint lubrication. *Annals of the Rheumatic Diseases*, 33(4):318–26.

[Swann et al., 1985] Swann, D. a., Silver, F. H., Slayter, H. S., Stafford, W., and Shore, E. (1985). The molecular structure and lubricating activity of lubricin isolated from bovine and human synovial fluids. *The Biochemical Journal*, 225(1):195–201.

[Swann et al., 1981] Swann, D. a., Slayter, H. S., and Silver, F. H. (1981). The molecular structure of lubricating glycoprotein-I, the boundary lubricant for articular cartilage. *The Journal of Biological Chemistry*, 256(11):5921–5.

[Swann et al., 1977] Swann, D. a., Sotman, S., Dixon, M., and Brooks, C. (1977). The isolation and partial characterization of the major glycoprotein (LGP-I) from the articular lubricating fraction from bovine synovial fluid. *The Biochemical Journal*, 161(3):473–85.

[Tadmor et al., 2003] Tadmor, R., Chen, N., and Israelachvili, J. (2003). Normal and shear forces between mica and model membrane surfaces with adsorbed hyaluronan. *Macromolecules*, 36(25):9519–9526.

[Tadmor et al., 2002a] Tadmor, R., Chen, N., and Israelachvili, J. N. (2002a). Thin film rheology and lubricity of hyaluronic acid solutions at a normal physiological concentration. *Journal of Biomedical Materials Research*, 61(4):514–23.

[Tadmor et al., 2002b] Tadmor, R., Herna, E., Chen, N., Pincus, P., and Israelachvili, J. N. (2002b). Debye length and double-layer forces in polyelectrolyte solutions. *Macromolecules*, 35:2380–2388.

[Takagi et al., 2003] Takagi, J., Strokovich, K., Springer, T. a., and Walz, T. (2003). Structure of integrin alpha5beta1 in complex with fibronectin. *The EMBO Journal*, 22(18):4607–15.

[Tomasek et al., 2002] Tomasek, J. J., Gabbiani, G., Hinz, B., Chaponnier, C., and

Brown, R. a. (2002). Myofibroblasts and mechano-regulation of connective tissue remodelling. *Nature Reviews. Molecular Cell Biology*, 3(5):349–63.

[Toole, 2004] Toole, B. P. (2004). Hyaluronan: from extracellular glue to pericellular cue. *Nature Reviews. Cancer*, 4(7):528–39.

[Vogel, 2006] Vogel, V. (2006). Mechanotransduction involving multimodular proteins: converting force into biochemical signals. *Annual Review of Biophysics and Biomolecular Structure*, 35:459–88.

[Wan et al., 2013] Wan, A. M. D., Chandler, E. M., Madhavan, M., Infanger, D. W., Ober, C. K., Gourdon, D., Malliaras, G. G., and Fischbach, C. (2013). Fibronectin conformation regulates the proangiogenic capability of tumor-associated adipogenic stromal cells. *Biochimica et Biophysica Acta*, 1830(9):4314–4320.

[Wan et al., 2012] Wan, A. M. D., Schur, R. M., Ober, C. K., Fischbach, C., Gourdon, D., and Malliaras, G. G. (2012). Electrical control of protein conformation. *Advanced Materials*, 24(18):2501–5.

[Wang and Ateshian, 1997] Wang, H. and Ateshian, G. A. (1997). The normal stress effect and equilibrium friction coefficient of afticular cartilage under steady frictional shear. *Journal of Biomechanics*, 30(8):771–776.

[Wegener et al., 2007] Wegener, K. L., Partridge, A. W., Han, J., Pickford, A. R., Liddington, R. C., Ginsberg, M. H., and Campbell, I. D. (2007). Structural basis of integrin activation by talin. *Cell*, 128(1):171–82.

[Wijelath, 2002] Wijelath, E. S. (2002). Novel vascular endothelial growth factor binding domains of fibronectin enhance vascular endothelial growth factor biological activity. *Circulation Research*, 91(1):25–31.

[Wright and Dowson, 1976] Wright, V. and Dowson, D. (1976). Lubrication and cartilage *. *Journal of Anatomy*, (December 1974):107–118.

[Yan et al., 2004] Yan, X., Perry, S. S., Spencer, N. D., Pasche, S., De Paul, S. M., Textor, M., and Lim, M. S. (2004). Reduction of friction at oxide interfaces upon polymer adsorption from aqueous solutions. *Langmuir*, 20(2):423–8.

[Yim et al., 2009] Yim, E. S., Zhao, B., Myung, D., Kourtis, L. C., Frank, C. W., Carter, D., Smith, R. L., and Goodman, S. B. (2009). Biocompatibility of poly(ethylene glycol)/poly(acrylic acid) interpenetrating polymer network

hydrogel particles in RAW 264.7 macrophage and MG-63 osteoblast cell lines. *Journal of Biomedical Materials Research. Part A*, 91(3):894–902.

[Yu et al., 2012] Yu, J., Banquy, X., Greene, G. W., Lowrey, D. D., and Israelachvili, J. N. (2012). The boundary lubrication of chemically grafted and cross-linked hyaluronic acid in phosphate buffered saline and lipid solutions measured by the surface forces apparatus. *Langmuir*, 28(4):2244–50.

[Zamir and Geiger, 2001] Zamir, E. and Geiger, B. (2001). Molecular complexity and dynamics of cell-matrix adhesions. *Journal of Cell Science*, 114(Pt 20):3583–90.

[Zappone et al., 2008] Zappone, B., Greene, G. W., Oroudjev, E., Jay, G. D., and Israelachvili, J. N. (2008). Molecular aspects of boundary lubrication by human lubricin: effect of disulfide bonds and enzymatic digestion. *Langmuir*, 24(4):1495–508.

[Zappone et al., 2007] Zappone, B., Ruths, M., Greene, G. W., Jay, G. D., and Israelachvili, J. N. (2007). Adsorption, lubrication, and wear of lubricin on model surfaces: polymer brush-like behavior of a glycoprotein. *Biophysical Journal*, 92(5):1693–708.

[Zhang et al., 2008] Zhang, M., Nigwekar, P., Castaneda, B., Hoyt, K., Joseph, J. V., di Sant'Agnese, A., Messing, E. M., Strang, J. G., Rubens, D. J., and Parker, K. J. (2008). Quantitative characterization of viscoelastic properties of human prostate correlated with histology. *Ultrasound in Medicine & Biology*, 34(7):1033–42.

[Zhang et al., 2004] Zhang, Y., Lu, H., Dazin, P., and Kapila, Y. (2004). Squamous cell carcinoma cell aggregates escape suspension-induced, p53-mediated anoikis: fibronectin and integrin alphav mediate survival signals through focal adhesion kinase. *The Journal of Biological Chemistry*, 279(46):48342–9.